Università degli Studi di Cagliari

# DOTTORATO DI RICERCA

IN SCIENZE E TECNOLOGIE CHIMICHE

Ciclo XXIII

# TITOLO TESI

SULFUR CHEMICAL STATE AT MINERAL SURFACES – AN XPS AND XAES INVESTIGATION

Settore/i scientifico disciplinari di afferenza

CHIM/01


Presentata da: Americo Rigoldi

Coordinatore Dottorato Prof. Mariano Casu

Tutor Prof.ssa Antonella Rossi


Esame finale anno accademico 2009 - 2010

# CONTENTS


| | | | | |
|---|---|---|---|---|
| | | | Abstract | 4 |
| **1** | | | **INTRODUCTION** | **7** |
| 1.1 | | | Sulphur chemical state identification | 8 |
| 1.2 | | | Scope of the thesis | 10 |
| | | | References | 11 |
| **2** | | | **LITERARY REVIEW** | **12** |
| 2.1 | | | Sulphur on enargite surface | 13 |
| | 2.1.1 | | Properties of enargite | 13 |
| | 2.1.2 | | Chemical state of the elements on enargite surface | 14 |
| | 2.1.3 | | Auger parameter and chemical state plot | 16 |
| | 2.1.4 | | Layer thickness of the sulphur-enriched sulfur layer | 19 |
| 2.2 | | | KLL Auger transition | 19 |
| | | | References | 21 |
| **3** | | | **X-RAY PHOTOELECTRON SPECTROSCOPY AND X-RAY EXCITED AUGER ELECTRON SPECTROSCOPY** | **24** |
| 3.1 | | | Physical Principle | 25 |
| 3.2 | | | Notation | 27 |
| 3.3 | | | Spectra | 28 |
| | 3.3.1 | | Chemical shift | 29 |
| | 3.3.2 | | Spin-orbit coupling | 29 |
| | | 3.3.2.1 | j-j coupling | 30 |
| | | 3.3.2.2 | L-S coupling | 31 |

3.3.3 Multiplet splitting 33
3.3.4 Satellite peaks 33
3.3.5 Energy scale correction for charging 34
3.3.6 Calibration 34
3.4 Data processing 34
3.4.1 Satellite subtraction 35
3.4.2 Background subtraction 35
3.4.3 Peak fitting 35
3.5 Auger parameter 37
3.6 Quantitative Analysis 40
References 43

**4 EXPERIMENTAL 45**
4.1 Materials 46
4.1.1 Reference materials 46
4.1.1.1 Sulphur, sulphides and sulphates 46
4.1.1.2 Model systems: Sulphur and polysulphides mixtures 47
4.1.2 Mineral samples 48
4.2 Methods 48
4.2.1 X-ray photoelectron spectroscopy 48
4.2.2 Theta Probe 49
4.2.3 ESCALAB MKII 51
4.2.3.1 X-ray excited Auger electron spectroscopy 54
4.2.4 SIGMA 2 55
4.2.5 Data processing and quantitative analysis 57
References 61

| | | | |
|---|---|---|---|
| **5** | | **RESULTS AND DISCUSSION** | **62** |
| 5.1 | | Reference compounds | 63 |
| | 5.1.1 | Group IA sulphates | 63 |
| | 5.1.2 | Chemical state of sulphates | 74 |
| | 5.1.3 | Elemental Sulphur ($S_8$) | 78 |
| | 5.1.4 | Sulphides and poly-sulphides of group I elements | 80 |
| | 5.1.5 | Chemical state of sulphides | 89 |
| | 5.1.6 | Copper and iron sulphide | 90 |
| | 5.1.7 | The chemical state of metal sulphides | 97 |
| | 5.1.8 | Effect of grinding time of polysulphides | 98 |
| 5.2 | | Model systems: mixtures of sodium tetrasulphide and elemental sulphur | 106 |
| 5.3 | | Minerals | 112 |
| | 5.3.1 | Pyrite | 112 |
| | 5.3.2 | Arsenopyrite | 119 |
| | 5.3.3 | Chalcopyrite | 124 |
| | 5.3.4 | Enargite | 129 |
| | 5.3.5 | Chemical state of sulphur in minerals | 134 |
| | | References | 136 |
| **6** | | **CONCLUSIONS** | 138 |
| | | APPENDIX | 141 |

# Abstract

During the interaction of sulphide minerals with the environment many reactions may occur. The knowledge of sulphur chemical state is important in order to clarify the mechanisms of oxidation/dissolution and precipitation reactions also in biotic conditions on the surface of these minerals. To date different hypotheses have been proposed for identifying the sulphur compounds that may form but no consensus is reached so far because the identification has been carried out either only on the basis of the photoelectron signals or combining the photoelectron signal with the centroid of the X-ray induced SKLL Auger line.

The objectives of this thesis are: the development of an analytical strategy for the unambiguous identification of sulphur chemical state in nanometer thick layers that form on mineral surfaces after leaching. To this purpose the acquisition of detailed spectra of a series of metal sulphides and of model systems made of mixtures of sulphur and polysulphides prepared under controlled conditions is necessary. Second objective was the establishment of the curve-fitting procedure to allow the separation of the different components present on the surface (sulphide, polysulphides, sulphates) not only of the S2p XP-spectra but also of the SKLL spectra. Based on these results the Auger parameter values will be determined and will be used together with the chemical state plot to distinguish the chemical state of sulphur species formed on the mineral surfaces after different surface treatments. In this way, the surface reactivity of sulphide minerals and more in general, of sulphur –bearing particles will be determined

The present work is organized in six chapters: the first one presents a short overview on the environmental problems that may occur when sulphide minerals, especially, those bearing eco-toxic elements such as arsenic, are exposed to the acidic mine drainage in the presence of oxidants and/or of microorganisms which enhance oxidation kinetics. It then outlines the analytical strategy that was adopted in this work for the identification of the sulphur chemical state.

In the second chapter a literature survey is provided: it underlines the role of sulphur in sulphide bearing minerals: Section 2.1 reports information about the mineral enargite and the chemical state of sulphur on its surface as it is available to date. Section 2.2 deals with the literature on the possibility of using the KLL Auger

transition. In chapter 3 a brief description of X-ray photoelectron and X-ray excited Auger electron spectroscopy is given while the materials and methods used in the present work are presented in chapter 4.

In chapter 5 – results and discussion - the X-ray photoelectron spectroscopy (XPS) and X-ray excited Auger electron spectroscopy (XAES) analyses on alkaline and transition metal sulphide and sulphates, polysulphides and sulphide minerals are presented. In particular the spectra recorded on the S2p and S KLL lines of the sulphides and sulphates are shown: they were collected for getting the peak fitting parameters and apply them to the model systems obtained by mixing sulphur with sodium tetrasulphide and to investigate the composition of mineral surfaces. Minerals were analysed freshly cleaved, ground and after air exposure. The chemical state of sulphur in sulphates, sulphides (alkali- and transition metal compounds, minerals) and polysulphide is then discussed. For the first time the X-ray excited Auger SKLL lines were fitted with parameters based on standards. In this way, which can be considered as an extension of previous work, a separation of the different components and a more precise determination of their kinetic energy were achieved. The Auger parameter and the chemical state plot were obtained by combining the S2p photoelectron lines and the SKLL Auger lines. On this basis a clear distinction of the chemical state of sulphur in sulphates, in alkali sulphides and in transition metal sulphides was possible. The chemical state of sulphur in the bulk of minerals such as enargite or pyrite was determined. The chemical state of sulphur that formed on the surface of compounds after exposure to air or after grinding was found to vary according the coordinating metal and its concentration.

It can be assessed that the analytical approach developed in the presented thesis and based on the curve – fitting procedure applied to the X-ray induced Auger electron spectroscopy appears to be a very promising method for identifying the chemical state of sulphur and for providing a new insight in the surface chemistry of sulphide minerals.

# Chapter 1

# Introduction

*This chapter provides a short overview on the environmental problems that may occur when sulphide minerals, especially, those bearing eco-toxic elements such as arsenic, are exposed to the acidic mine drainage in the presence of oxidants and/or of microorganisms which enhance oxidation kinetics. Special attention was devoted to the role played by sulphur in the stability of the minerals since it was shown that a very thin sulphur-enriched layer on the mineral surfaces may affect the oxidation/dissolution reactions. Hereafter the analytical strategy that was adopted in this work for the identification of the sulphur chemical state is outlined.*

## 1.1 Sulphur chemical state identification

The identification of the oxidation state, the chemical environment and the coordination of sulphur is important for understanding the chemical reactions at the surface of sulphide minerals. Sulphide minerals ore deposits are the main natural sources of several precious and base metals, and as such they are of remarkable economic value. On the other hand, they are thermodynamically unstable in supergene conditions, i.e. when in contact with the atmosphere, and upon oxidation, they may release into the environment several ecotoxines such as heavy metals, As, Se and Te. The interaction of the metal sulphides with the environment occurs at their surface; therefore the study of metal sulphide surfaces is of utmost importance for two reasons:

- some processes of ore beneficiation, most notably flotation, depend on the mineral surface properties; therefore, studies of sulphide surfaces may provide clues to a better understanding of mineral dressing problems arising in commercial plants and possibly to a more effective application of mineral separation processes;
- the first steps of oxidation/dissolution of sulphides in the supergene environment occur at the mineral surface; hence, understanding of the dissolution mechanism occurring at their surface is critical for the assessment of the potential environmental impact of mining and smelting activities.

With these two objectives in mind, several studies were conducted on sulphide surfaces (Nesbitt et al 1995 [1], 1999 [2]; England et al. 1999 [3]; Fullston et al., 1999 [4], to mention but a few). In a previous Ph.D. thesis [5] – which was carried out within the research group wherein also this work, was conducted – oxidation/dissolution experiments were performed in acidic conditions, also in the presence of iron- and sulphur oxidizing microorganisms, on enargite ($Cu_3AsS_4$), a mineral to which some attention was recently drawn because it is locally abundant in certain types of ore deposits. The reasons for having recourse to X-ray photoelectron spectroscopy (XPS) for this investigation are related to its high surface sensitivity, intrinsic no-destructiveness and chemical state identification suitability.

Enargite surface properties drew, comparatively to other sulphides and sulphosalts, little attention, but in recent years a number of studies have been carried out, including electrochemical [6,7] and XPS [4] studies, mostly conducted in alkaline

conditions, with the ultimate goal of predicting the behaviour of enargite in flotation. A detailed characterization of different natural and synthetic enargites was performed by XPS surface analysis [8] and a valuable database for Cu, As and S in enargites under natural, cleaved and sputtered conditions was therein proposed. XPS investigations of enargite surfaces were also carried out before [9] and after treatment with air-saturated distilled water, and in acidic ($H_2SO_4$) conditions as well as in acidic ferric solutions [10,11], to simulate natural environments where enargite is exposed to extremely acidic conditions generated by pyrite oxidation.

The results confirmed the rather refractory behaviour of enargite compared to other sulphides, as established by other authors; notably, there is no significant shift of the binding energies of copper and arsenic, even in the most extreme conditions ($H_2SO_4$ or acidic ferric solutions), but the formation of a metal depleted/sulphur enriched layer, 5-10 nm thick, was observed [10]. On the other hand, the untreated surface of natural crystals, exposed for a number of years to atmospheric conditions, show evidence of Cu-O and As-O bonds formation [8] indicating that an oxidized surface has to be considered as the starting condition on natural enargite that has not undergone any grinding or cleavage.

The most intense photoelectron line, S2p, for a sulphide mineral is complex on account of the spin-orbit coupling that splits the signal into two components: $S2p_{3/2}$ and $S2p_{1/2}$ only separated by 1.2 eV and because of the wide variety of formal oxidation states for sulphur, that may result after a leaching process. In fact, between the extremes consisting of $S^{2-}$ (sulphide) and $S^{6+}$ (sulphate), a variety of intermediate oxidation states and thus of different compounds can be formed during oxidation, dissolution and precipitation reactions. It was suggested [6] that the comparatively refractory behaviour of enargite may be due to the creation of a passive film of a rather elusive, ill-defined $CuS_2$ compound [12]. The exact nature of this hypothetic species is still unclear.

## 1.2 Scope of the thesis

Scope of this thesis is the development of an analytical strategy for the unambiguous identification of sulphur chemical state in nanometer thick layers that form on mineral surfaces after leaching. To this purpose the acquisition of detailed spectra of a series of metal sulphides and of model systems made of mixtures of sulphur and polysulphides prepared under controlled conditions is necessary. Furthermore the establishment of the curve-fitting procedure to allow the separation of the components not only of the S2p XP-spectra but also of the SKLL spectra is required. In addition, the Auger parameter values, compared with other results (when available) will be determined will be used to distinguish the species formed on the mineral surfaces after different surface treatments. In this way, the surface reactivity of sulphide minerals and more in general, of sulphur –bearing particles will be determined.

This approach is applied for the first time in this work.

## References


[1] Nesbitt H.V., Muir I.J., Pratt A.R., *Geochimica et Cosmochima Acta* 1995; Vol.59, No.9: 1773-1786

[2] Nesbitt H.W., Reinke, M., *Am. Mineral*. 1999; 84:639-649

[3] England K.E.R, Pattrick R.A.D., Vaughan D.J., *Mineral. Mag.* 1999; 63: 559-566

[4] Fullston D., Fornasiero D., Ralston J., *Langmuir* 1999; 15: 4530-4536

[5] Fantauzzi M., *PhD Thesis* 2005; University of Cagliari – Italy

[6] Cordova R., Gomez H., Real S.G., Schrebler R., Vilche J.R., *J. Electrochem. Soc.* 1997; 144: 2628-2636.

[7] Fullston D., Fornasiero D., Ralston J. *Langmuir* 1999; 15: 4524-4529

[8] Rossi A., Atzei D., Da Pelo S., Frau F., Lattanzi P., England K.E.R., Vaughan D.J., *Surface and Interface Analysis* 2001; 31: 465-470

[9] Fantauzzi M., Atzei D., Elsener B., Lattanzi P.F., Rossi A., *Surface and Interface Analysis* 2006; 38: 922-930

[10] Elsener B., Fantauzzi M., Atzei D. and Rossi A., *European Journal of Mineralogy* 2007; Vol.9, No. 3: 353-361

[11] Fantauzzi M., Atzei D., Elsener B., Lattanzi P., Rossi A., *Surface and Interface Analysis* 2007; 39: 908–915

[12] Yin Q., Kelsall G.H., Vaughan D.J., England K.E.R. *Geochimica et Cosmochima Acta* 1995; 59: 1091-1100

# Chapter 2

# Literature review

*In this chapter a literature survey is given underlining the role of sulphur in bearing sulphide minerals: Section 2.1 reports information about the mineral enargite and the chemical state of sulphur on its surface. Section 2.2 deals with the literature on the possibility of using the KLL Auger transition.*

## 2.1 Sulphur on enargite surface

Enargite is a copper arsenic sulphide with formula $Cu_3AsS_4$, frequently associated, as a minor component. to complex sulphide minerals mined for the production of metallic copper or for gold recovery. It is found in significant amounts in the so-called "high sulphidation" volcanic-hosted epithermal deposits [1]. Along with other arsenic-bearing sulphides, it is of environmental concern on account of the potential release of toxic arsenic species in acid mine drainage (AMD). A thorough study of the surface chemistry of enargite, i.e. the precise determination of the chemical state of the elements arsenic, copper and especially sulphur in different conditions of the enargite surface, is a fundamental tool in understanding oxidation, dissolution and precipitation phenomena and thus in AMD control.

### 2.1.1 Properties of enargite [2]

Enargite is a blackish gray mineral with a metallic luster, Mohs hardness = 3, and density = 4.5 g/cm$^3$. Enargite crystallizes in the orthorhombic system, pyramidal class, space group $Pnm2_1$. It occurs in granular masses, but well-formed crystals are not rare; its habit may be tabular (001), or prismatic, elongated along c. Enargite shows an excellent cleavage along (110); other cleavage planes are (100) and (010). The crystal type is that of wurtzite (ZnS), with Zn positions occupied by Cu and As; both elements are in fourfold coordination with S. The unit cell parameters are a=7.339 Å, b=6.428 Å, c=6.145 Å. Enargite is a semiconductor of the type $A_3^I B^V C_4^{II}$. The flat band potential is about -0.16V vs the standard hydrogen electrode, SHE. Copper is nominally in the monovalent state, and arsenic in the pentavalent state. In most natural occurrences, enargite is associated with pyrite, and other copper and/or arsenic and/or base metal sulphides (chalcopyrite, chalcocite, covellite, digenite, tennantite, sphalerite, galena). Enargite may contain minor amounts of other elements (Sb, Ag, Fe) [2].

## 2.1.2 Chemical state of the elements on enargite surface

The surface chemistry of sulphide minerals such as pyrite [3 and reference cited therein], arsenopyrite [4 and reference cited therein] and chalcopyrite [5] is well documented. A number of papers has been published regarding the surface chemistry of enargite [6 - 11]. In an early work the research group, the author of this work participates in, reported results on the XPS characterization of synthetic and natural enargites [12, 13]. Qualitative and quantitative surface analyses of natural enargites (from Peru and the Furtei mine, Sardinia) were performed and the results were compared to those found for synthetic enargite. Most natural and synthetic samples showed comparable binding energies for all elements, and quantitative surface compositions matching well the bulk composition (as determined by electron microprobe) [12 - 14].

*Table 2.1:* Binding Energies (eV) of the different photoelectron lines and kinetic energies (eV) of the Auger lines in natural and synthetic enargite samples (C1s = 285.0 eV). Data from [12, 14] (EN stands for Enargite).

| Element line | EN Synthetic Powder [12] | EN from Peru crystal as received [12] | EN from Peru crystal cleaved [14] | EN Furtei Mine crystal as received [14] | EN Furtei Mine crystal cleaved [14] | EN Genaro Mine crystal as received [14] | EN Genaro Mine crystal cleaved [14] |
|---|---|---|---|---|---|---|---|
| $As3d_{5/2}$ (I) | 44.0 ± 0.2 | 43.8 ± 0.2 | 43.9 ± 0.1 | 44.3 ± 0.1 | 43.8 ± 0.2 | 43.3 ± 0.1 | 43.5 ± 0.1 |
| $As3d_{5/2}$ (II) | | 45.5 ± 0.2 | | | | 45.3 ± 0.1 | |
| AsLMM | 1222.8 ± 0.2 | 1223.1 ± 0.2 | 1222.8 ± 0.1 | 1222.5 ± 0.1 | 1222.7 ± 0.2 | 1223.3 ± 0.2 | 1223.0 ± 0.1 |
| $Cu2p_{3/2}$ | 932.6 ± 0.2 | 932.5 ± 0.2 | 932.6 ± 0.1 | 932.4 ± 0.2 | 932.8 ± 0.2 | 932.4 ± 0.1 | 932.6 ± 0.1 |
| CuLMM | 916.8 ± 0.2 | 917.1 ± 0.2 | 916.8 ± 0.1 | 917.0 ± 0.2 | 916.7 ± 0.2 | 916.8 ± 0.2 | 917.0 ± 0.2 |
| $S2p_{3/2}$ (I) | 162.4 ± 0.2 | 162.0 ± 0.2 | 162.1 ± 0.1 | 162.8 ± 0.2 | 161.5 ± 0.2 | 162.0 ± 0.1 | 162.1 ± 0.1 |
| $S2p_{3/2}$ (II) | 164.2 ± 0.2 | 163.7 ± 0.1 | - | 164.3 ± 0.2 | 164.2 ± 0.2 | 163.5 ± 0.1 | 164.0 ± 0.2 |
| $S2p_{3/2}$ (III) | | 168.7 ± 0.1 | | | | 168.5 ± 0.1 | |
| SKLL | 2115.0 ± 0.2 | 2115.6 ± 0.2 | 2116.7 ± 0.2 | 2115.0 ± 0.2 | 2116.3 ± 0.2 | 2115.7 ± 0.2 | 2115.8 ± 0.1 |

A comparison of the binding energies of arsenic, copper and sulphur atoms on freshly cleaved and different “as-received” samples (table 2.1) stresses that arsenic and

copper exhibit remarkably constant binding energies whereas the sulphur atom at the surface of enargite is more susceptible to changes in the enargite surface state and composition. The same result was found in a study on enargite surface reactivity in acidic ferric solutions simulating the AMD environment [15], where the chemical state of copper and arsenic did not change during immersion in acidic, oxidizing solutions. Also in this case, the main changes were found for the sulphur atoms at the surface of enargite.

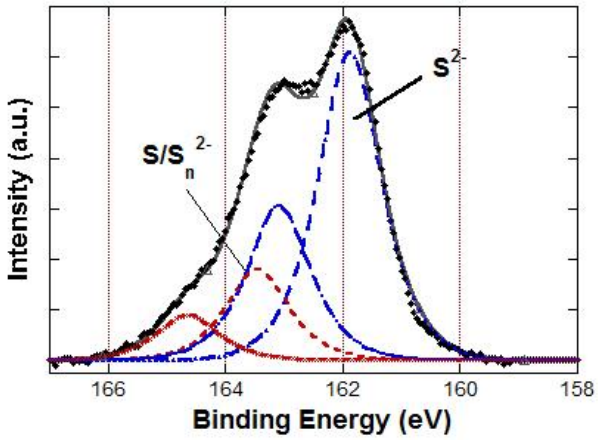


*Figure 2.1:* High-resolution spectrum of S2p region for a Enargite sample exposed to $FeCl_3$ 0.025M solution for 24 hours [14].

The most intense *sulphur* line, S2p, is asymmetric due to spin - orbit splitting in $2p_{3/2}$ and $2p_{1/2}$ components with a 2 : 1 ratio [16] and a binding energy difference of 1.2 eV [17]. The sulphur S2p spectrum of enargite (figure 2.1) is composed of two components, one with the $S2p_{3/2}$ signal at 162.0 ± 0.2 eV (blue curves in Figure 2.1) and the other at 163.5 ± 0.2 eV (red plot in Figure 2.1). The lower binding energy component can be attributed to the sulphur atoms in the bulk of enargite (see table 1). The attribution of the component at higher binding energy, the intensity of which by ARXPS measurements [14, 15] increases after immersion into acidic solutions [15] and which is located at the outermost surface, has been (and still is) controversial. Essentially, three different attributions were proposed: elemental sulphur, polysulphide or the formation of metal-deficient surface layer [14, 15]. Part of the ambiguity in the precise attribution of the chemical state of this sulphur compound may reside in the fact that an attribution only based on XPS binding energies of photoelectron core lines [6 – 13] is intrinsically difficult.

### 2.1.3 Auger parameter and chemical state plot

The use of the Auger parameter concept and especially the two- dimensional "chemical state plot" introduced by Wagner [19] was shown to provide for enargite [14, 15] and other geological materials [18] more reliable information on the chemical state of the elements. This requires the acquisition of high-resolution spectra of the corresponding X-ray induced Auger lines AsLMM, CuLMM and SKLL and the determination of the kinetic energy of the principal Auger signals (table 1, 2).

Indeed, when both the binding energy of the photoelectron and the kinetic energy of the Auger electron are measured, a new parameter known as the Auger parameter ($\alpha$) can be determined. Wagner originally defined the Auger parameter as the difference between the kinetic energy of the most intense Auger line and the most intense photoelectron line, making reference to the Fermi level rather than the vacuum level. The definition of the Auger parameter $\alpha'$ [20] used most frequently is

$$\alpha' = \alpha + h\nu = E_k \text{ (Auger)} + E_b \text{ (photoelectron)} \qquad (1)$$

The modified parameter $\alpha'$, as so defined, is then independent of $h\nu$ and always positive and it is simply the sum of the kinetic energy of the Auger signal and the binding energy of the photoelectron signal. This sum will be the same, independent of sample charging. Yu et al. [21], Peisert et al. [22] and Mugford [23] reported in the nineties the Auger parameters of solid sulphur-containing compounds. Mugdorf's work was performed using the AgL$\alpha$ radiation in the so-called high-energy XPS mode. In a previous work of the research group where the thesis has been carried out the Auger parameters for a series of reference compounds and for enargite were determined (table 2) [14].

*Table 2:* Binding energy and Auger kinetic energy of sulphur $S2p_{3/2}$ (±0.2 eV) and SKLL (±0.2 eV) signals of sulphur compounds with the Auger parameter for sulphur compounds [14].

| **Compound** | **$S2p_{3/2}$ BE (eV)** | **SKLL KE (eV)** | **α'(eV)** |
|---|---|---|---|
| CuS | 162.7 | 2115.6 | 2278.3 |
| $Cu_2S$ | 162.1 | 2115.9 | 2278.0 |
| FeS | 162.8 | 2116.1 | 2278.9 |
| Pyrite | 162.5 | 2116.2 | 2278.7 |
| ENSynthetic | 162.4 | 2115.0 | 2277.4 |
| ENPeru as rec | 162.0 | 2115.6 | 2277.6 |
| ENPeru cleaved | 162.1 | 2116.7 | 2278.8 |
| ENFurtei as rec | 162.8 | 2115.0 | 2277.8 |
| ENFurtei cleaved | 161.5 | 2116.3 | 2277.8 |
| $As_2S_3$ | 163.6 | 2113.4 | 2277.0 |
| $CuSO_4$ | 169.2 | 2106.6 | 2275.8 |

It is worth noticing that the kinetic energy of the SKLL Auger line was simply determined at its maximum intensity: no attempt to further process the Auger signal was made. The Auger parameter in the chemical state plot is found as a series of diagonal lines representing equal Auger parameters.

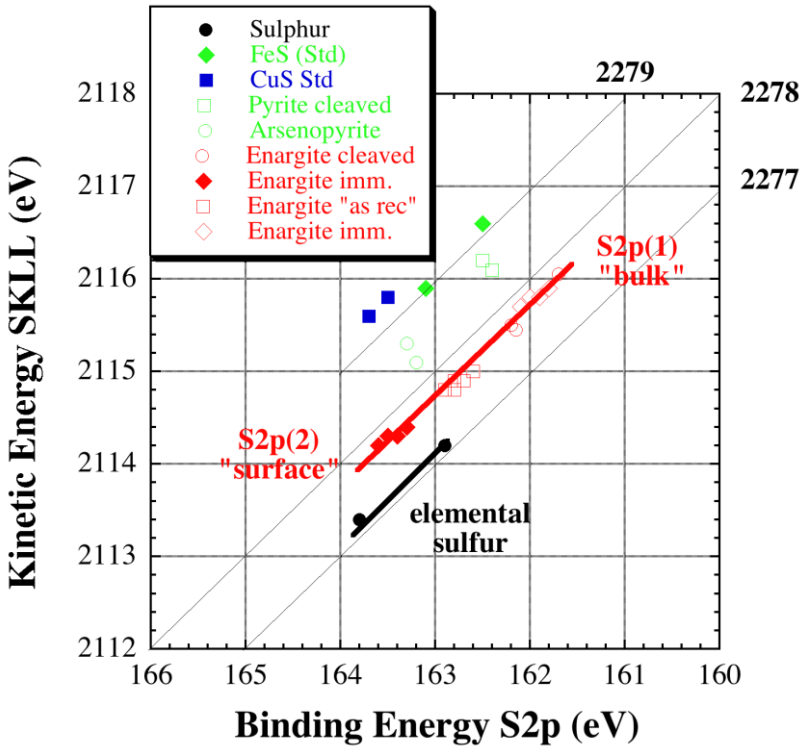


*Figure 2.2:* Chemical state plot of sulphur compounds [15].

The chemical state plot of sulphur compounds (figure 2.2) shows all the sulphides in the upper right corner, the sulphates in the lower left corner (not shown). All enargite samples fall on the same line with Auger parameter α' 2277.8 ± 0.2 eV, clearly separated from elemental sulphur (α' 2277.2 ± 0.2 eV) and the other sulphide minerals (pyrite, arsenopyrite) or reference compounds (FeS, CuS). The fact that both sulphur signals (figure 2.1), the low BE S 2p(1) associated to the bulk and the high BE S 2p(2) associated to sulphur at the surface, have the same Auger parameter has to be verified (as the maximum of the SKLL peak was only taken to determine the kinetic energy). The authors concluded that, based on the chemical state plot, the assignment of the high BE sulphur compound to elemental sulphur could be excluded. The distinction between a polysulphide layer ($S_n^{2-}$, $2 < n < 8$) or a copper-deficient sulphur layer is difficult and requires further investigations.

### 2.1.4 Layer thickness of the sulphur-enriched surface layer

Quantitative analysis with the three-layer model [24] showed that on "as received" crystals of natural enargite, that had been exposed for a long time to the atmosphere, an oxidised layer of 0.5 nm thickness enriched in arsenic had been formed [13]. Similarly, after 24 h exposure of the enargite samples to acidic oxidizing solutions a strongly sulphur enriched layer of up to 0.7 nm was found [15]. The calculated thickness – based simply on the integrated XPS intensity of the high BE sulphur S2p (2) compound (Fig. 2.1) - would correspond to slightly more than one monolayer. Including copper ions into the sulphur-rich enargite surface layer the thickness may range from 1 to 2 nm. In addition, the thickness of this altered layer was found to increase with increasing enargite dissolution [15, 25]. This layer and the underlying altered interface very likely influence the interaction of enargite with the natural environment and its behaviour in mineral processing plants and should be taken into account in the assessment of the potential impact of enargite-bearing ores on the environment [13 – 15, 25] also as a consequence of the effect of the presence of iron- and sulphur oxidizing microorganisms [26].

## 2.2 KLL Auger transition

As outlined above, the SKLL Auger transition signals did not allow distinguishing the two components as in the S2p photoelectron lines (fig. 2.1). The Auger parameter was calculated based on the position of the centre of gravity of the SKLL signal. In this study a new approach based on curve fitting of the X-ray excited Auger lines was tested. This requires a) SKLL signals with good signal / noise ratio acquired on well-defined standards creating the necessary database, and b) a thorough theoretical analysis of the Auger transition. Unfortunately, under the experimental conditions available for this thesis it was impossible to collect the S1s because its binding energy (2472 eV) is not accessible with the conventional XPS source.

The determination of the Auger transition rates and total Auger probability for the KLL transitions for various atoms (Z=1 to 80) was calculated in the past [27] and many authors applied those calculations to real samples for example in the study of KLL Auger spectra of sodium, magnesium [28] and fluorine [29]. Both sodium and

magnesium oxides as well as different fluorine salts show all five well resolved lines as predicted in the extreme L-S coupling theory. In the fluorine salts a cation-dependence of the Auger transition energies and line-widths is observed. Studies on KLL Auger transition of copper, nickel, sodium and magnesium has been performed recently [30, 31] in order to test atomic theory and update models available. The main result of these studies was the evidence of intensive satellite structure of intrinsic origin in copper and nickel [30] and correlations between lines of the spectra and shake-up/shake off processes [31].

First information about chemical shift in Auger spectra on sulphur compounds date back to the 1970 [32, 33]. Sodium thiosulphate is a historic compound for which the chemical shift in sulphur was first observed. The Auger lines of $Na_2S_2O_3$ studied by Fahlman et al. [32] show a double peaked shape with an energy separation of 4.3 eV between the peak corresponding to the oxidation number $6^+$ and that corresponding to the oxidation number $2^-$. Evidence was provided that the Auger transition energy depends on the chemical state of the sulphur atom and the higher oxidation number has the lower transition energy. No double structure was observed for the sodium Auger line, and this means that both sodium atoms of the molecule are in the same chemical state. The difference in Auger chemical shift was attributed to final state effects, i.e. to differences in relaxation energies [34]. Moretti [20] reviewed final state relaxation energies and their relation with the Auger parameter [20]. For solid sulphur compounds, relaxation energy was studied and discussed in terms of initial state charge and dielectric screening models [22].

## References


[1] Arribas A., *Mineral Assoc. Short Course* 1995; 23:419

[2] Lattanzi P., Da Pelo S., Musu E., Atzei D., Elsener B., Fantauzzi M., Rossi A., *Earth Science Review* 2008; 86: 62-88

[3] Chandra A.P., Gerson A.R., *Surf. Sci. Rep.* 2010; 65: 293- 315

[4] Corkhill C.I., Vaughan D.J., *Appl. Geochem.* 2009; 24: 2342-2361

[5] England K.E.R., Pattrick, R.A.D., Vaughan D.J., *Mineral. Mag.* 1999; 63: 559

[6] Fullston D., Fornasiero D., Ralston J., *Langmuir* 1999; 15: 4530-4536

[7] Da Pelo S., *PhD Thesis* 1998 (in Italian); University of Cagliari – Italy, English abstract in Plinius 1999; 21-70

[8] Velasquez P., Ramos-Barrado J.R., Leinen D., *Surf. Interface Anal*. 2002; 34: 280-283

[9] Pratt A., *Surf. Interface Anal*. 2004; 36: 654-657

[10] Viñals J., Roca A., Hernandez M.C., Benavente O., *Hydrometallurgy* 2003; 68: 183-193

[11] Asbjörnsson J., Kelsall G. H., Pattrick R. A. D., Vaughan D. J., Wincott P. L., Hope G. A, *Journal of The Electrochemical Society*, 2004; 151 (7): E250-E256

[12] Rossi, A.; Atzei, D.; Da Pelo, S.; Frau, F.; Lattanzi, P.; England, K.E.R.; Vaughan, D.J. *Surf. Interface Anal*. 2001; 31: 465-470

[13] Rossi A., Atzei D., Elsener B., Da Pelo S., Frau F., Lattanzi P., D.J. Wincott P. L., Vaughan D. J., in *Water-Rock Interaction* 2001; Vol. 1: 427 Cidu R. (ed.), A.A. Balkema Publishers, Rotterdam;

[14] Fantauzzi M., Atzei D., Elsener B., Lattanzi P., Rossi A., *Surf. Interface. Anal.* 2006; 38: 922-930

[15] Fantauzzi M., Elsener B., Atzei D., Lattanzi P., Rossi A., *Surf. Interface Anal.* 2007; 39: 908-915

[16] Briggs D., Grant J.T., *Surface Analysis by Auger and X-ray Photoelectron Spectroscopy* 2003; IM Publications

[17] Moulder J.F., Stickle W.F., Sobol P.E., K.D. Bomben. *Handbook of X-ray Photoelectron Spectroscopy: A Reference Book of Standard Spectra for Identification and Interpretation of XPS Data*. Physical Electronics Division: Eden Praire, MN, 1995; ISBN: 096 481 241X.

[18] Perry D.L., Taylor J.A., Wagner C.D., X-ray Induced Photoelectron and Auger Spectroscopy, in *Instrumental Surface Analysis of Geological Materials*,. Perry, D.L: (ed.) VCH Publishers Weinheim, 1990, 45

[19] Wagner C.D., Joshi. A., *Journal of Electron Spectroscopy and Related Phenomena* 1991; 47: 283 and references quoted therein.

[20] Moretti G., *Journal of Electron Spectroscopy and Related Phenomena* 1998; 95: 95-144

[21] Yu X.-R., Liu F., Wang Z.-Y., Chen Y., *Journal of Electron Spectroscopy and Related Phenomena* 1990; 50: 159-166

[22] Peisert H., Chassé T., Streubel P., Meisel A., Sgargan R., *Journal of Electron Spectroscopy and Related Phenomena* 1994; 68: 321-328

[23] Mugford S.C., *A study by X-ray photoelectron spectroscopy of sulphur chemistry in relation to corrosion*, April 1990; Faculty of Engineering, Surrey University, Guildford

[24] Rossi A, Elsener B, *Surf. Interface Anal*. 1992; 18: 499

[25] Elsener B, Atzei D, Fantauzzi M, Rossi A, *European Journal of Mineralogy* 2007; 19: 353-361

[26] Fantauzzi M., Rossi G., Elsener B., Loi G., Atzei D., Rossi A., *Anal. Bioanal. Chem.* 2009; 393: 1931-1941

[27] Callan E.J., *Phys. Rev.* 1961; 124 No.3: 793-799

[28] Fahlman, R. Nordberg, C. Nordling, K. Siegbahn, *Zeitschrift für Physik* 1966; 192: 476-483

[29] Albridge R.G., Hamrin K., Johansson G., Fahlman A., *Zeitshrift für Physik* 1968; 209: 419-427

[30] Kövér L., Cserny I., Tóth J., Varga D., Mukoyama T., *Journal of Electron Spectroscopy and Related Phenomena* 2001; 114-116: 55-61

[31] Kantia T., Partanen L., Aksela S., Aksela H., *Journal of Electron Spectroscopy and Related Phenomena* 2010; 180: 58-65

[32] Fahlman, K. Harmin, R. Nordberg, C. Nordling, K. Siegbahn, *Physics Letters* 1966*;* 20 No.2: 156

[33] Asplund L., Kelfve P., Siegbahn H., Goscinski O., Fellner-Feldegg H., Hamrin, K., Blomster B., Siegbahn K., *Chem. Phys. Lett.* 1976; 40 No.3: 353-356

[34] Nishikida S., Ikeda S., *B. Chem. Soc. Jpn.* 1978; 51 No.7: 1996-2001

# Chapter 3

## X-ray photoelectron spectroscopy and X-ray excited Auger electron spectroscopy

*In this chapter a brief description of X-ray photoelectron and X-ray excited Auger electron spectroscopic is provided.*

# X-RAY PHOTOELECTRON SPECTROSCOPY (XPS)

## 3.1 Physical principle [1, 2, 3]

Herz in 1887 discovered and described the emission of electrons from a material under UV irradiation. Einstein in 1905 gave the correct interpretation of the photoelectric effect and for this he was awarded the Nobel prize for Physics in 1921. Following his work, Rutherford and his group succeeded in the measurement of energies of the electrons emitted from metals bombarded by hard X-rays. After the end of the Second War World and the development of high-vacuum systems the measurement of the kinetic energy of the emitted electrons with zero energy loss became feasible. Siegbahn coined in 1967 the acronym ESCA (electron spectroscopy for chemical analysis) since he was able to measure accurately the energy of the electrons emitted from the core levels of the atoms irradiated with soft X-rays and he was the first to publish that changes in the kinetic energy of the electrons could be related to changes in the chemical bonds of the element [4].

In X-ray photoelectron spectroscopy soft X-ray sources are traditionally used: the beam can penetrate many micrometers into materials; the absorption by an atom in the solid may lead to the photoemission of the electrons from the core-levels as well as from the valence levels. The photon energy, hν, must be greater than the binding energy (BE) in order to obtain electron photoemission. A fraction of the electrons are emitted from the sample in vacuum, without suffering energy loss during their travel through the solid, and they are discriminated on the basis of their kinetic energy to produce a spectrum of the electron intensity, expressed as counts, counts/s, counts/s*eV, versus electron energy. The kinetic energy (KE) of the electron is the experimental quantity measured by the spectrometer, but this is dependent on the photon energy of the X-rays employed and is therefore not an intrinsic property of the materials being studied. On the other hand, the binding energy (BE) is a parameter that identifies the electron specifically, both in terms of its parent element and atomic energy level from which it was photoemitted. The fundamental relationship between the parameters involved in an XPS experiment is:

$$KE = h\nu - BE - \Phi$$

where Φ is the spectrometer work-function i.e. the potential difference for electrons between the Fermi level and the maximum potential just outside a specified surface (ISO 18115:2001). The electron binding energy in a conducting solid is in effect, relative to the Fermi level. Thus, it is essential that the energy scale be accurately linear and correctly calibrated (ISO 15472:2001). The electron binding energies differ from element to element and therefore an accurate measurement of the binding energy allows almost a straightforward elemental identification. All elements can be identified under the common laboratory conditions, with the exception of hydrogen and helium.

Once a photoelectron has been emitted, the ionized atom must relax. This can be achieved by emission of an X-ray photon (X-ray fluorescence) or ejection of an Auger secondary electron. Thus, Auger electrons are produced as a consequence of the XPS primary process, and this secondary phenomenon is often referred to as XAES (X-ray induced Auger electron spectroscopy or X-ray excited Auger electron spectroscopy). Auger peaks can provide valuable chemical information about an atom but they can also interfere with photoelectronic peaks. Signal superposition can be avoided by changing the X-ray source.

The sampling depth of the XPS technique varies with the KE of the electrons being used. It is determined by a quantity $\Lambda = \lambda * \cos\theta$ known as electron attenuation length (AL). It depends on the inelastic mean free path λ (IMFP), which depends firstly on the KE of the electron and the density of the solid being passed through by the electron, and on the emission angle θ, i.e. the angle at which particles leave a specimen measured with respect to the normal to the specimen surface. Typical sampling depth is ca. 3Λ. In the energy range of interest in electron spectroscopy, i.e. 200-2000 eV, Λ is equal to very few nanometers (< 10 nm). This is the reason why XPS is a surface-sensitive technique.

## 3.2. Notation [5]

The formalism used for XPS to describe which electrons are involved in each of the observed transitions differs from that used for Auger electron spectroscopy (AES): XPS uses the so-called spectroscopists' notation whereas Auger electrons are identified by the equivalent X-ray notation.

In the former, transitions are labeled according to the scheme $nl_j$ where n is the principal quantum number, l is the electron angular momentum quantum number and j [given by |l+s| (s is the spin angular momentum quantum number)] is the so-called total angular momentum quantum number. In the X-ray notation, the principal quantum numbers are identified with letters K, L, M etc. whereas subscript numbers refer to the j values, more information about notation was provided in § 3.3.2. The relationship between the two notations is given in Table 3.1.

*Table 3.1:* The spectroscopic terms are listed opposite their X-ray equivalents.

| Quantum numbers | | | X-ray suffix | X-ray level | Spectroscopic level |
|---|---|---|---|---|---|
| *n* | *l* | *j* | | | |
| 1 | 0 | 1/2 | 1 | K | $1s_{1/2}$ |
| 2 | 0 | 1/2 | 1 | $L_1$ | $2s_{1/2}$ |
| 2 | 1 | 1/2 | 2 | $L_2$ | $2p_{1/2}$ |
| 2 | 1 | 3/2 | 3 | $L_3$ | $2p_{3/2}$ |
| 3 | 0 | 1/2 | 1 | $M_1$ | $3s_{1/2}$ |
| 3 | 1 | 1/2 | 2 | $M_2$ | $3p_{1/2}$ |
| 3 | 1 | 3/2 | 3 | $M_3$ | $3p_{3/2}$ |
| 3 | 2 | 3/2 | 4 | $M_4$ | $3d_{3/2}$ |
| 3 | 2 | 5/2 | 5 | $M_5$ | $3d_{5/2}$ |
| | etc. | | etc. | etc. | etc. |

## 3.3 Spectra [5,6]

The first step in characterizing the surface chemistry of the specimen under investigation is recording a survey, or wide scan over a region that provides the peaks that the different elements can emit after irradiation with the source. Usually, the range 0-1200 eV (obtainable both with Al kα and Mg kα sources) is sufficient. Peak identification is achieved by means of electron energy reference tables. This procedure is applied for the identification of the elements present when the sample composition is unknown and for ascertaining the composition when it is known. In the latter case, the peak identification ensures the operator that the spectrum reflects the sample composition and possibly, it allows the identification of contaminants such as carbon or oxygen due to the reaction of the sample surface with the ambient atmosphere [7].

As stated above, the electrons excited and emitted without energy loss, contribute to the characteristic peaks in the spectrum whereas those that undergo inelastic photoemission contribute to the spectrum with weak signals when the losses are discrete and with the step-like increase in the background when emitted after random scattering. There is also a contribution to the background from the continuous photon radiation emitted from the anode due to the deceleration of incident electrons within the conventional Al or Mg sources; this radiation is called "Bremsstrahlung" radiation: its spectral distribution is continuous up to the energy of the incident electrons. In XPS, the bremsstrahlung may also photoionize inner shells that would be energetically impossible by characteristic Al or Mg Kα X-rays. As a result, Auger electron features may appear at negative binding energy values and, in addition, the intensities of other Auger electron features may be greater than if the inner shell vacancies would be created only by the characteristic X-rays. The Bremsstrahlung-excited Auger electron features can be helpful in determining the Auger parameters needed to identify chemical states and in this work it was used for recording the SKLL spectra. The Bremsstrahlung is removed when the source is monochromatic.

After the survey spectrum, the acquisition of spectra around the element peak of interest with a higher resolution follows. Curve fitting routine applied to these spectra allows the differentiation of overlapping peaks thus providing more detailed and

valuable chemical information of the specimen and making quantitative analysis possible even when an inhomogeneous elemental distribution occurs within the depth.

### 3.3.1 Chemical shift

The chemical shift is defined as the change in peak energy arising from a change in the chemical environment of the atom (ISO 18115:2001). In agreement with this definition, the electrostatic potential of the core electrons will be modified if an atom is bonded to another one, since its valence electron density will be altered with respect to its elemental state. As a consequence, a change of the BE of the signal (chemical shift) should be observable in the spectrum. The chemical shift can vary from a fraction up to several eV. Owing to line width of the X-ray source used in XPS (0.3 - 0.9 eV) data processing, shift of an element in several of its compounds enable to identify its chemical state [8].

### 3.3.2 Spin-orbit coupling [6]

Since an electron is a charged particle, its orbit around a nucleus induces a magnetic field whose intensity and direction depend on the electron velocity and on the radius of the orbit respectively. The two latter quantities can be characterized by an angular momentum, called the orbital angular momentum, which of course is quantized since the electron can travel only on certain discrete orbitals. The characteristic quantum number is l, and l can take the values 0, 1, 2, 3, 4, …. Another property of an orbiting electron is the electronic spin, which can be positive or negative and also induces an inherent magnetic field; the latter in turn has an associated spin momentum, characterized by a spin quantum number s, which can take either of the values ±1/2. Thus the total electronic angular momentum is a combination of the orbital angular and spin momenta, and this combination is in fact simply the vector sum of the two momenta. However, it is most important in the present context to notice that the vector summation can be carried out in two ways, summarized in the names of j-j coupling and of L-S (also called Russell-Saunders) coupling, respectively.

### 3.3.2.1 j-j coupling

In j-j coupling the total angular momentum of a single isolated electron is obtained by vector summation of the individual electron spin and angular momenta. According to § 3.2 j can take the values 1/2, 3/2, 5/2 etc. To arrive at the total angular momentum for the whole atom, summation is then performed for all electrons, the result being the total atomic angular momentum with an associated quantum number J, where $J = \Sigma j$. This description of the summation is known as j-j coupling. This kind of coupling is the best description of electronic interaction in elements of high atomic number, i.e. Z> ~75, the annotation based on it has been used for both Auger and spectroscopic features for all parts of the Periodic Table. This does not matter for the features arising from photoelectron production, since the final state of the atom is singly ionized, but in the Auger process, where the final state is doubly ionized, interactions between the two holes in the final state can lead to situations where j-j description is inadequate.

The X-ray notation is almost always used for Auger transitions, so that, for example, in j-j coupling there would be six predicted KLL transition, i.e. $KL_1L_1$, $KL_1L_2$, $KL_1L_3$, $KL_2L_2$, $KL_2L_3$, $KL_3L_3$. The spectroscopy annotation is directly equivalent to that for the X-ray, and is more obviously related to the various quantum numbers. In it, the principal quantum number appear first, then states with l = 0, 1, 2, 3, … are designated s, p, d, f, …, respectively, and follow the first number, and finally the j values are appended as suffixes. Thus the state written $L_3$ in the X-ray notation, in which n =1 2, l = 1 and j = 3/2, would be written $2p_{3/2}$ in the spectroscopy notation. It is conventional to identify by means of the spectroscopic notation the atomic level from which it was ejected.

*Table 3.2:* Notation in L-S coupling.

| Transition | Configuration | *L* | *S* | Term |
|---|---|---|---|---|
| $KL_1L_1$ | $2s^02p^6$ | 0 | 0 | $^1S$ |
| $KL_1L_{2,3}$ | $2s^12p^5$ | 1 | 0 | $^1P$ |
| | | 1 | 1 | $^3P$ |
| $KL_{2,3}L_{2,3}$ | $2s^22p^4$ | 0 | 0 | $^1S$ |
| | | [1 | 1 | $^3P$][a] |
| | | 2 | 0 | $^1D$ |

[a]Forbidden

*Table 3.3:* Notation in intermediate coupling.

| Transition | Configuration | *L-S* term | *L* | *S* | *J* | IC term |
|---|---|---|---|---|---|---|
| $KL_1L_1$ | $2s^02p^6$ | $^1S$ | 0 | 0 | 0 | $^1S_0$ |
| $KL_1L_{2,3}$ | $2s^12p^5$ | $^1P$ | 1 | 0 | 1 | $^1P_1$ |
| | | | 1 | 1 | 0 | $^3P_0$ |
| | | $^3P$ | 1 | 1 | 1 | $^3P_1$ |
| | | | 1 | 1 | 2 | $^3P_2$ |
| $KL_{2,3}L_{2,3}$ | $2s^22p^4$ | $^1S$ | 0 | 0 | 0 | $^1S_0$ |
| | | | 1 | 1 | 0 | $^3P_0$ |
| | | $^3P$ | [1 | 1 | 1 | $^3P_1$][a] |
| | | | 1 | 1 | 2 | $^3P_2$ |
| | | $^1D$ | 2 | 0 | 2 | $^1D_2$ |

[a]Forbidden

### 3.3.2.2 L-S coupling

The other way of carrying out the vector summation is first to sum all the individual electronic angular momenta and then all the individual electronic spin momenta. These two total momenta are then characterized by two quantum numbers, i.e. the total atomic orbital angular momentum quantum number L, which is equal to Σl, and the total atomic spin quantum number S, which is equal to Σs. Coupling of the two total momenta to give the total atomic angular momentum can then be characterized as before by quantum number J, which is now, however, equal to | L ± S |. Since L

and S can take the values 0, 1, 2, 3, …, J can take any integral value between | L + S | and |L – S | and for this reason the origin of the name "L-S coupling" is obvious. L-S coupling has been found to apply to elements of low atomic number, i.e. Z<~20. In this coupling scheme the annotation is that of term symbols of the form $^{(2S+1)}L$ describing the electron distribution in the final state. By analogy with the spectroscopic notation of Table 3.1, states with L = 0, 1, 2, 3, …are designated by capitals S, P, D, F,…, whereas the total spin quantum number S enters as the prefix (2S + 1). (Here the state S corresponding to L = 0 should not be confused with S, the total spin quantum number.) As for j-j coupling, L-S coupling predicts six possible components in the KLL series, listed in Table 3.2, but one of these is forbidden owing to the principle of conservation of parity. Also shown in table 3.2 is a frequently used way of describing the final state configuration following an Auger transition ABC, by writing down the electron populations in the levels B and C, e.g. $2s^1 2p^5$ for $KL_1L_{2,3}$.

The L-S classification and notation has been used mostly by those recording Auger spectra at high –energy resolution in order to provide data for comparison with theoretical calculations (ref. in § 2.2), and is not normally encountered in everyday use. The same is true of the mixed, or intermediate, coupling scheme which must be used in the region of the Periodic Table where neither L-S nor j-j coupling is adequate to describing the final state configuration. In intermediate coupling, each L-S term is split into multiplets of different J values, so that the term symbols are now in the form $^{(2S+1)}L_j$. As can be seen from Table 3.3, ten possible final states are predicted in the KLL series, but one is forbidden for the same reason as before. There have been several examples of experimental evidence for the existence of nine lines in a KLL spectrum.

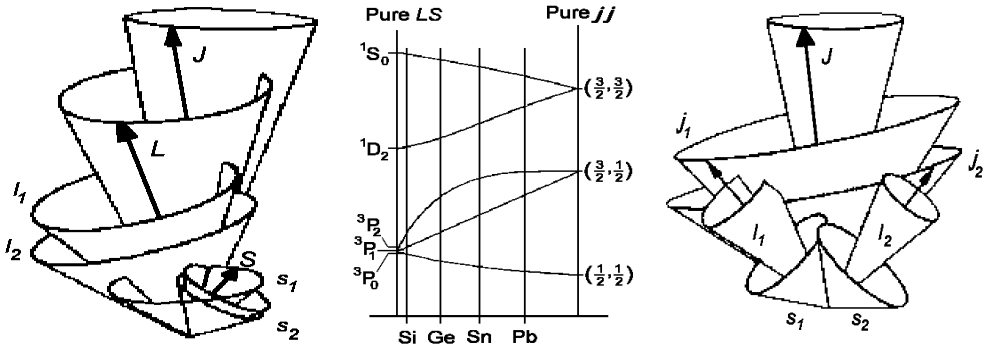


*Figure 3.1:* From the left, L-S coupling, L-S / j-j correlation for elements of the 4th main group and j-j coupling [9].

### 3.3.3 Multiplet splitting

Multiplet splitting of a photoelectron peak may occur in a compound that has unpaired electrons in the valence band, and arises from different spin distributions of the electrons of the band structure. This results in a doublet of the core level peak being considered. Multiplet splitting effects are observed for several transition metals.

### 3.3.4 Satellite peaks

The initial-state energy changes are mainly due to the chemical bond formed by the atom. Final state effects that occur after photoelectron emission, such as core hole screening, relaxation of electron orbitals and polarization of surrounding ions cause other peaks to appear in XPS spectra known as satellites.

Shake-up satellites may occur when the outgoing photoelectron simultaneously interacts with a valence electron and excites it (shakes it up) to a higher energy level; the energy of the core electron is then slightly reduced giving a satellite structure a few eV *below* (but *above* on a binding energy scale) the core level position. Another feature is the shake-off satellite where the valence electron is completely ejected from the ion.

### 3.3.5 Energy scale correction for charging

Photoemission from an insulating sample causes electrostatic charging to occur in the positive direction. This causes a shift in the peak position in the direction of higher BE. The energy scale correction by referring all the peaks to that of the aliphatic C1s at 285.0 eV is the one used in this thesis and is generally accepted. Other methods are discussed in [10].

### 3.3.6 Calibration

An accurate spectrometer calibration is required to extract chemical shift information by comparing the measured BE with bibliography or databases, to use spectral addition or subtraction to enhance experimental data interpretation and to provide a qualified analysis.

The linearity of the BE scale is checked by comparing the $Au4f_{7/2}$, the $Ag3d_{5/2}$, the $Cu2p_{3/2}$ and the CuLMM positions with their expected values. A guideline to the calibration procedure and to the reference peaks can be found in ISO 15472:2001 [11].

## 3.4 Data processing

Data processing is required to obtain the maximum amount of information from a spectrum. There are several commercially available programs to perform curve fitting routines quickly and easily. CASA XPS (Casasoftware Ltd., UK) was used in this work.

Data processing, is a multi-steps process. The following action has to be taken:

- spectra inspection
- spike removal
- satellite subtraction
- background subtraction
- peak fitting

### 3.4.1 Satellite subtraction

Subtraction of the satellites due to use of a non-monochromatic X-ray source must be carried out carefully out as spectral distortion may result from an incorrect removal. Some authors [12; 13] suggest keeping all satellites to preserve all the data.

### 3.4.2 Background subtraction

As for satellite subtraction, a background removal can be done and, if incorrectly performed, will cause problems with any quantification model. Three kinds of background subtraction are applied in XPS data analysis: the linear, the integral, based on Shirley method, and Tougaard, based on elastic and inelastic energy loss processes. The linear background often does not satisfactorily approximate the experimental curve. The Shirley background adopted in this work tries to remove as much asymmetry as possible from the peak, under the assumption that the background is only due to inelastic scattering of the high kinetic energy electrons. The details of the calculation of Shirley background with Sherwood's iteration can be found in [12]. Some authors suggest the evaluation of the background during the fitting routine to avoid spectral distortion [12, 13, 14].

### 3.4.3 Peak fitting

In many cases the information provided by photoelectron spectroscopy is contained in a spectrum that consists of a number of overlapping peaks. This happens when the FWHM height of a photoelectron line is wider than the same parameter for a standard acquired under the same experimental conditions. Some criteria can be useful to establish the number of components peaks:

- Visual inspection of the peak shape to check for asymmetry and the presence of shoulders or humps;
- Calculation of the FWHM height ratio between a test spectrum and a reference spectrum. If the ratio is <1.05, one peak is assigned. If it is close to 1.15 and not

valleis appear or the test spectrum is 20% wider than that of the reference spectrum, two peaks are assigned;

- Visual inspection of the first and second derivative spectra;
- Minimization of the sum of the squared residuals.

Whenever possible, it is convenient to employ a monochromatic X-ray source but this may lead to substantial loss of intensity. The two ways for spectrum interpretation are deconvolution and curve fitting of the spectrum. The first one aims at the removal of instrumental broadening from the experimental data and should not be confused with curve fitting also known as peak synthesis or peak fitting, that is based on the use of Gaussian / Lorentzian functions. The second approach was adopted in this work and will be briefly described hereafter.

A spectrum can be synthesized by summing a series of functions representing individual peaks in order to produce a final function that closely represents the experimental spectrum. The peak function is generally designed to be a function of appropriate peak variables such as position, intensity, width, and function type and peak tail characteristics. Such a curve synthesis provides a useful initial guess for the refining process of non-linear least squares curve fitting.

A number of types of function have been used for this purpose. A core level photoemission peak inherently has Lorentzian shape whose width is the inverse of the core lifetime. The phonons, the vibrational response of the host lattice, produce broadening of essentially Gaussian character. The Voigt function is the convolution of these contributions and is sometimes approximated by the sum or the product of a mixed Gaussian/Lorentzian function. The second one has been adopted in this work. Tail parameters may be included in the Gaussian/Lorentzian function to take into account the asymmetric line shape. Curve fitting of this type assumes that a particular peak profile is uniquely characterized once its full width at half maximum (FWHM) has been fixed, and cannot be resolved into subcomponents. This is done by acquiring a series of standard materials in the same experimental conditions of the samples under investigation.

Several non-linear least squares algorithms for the optimization of the curve synthesis process have been proposed. The one used in this work is based on Marquardt's

method [15]. More details can be found in [12] and in the CASA XPS pdf user's manual, version 1.0, March 2000.

## 3.5. Auger Parameter [16, 17]

In 1971 Charles Wagner introduced the Auger parameter concept that increases the usefulness of XPS for identifying chemicals states. He noticed [16, 17] that the difference in two kinetic energies (Auger and photoelectron), which is accurately measurable in the presence of static charging, can be very useful in the characterization of insulator and semiconductor materials.

The original Auger parameter was defined as the difference in kinetic energies of prominent and conveniently situated Auger and photoelectron peaks from the same elements, recorded in the same spectrum, i.e.

$$\alpha' = KE(C'C''C''') - KE(C) \qquad (1)$$

Where KE (C'C''C''') is the kinetic energy of the Auger transition involving electrons from C', C'' and C''' core levels C.

Eq. (1) could produce negative values for α but, being KE (photoelectron) = hν – BE (photoelectron), it is possible to define α', the modified Auger Parameter:

$$\alpha' = KE(C'C''C''') + BE(C) \qquad (2)$$

The so-defined modified parameter $\alpha'$ is then independent of hν and always positive and it is simply the sum of the kinetic energy of the Auger signal and the binding energy of the photoelectron signal.

The Auger parameter concept was based on the following ideas:

- there is a fixed difference between two line energies (Auger and photoelectron) of the same element in the same sample;
- Charge corrections to the individual peak measurements are unnecessary because they simply cancel during the estimation of the Auger parameter;

- Work function corrections are also unnecessary, and vacuum level data can directly be compared to Fermi level data.

The concept of the Auger parameter (eq. 2) is of considerable analytical value, because it is independent of charging effects and changes with the chemical environment of the element under consideration.

The Auger parameter is still a one-dimensional quantity like the photoelectron binding energy or the Auger kinetic energy alone. Actually, a more useful general approach than the Auger parameter alone is the display of photoelectron and Auger data in the form of a scatter plot. The positions of the sharpest Auger line and the most intense photoelectron line, recorded on a two dimensional plot of compounds of each element, form the basis for an alternative approach to chemical state identification. In this plot, called *Wagner plot* or *chemical state plot*, the Auger kinetic energy is on the ordinate and the photoelectron binding energy is on the abscissa and oriented in the negative direction. Eq. (2) shows that the Auger parameters are the intercepts of the linear relationship KE (Auger) vs. BE (photoemission) to be read directly on the straight lines with slope -1.

In the chemical state plot the position of the different chemicals states depends on both initials and final state effects. The initial state effects include the contribution to the chemical shift of both the valence charge and the Madelung potential (which takes into account the charges of all the other atoms in a compound) at the core-ionized atom. The final state effects include information about the extra-atomic polarization energy, which is directly measured by the Auger parameter $\alpha' = KE + BE$.

In the final state of the photoemission process an atom is left with a core-hole and this positive charge will polarize the surrounding atoms and the valence electrons. There will be a relaxation energy that will lower the binding energy values. The relaxation energy can be divided into two parts: an atomic contribution, that depends on the atomic number and the core orbital involved in the process, and an extra-atomic contribution which is the relaxation energy associated with the rest of the system (with the flow of electron density from the surrounding toward the core-ionized atom) [17].

In the simplest approximation, assuming that the intra-atomic relaxation energy is independent of the chemical environment, the shifts in the core ionization energy, ΔBE, and in the kinetic energy of an Auger transition, ΔKE, are given by the following equations [18]:

$$\mathbf{\Delta BE = \Delta V - \Delta R^{ea}} \quad \mathbf{(3)}$$

$$\mathbf{\Delta KE = -\Delta V + 3\ \Delta R^{ea}} \quad \mathbf{(4)}$$

ΔV reflects differences in the initial orbital energy of the electron in the initial (un-ionized) state; and $\Delta R^{ea}$ reflects differences in the final-state extra-atomic relaxation energy. The shift in the Auger parameter Δα' provides, according to eq. (5), a direct measurement of the shifts in the extra-atomic relaxation energy [18]:

$$\Delta\alpha' = \Delta BE + \Delta KE = 2\ \Delta R^{ea} \quad (5)$$

Three different situations can be found in the Wagner chemical state plot:

1) *Identical Auger parameter*

   The individual data point of different compounds or samples are found on a diagonal line with equation KE = α' - BE with a slope ΔKE / ΔBE = -1 in the Wagner plot (the lines show a positive slope in the graph owing to the negatively oriented x-axis). Such compounds show the same Auger parameter $\alpha'$ and identical chemical state.

2) *Initial and final state effects have similar values*

   The BE values for an element in different compounds or samples are similar: $\Delta BE = \Delta V - \Delta R^{ea} = 0$, so $\Delta V = \Delta R^{ea}$ (initial and final state effects have similar values). Differences in $\alpha'$ are due to differences in the bond nature: the more positive the Auger parameter shift, the more covalent the bond; the more negative the Auger parameter shift, the more ionic the bond.

3) *Similar initial state effects*

   The data point for an element in different compounds or samples fall on a line with slope ΔKE / ΔBE = -3. This indicates similar initials state effects (ΔV in eqs. 3 and 4, the difference in the Madelung potential $V_M$ and the term related to the ground state valence charge q of the core-ionized atom).

## 3.6 Quantitative analysis

In order to quantify spectra from XPS, one must convert peak intensities (usually peak areas) to atomic concentrations. The easiest case concerns homogeneous samples. The situation is more complicated for samples with surface films that are either thinner than the information depth of the technique or discontinuous.

As will be shown in the sequel, experimental peak intensities depend upon several parameters, which are dependent on the photoemitting element, the matrix, the physics of the X-ray photoemission phenomenon, the mechanics and dynamics of the electron travelling through the sample, the spectrometer geometry, experimental design, etc. Thus, the experimental peak intensities can be considered "raw" data that have to be corrected in order to obtain comparable quantities. The peak intensity correction factors are usually referred to as *sensitivity factors*. There are three main approaches for evaluating the sensitivity factors. (i) They can be found in the literature or experimentally determined in-house. (ii) Alternatively, sensitivity factors can be calculated taking into account all the physical parameters involved in XPS peak "generation". (iii) The last approach is known as the first principle method [10]. This method has been used here and will be described in some detail. The most generic expression used in XPS quantitative analysis is:

$$A\ at.\% = \frac{I_A/S_A}{\sum_i I_i/S_i} \cdot 100$$

where A is the element or the chemical species, $I_i$ is the experimental intensity of the chosen XPS peak generated from the species I, $S_i$ is the sensitivity factor for that particular XPS peak generated from the species i.

In the first principle method, the intensity $I_i$ of a particular peak of the generic species I, is given by the following expression:

$$I_i = \sigma_i(h\nu)D(E_i)\int_0^{\pi} d\gamma \int_0^{2\pi} d\Phi L_i(\gamma) \int_{-\infty}^{+\infty} dx \int_{-\infty}^{+\infty} dy J_0(xy) sec\delta T(xyz\Phi E_i) \int_0^{\infty} dz\, N_i(xyz) e^{-z/\lambda_M(E_i)cos\theta}$$

whose solution for the atomic density $N_i$ could be used in the above expression for the atomic concentration. It may be rewritten as:

$$A\ at.\% = \frac{N_A}{\Sigma_i N_i} \cdot 100$$

σ is the photoionization cross-section which is defined as the "effective area" of the collision between an incident X-ray photon and an atom of the species i in the sample. σ depends upon the photon energy hν, the element of I and the quantic numbers n, l, s and j describing the initial state of the photoemitted electron [19].

D is the detector efficiency function that describes the efficiency of the spectrometer detector versus the electronic kinetic energy $E_i$, i.e. the ratio of the electron actually counted and the total number of electrons arrived at the detector.

L is the angular asymmetry function that takes into account the non-isotropic nature of the electronic photoemission phenomenon. It depends upon the X-ray source and the quantic numbers n, l, s and j describing the initial state of the photoemitted electron [20].

$J_0$ is the X-ray photon flux versus the x and y coordinates. T is the so-called *transmission function* of the spectrometer. It can be defined as the number of electrons actually counted and the number of electrons entering the detection system of the spectrometer.

λ is the inelastic mean free path of the emitted electrons, which depends upon the electron KE and the density of the material M (i.e. the sample).

The above rigorous expression for peak intensity $I_i$ is indeed very complex, but can be simplified with certain assumptions. First of all, under the hypothesis that the sample is homogeneous down to a depth greater than the sampling depth of the XPS technique:

$$\int_0^\infty dz\, N_i(xyz) e^{-z/\lambda_M(E_i)cos\theta} = N_i \lambda_M(E_i) cos\theta = N_i \Lambda_{Mi}$$

Thus, the above expression for intensity of a photoelectron line $I_i$ can be rewritten as:

$$I_i = \sigma_i(h\nu)D(E_i)\int_0^{\pi} d\gamma \int_0^{2\pi} d\Phi L_i(\gamma) \int_{-\infty}^{+\infty} dx \int_{-\infty}^{+\infty} dy J_0(xy) sec\delta T(xyz\Phi E_i) N_i \Lambda_{Mi}$$

where $\Lambda = \lambda * \cos\theta$ is the *attenuation length*, i.e. is the maximum path-length that can be travelled by the photoelectron (with a certain KE) in the material M without loosing energy in inelastic scattering events.

## References


[1] Scorciapino M.A., *PhD Thesis* 2007; University of Cagliari – Italy

[2] Fantauzzi M., *PhD Thesis* 2005; University of Cagliari – Italy

[3] Addari D., *PhD Thesis* 2005; University of Cagliari – Italy

[4] Siegbahn K, Nordling C., A. Fahlman, R. Nordberg, K. Hamrin, J. Hedman, G. Johansson, T. Berkmark, S.E. Karlson, I. Lindgren, B. Lindberg, *ESCA: Atomic Molecular and Solid state structure studied by means of electron spectroscopy* 1967; Almquist and Wiksells Uppsala

[5] Watts J.F., Wolstenholme J., *An introduction to Surface Analysis by XPS and AES* 2003; ed. J. Wiley & Sons Ltd.

[6] Briggs D., Grant J.T., *Surface Analysis by Auger and X-Ray Photoelectron Spectroscopy* 2003; ed. by D. Briggs

[7] Castle J.E., *Journal of Vacuum Science and Technology A 2007;* 25: 1-27

[8] Moulder J.F., Stickle W.F., Sobol P.E., Bomben K.D., *Handbook of X-ray Photoelectron Spectroscopy* 1992: ed J. Chastain – Perkin-Elmer Corporation

[9] http://www.pci.tu-bs.de/aggericke/PC3e_osv/Kap_V/Russel.htm (last access 20 February 2011)

[10] Seah M.P., Briggs D. in *Pratical Surface Analysis* 1990; 2nd ed., Vol.1: J. Wiley & Sons, Chichester, eds. by D. Briggs and M.P. Seah

[11] Seah M.P., *Surface and Interface Analysis* 2001; 31: 721

[12] Sherwood P.M.A. in *Pratical Surface Analysis* 1983, 1st ed. Vol.1: J. Wiley & Sons, Chichester, eds. D. Briggs, M.P. Seah

[13] Salvi A.M., Castle J.E., Watts J.F., Desimoni E., *Applied Surfaces Science* 1995; 90: 333-341

[14] Wertheim G.K., Dicenzo S.B., *Journal of Electron Spectroscopy and Related Phenomena* 1985; 37:57-67

[15] Bevington P.R., Robinson D.K., *Data reduction and error analysis for the physical sciences* 1992: 161-163, 2nd ed., McGraw Hill, Boston

[16] Wagner C.D., Joshi A., *Journal of Electron Spectroscopy and Related Phenomena* 1988; 47**:** 283 (and references quoted therein)

[17] Moretti G., *Journal of Electron Spectroscopy and Related Phenomena,* 1998; 95: 95-144

[18] Wagner C.D., *Faraday Discuss. Chem. Soc.*1975; 60: 291

[19] Scofield J.H., *Journal of Electron Spectroscopy and Related Phenomena* 1976; 8: 129

[20] Reilman R.F, Msezane A., Manson S.T., *Journal of Electron Spectroscopy and Related Phenomena* 1976; 8: 389

# Chapter 4
# Experimental

*In this chapter the materials and methods used in the present work are presented. First, the reference compounds and the minerals employed are listed. Then, the protocol for the preparation of the mixtures of sulphides and polysulphides is described along with the procedures adopted for performing the X-ray photoelectron and the X-ray excited Auger electron spectroscopic experiments.*

# 4.1. Materials

## 4.1.1 Reference materials

In the following paragraphs the reference compounds, the investigated model systems consisting of mixtures of sulphur and polysulphide and the mineral samples are described.

### 4.1.1.1 Sulphur, sulphides and sulphates

A series of alkaline sulphides and sulphates and of sulphides and sulphates of transition metal elements were analysed by XPS and XAES. Their suppliers are listed in table 4.1 along with their appearance and purity and the chemical abstract number (CAS).

*Table 4.1:* Sulphides and sulphates used in this work; purity, supplier, appearance and CAS are reported.

| Molecular formula | Purity | Supplier | Appearance | Color | CAS |
|---|---|---|---|---|---|
| $S_8$ | - | - | Solid | | 7704-34-9 |
| **Sulphides** | | | | | |
| $Li_2S$ anhydrous | 99% | Alfa Aesar | Hygroscopic powder | White | 12136-58-2 |
| $Na_2S$ anhydrous | 100% | Alfa Aesar | Hygroscopic solid | Colorless to yellow | 1313-82-2 |
| $Na_2S_4$ | 90-95%, $H_2O$ 5% max. | Alfa Aesar | Hygroscopic powder | Light brown/yellow/orange | 12034-39-8 |
| $K_2S_n$ | $K_2S$ 42% min. | Riedel de Haën | Lumps | Light brown to yellow with green dots | 37199-66-9 |
| FeS | 99.9% | Aldrich | Powder | Black | 1317-37-9 |
| $Cu_2S$ | 99.99% | Aldrich | Powder | Black | 22205-45-4 |
| CuS | 99.99+% | Aldrich | Powder | Black | 1317-40-4 |
| **Sulphates** | | | | | |
| $Li_2SO_4*H_2O$ | 99% | Merck | Powder | White | 10102-25-7 |
| $Na_2SO_4$ | 99% min. | Riedel de Haën | Powder | White | 7757-82-6 |
| $K_2SO_4$ | 99% | Merck | Powder | White | 7778-80-5 |
| $Rb_2SO_4$ | 99.8% | Aldrich | Powder | White | 7488-54-2 |
| $Cs_2SO_4$ | 99.99% | Aldrich | Powder | White | 10294-54-9 |

The air- or moisture sensitive compounds arrived stored in sealed bottles under nitrogen. All containers were opened in a glove box (UNILAB, manufactured by

MBraun.), filled with argon and located near to the XP-spectrometer. Residual oxygen and water in the glove box were monitored and resulted to be always 1 mg/kg and less than 1 mg/kg respectively. The solids were crushed using an agate pestle and mortar and then compressed into a disk, such as those used for preparation of KBr disks for infrared spectroscopy, to form a pellet. The pellet was then attached to a double-sided adhesive tape mounted on a standard sample holder (Figure 4.1). The sample was then sealed, in the interior of the glove box, into an air tight bell device and transferred, out of contact with the air, to the fast-entry air lock of the spectrometer (Figure 4.1) [1].

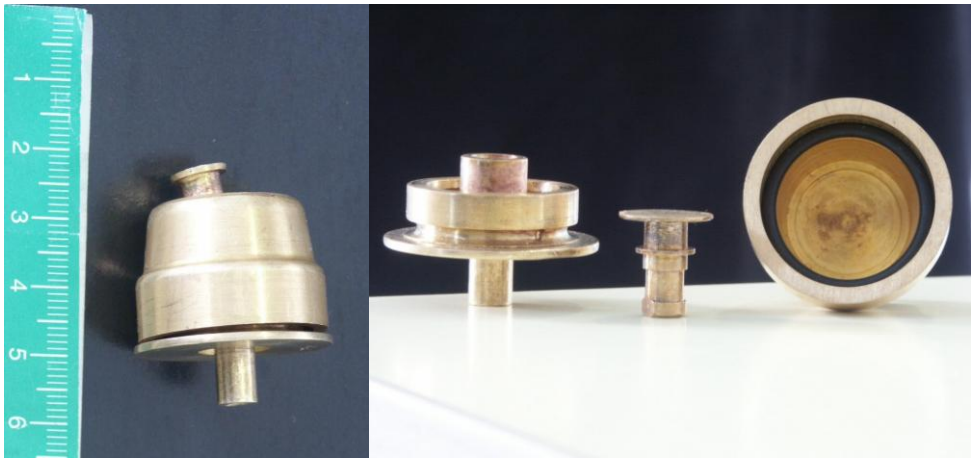

*Figure 4.1:* Bell-device for transferring the sample from the glove box to the fast entry air lock of the XP-spectrometer [1].

### 4.1.1.2 Model systems: Sulphur and polysulphides mixtures

In order to simulate the situation that may occur at the mineral surface, a series of mixtures, as model systems, were prepared using sodium tetrasulphide ($Na_2S_4$) and sulphur ($S_8$). The sodium tetrasulphide container was opened inside of the glove box and was crushed in an agate mortar for five minutes. A piece of solid elemental sulphur was ground for five minutes inside of the glove box. With two powdered samples two mixtures were prepared, one 50:50 and one 20:80 by weight, respectively corresponding to 42 – 58 atomic % and to 16:84 atomic %. The mixtures were weighted inside the glove box using a balance with a sensitivity of ± 0.01 g. Each mixture was further crushed for five minutes before preparing the pellet to be transferred to the spectrometer.

### 4.1.3 Mineral samples

The minerals investigated are listed in Table 4.2. All minerals were measured in the following conditions: (i) freshly cleaved, (ii) after air exposure for one week and (iii) after comminution in an agate mortar. Furthermore, pyrite samples were measured after different comminution conditions: in air, under argon in the glove box and in air and using acetone to limit iron oxidation.

*Table 4.2:* Minerals.

| Name | Chemical formula | Origin |
|---|---|---|
| Arsenopyrite | FeAsS | China |
| Chalcopyrite | $CuFeS_2$ | Unknown |
| Enargite | $Cu_3AsS_4$ | Leonard Mine, Butte, Montana, USA |
| Pyrite | $FeS_2$ | Unknown |

The minerals were characterized by means of X-ray diffraction. Enargite, arsenopyrite and pyrite samples were found to consist of a single phase, whereas various phases were present in chalcopyrite.

## 4.2. Methods

### 4.2.1. X-ray photoelectron spectroscopy

Three different spectrometers were used: the Theta Probe (Thermo Fisher Scientific), the ESCALAB MKII upgraded with 5 channelectrons and a hemispherical analyser (Vacuum Generator Ltd) now Thermo Fisher Scientific and the SIGMA 2 with the Alpha 100 analyser (Thermo Fisher Scientific). The first spectrometer is equipped with an AlKα monochromatic source, the other two are equipped with MgKα and AlKα non-monochromatic sources. The first series of measurements was carried out on a set of sulphides and sulphates (see Results, § 5.1.1 – 5.1.6) in order to determine the curve-fitting parameters using the high-resolution mode. The second series of measurements were performed using the ESCALAB MKII; only few selected samples, i.e. $K_2SO_4$, $Cu_2S$, CuS and FeS, were analysed with the SIGMA 2 to

investigate the charging effect on insulating samples in the high-energy region of the XP-spectrum where the SKLL signal can be detected.

In the sequel the main characteristics of the three spectrometers are reported and the experimental set-up is provided for each of them.

### 4.2.2 Theta Probe

The Theta Probe (Thermo Fischer Scientific, Waltham MA, USA) shown in figure 4.2 is equipped with a radian lens unit and a two dimensional detector that collects the photoemitted electrons over a 60° angular range, in parallel, without tilting the sample. The electrons are excited using an AlKα monochromatic micro-focused source with a spot size of 300 µm and a power of 70 W. The pass energy was set at 100 eV and the analyser was operated in the fixed analyzer transmission mode. The energy resolution in these conditions is found to be equal to 0.83 eV. This spectrometer is computer-controlled and the spectra are acquired by *Avantage* a Windows$^{TM}$ – based data system. In this work the instrument was used in the conventional mode, also called *standard lens mode*, since there were no requirements for angle-resolved information.

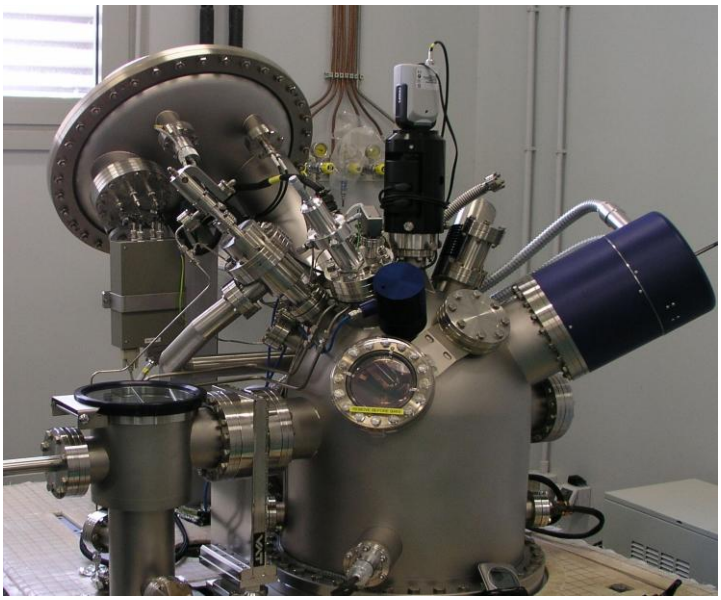

*Figure 4.2 :* THETA PROBE, Thermo Fisher Scientific Inc., East Grinstead, UK at Università di Cagliari.

A scheme of the spectrometer geometry is represented in figure 4.3 [2].

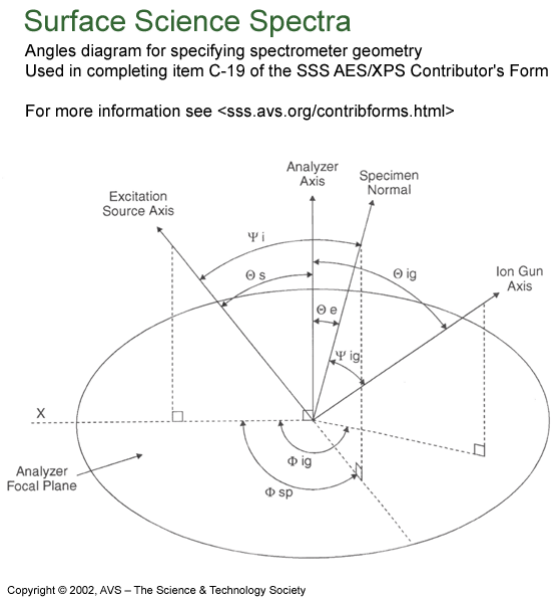


*Figure 4.3:* Angles diagram for specifying Theta Probe geometry from Surface Science Spectra [2].

Table 4.3 lists the most significant information for the Theta Probe configuration.

*Table 4.3:* Theta Probe configuration

| | |
|---|---|
| *Emission Angle ($\Theta_e$)* | 53° |
| *Incident Angle ($\Psi_i$)* | 30° |
| *Source-to-Analyser Angle ($\Theta_s$)* | 67.38° |
| *Specimen Azimuthal Angle ($\Phi_s$)* | 30.6° |
| *Sputter Source Incident Angle ($\Psi_{ig}$)* | 45° |
| *Sputter Source Polar Angle ($\Theta_{ig}$)* | 58.43° |
| *Sputter Source Azimuthal Angle ($\Phi_{ig}$)* | 24.2° |

The pump system consists of two turbo-molecular pumps, one operating in the fast entry air lock chamber, the other in the analysis chamber. In the analysis chamber a titanium sublimation pump is also fitted and these two pumps allow the achievement of a base residual pressure always lower than $5 \cdot 10^{-8}$ Pa. During the experiments the residual pressure resulted being equal to $5*10^{-7}$ Pa.

Further equipment is an ion gun (angle ion gun-to-sample normal: 45°), a combined low-energy electron/ion flood gun for charge compensation and a cooling stage.

The calibration of the spectrometer was performed according to the instructions of the manufacturer and the linearity of the binding energy scale was periodically checked according to ISO 15472:2001 [3].

The list of the regions collected is given in table 4.4.

*Table 4.4:* List of regions and relative energy ranges used for experiments, as well of step sizes and times per step.

| **Name** | **Energy Range (eV)** | **Step size (eV)** | **Time per step (ms)** |
|---|---|---|---|
| Survey | 0-1400 | 1 | 50 |
| Valence Band | -5-40 | 0.05 | 50 |
| S2p | 150-175 | 0.05 | 100 |
| S2s | 215-245 | 0.05 | 50 |
| SLMM | 1310-1360 | 0.05 | 50 |
| C1s | 275-300 | 0.05 | 50 |
| O1s | 520-545 | 0.05 | 50 |
| Cations | | | |
| As3d | 30-55 | 0.05 | 50 |
| AsLMM | 250-275 | 0.05 | 50 |
| Cu2p | 920-970 | 0.05 | 50 |
| CuLMM | 560-575 | 0.05 | 50 |
| Fe2p | 700-730 | 0.05 | 50 |
| FeLMM | 760-810 | 0.05 | 50 |
| K2p | 285-300 | 0.05 | 50 |

## 4.2.3 ESCALAB MKII

The ESCALAB MKII installed at Università di Cagliari in 1985 [figure 4.4] was manufactured by Vacuum Generator and was upgraded in the nineties. This instrument is a multi-technique surface analysis system that is mainly used as X-ray photoelectron spectrometer but is also provided with an electron source for Auger electron spectroscopy and two ion sources Ag21 for argon ion etching in situ and an AG61 for ISS.

It consists of a spherical sector analyser and a set of five channel electron multipliers.

The analyser is equipped with electrostatic lens and mechanical apertures: in this thesis the large area mode was selected. The lens was operated in the standard mode [potential was 0.2 V at 100 eV kinetic energy and 2.08V at 1000 eV kinetic energy]. The main part of the instrument is the Mu-metal analysis chamber where the residual pressure is usually maintained around $10^{-7}$ Pa by a turbo-molecular pump and a titanium sublimation pump. The sample is introduced through a fast entry chamber where a rotary pump keeps the residual pressure at $10^{-3}$ mbar. The pressure in the analysis chamber during measurements was always maintained below $5*10^{-5}$ Pa. The cooling of the stage at the liquid nitrogen temperature started before introducing the sample in order to cool down the stage. It was continuously cooled during the measurements to avoid sulphur sublimation that might occur under vacuum at room temperature [4].

A standard X-ray source with aluminium and magnesium anodes is mounted. The magnesium and aluminium coatings are deposited on a silver substrate, which covers the copper, to eliminate the excitation of the sample by the CuLα when the anode is old. The energy of the X-rays emitted from the source depends upon the anode material of which they are formed. If Mg kα is required, the cathode nearest the magnesium face is used otherwise the cathode nearest to the aluminium face is selected. The anode is designed to minimize the cross contamination of the X-ray radiation that was found to be always lower than 0.25%. A 1 μm aluminium windows shields the sample from stray electrons from the sources. Spectra were collected with the Al $k\alpha_{1,2}$ (1486.6 eV) operated at 20 mA and 15 kV (300 W) and with the Mg $k\alpha_{1,2}$ (1253.6 eV) operated at 20 mA and 15 kV (300 W) when the photoelectron signals were superimposed to the Auger-excited ones. The analyzer was operated in constant analyzer energy (CAE) mode, at 20 eV pass energy (PE) for high-resolution spectra, and at 50 eV PE for the acquisition of the survey spectra. The full width at half maximum (FWHM) of the $Ag3d_{5/2}$ line, at 20 eV was measured to be 1.1 eV. The intensity /energy response function was evaluated to be equal to $1/\sqrt{KE}$. In table 4.5 the energy range of the spectral regions acquired with the ESCALAB is shown. The emission angle was always 0°.

*Figure 4.4 :* VG ESCALAB 200, Thermo Fisher Scientific Inc., East Grinstead, UK at Università di Cagliari.

*Table 4.5:* List of regions and relative energy ranges used for experiments, step sizes and times per step are listed too.

| **Name** | **Energy Range (eV)** | **Step size (eV)** | **Time per step (ms)** |
|---|---|---|---|
| Survey (Al) | 0-1400 | 1 | 100 |
| Survey (Mg) | 0-1200 | 1 | 100 |
| Valence Band | -10-40 | 0.1 | 100 |
| S2p | 155-175 | 0.05 | 100 |
| SKLL | -645-595 | 0.05 | 100 |
| S2s | 218-238 | 0.05 | 100 |
| SLMM | 1310-1370 | 0.05 | 100 |
| C1s | 275-295 | 0.05 | 100 |
| O1s | 525-545 | 0.05 | 100 |
| Cations | | | |
| As3d | 30-55 | 0.05 | 100 |
| AsLMM | 250-275 | 0.05 | 100 |
| Cs3d | 715-745 | 0.05 | 100 |
| Cu2p | 920-970 | 0.05 | 100 |
| CuLMM | 560-575 | 0.05 | 100 |
| Fe2p | 700-740 | 0.05 | 100 |
| Fe3s | 82-102 | 0.05 | 100 |
| Fe3p | 43-63 | 0.05 | 100 |
| FeLMM | 760-810 | 0.05 | 100 |
| K2p | 292-316 | 0.05 | 100 |
| Li1s | 50-70 | 0.05 | 100 |
| Na1s | 1068-1092 | 0.05 | 100 |
| Rb3d | 105-125 | 0.05 | 100 |

Table 4.6 lists the most significant information for the ESCALB MKII configuration angles are defined as in figure 4.3.

*Table 4.6:* Angles referred to figure 4.3 for specifying ESCALB MKII geometry configuration for sources and analyser [5]

| | |
|---|---|
| *Emission Angle ($\Theta_e$)* | 0° |
| *Incident Angle ($\Psi_i$)* | 49° |
| *Source-to-Analyzer Angle ($\Theta_s$)* | 49° |
| *Specimen Azimuthal Angle ($\Phi_s$)* | 40° |
| *Sputter Source Incident Angle ($\Psi_{ig}$)* | 48° |
| *Sputter Source Polar Angle ($\Theta_{ig}$)* | 53° |
| *Sputter Source Azimuthal Angle ($\Phi_{ig}$)* | 85° |

A periodic calibration was performed to assess the linear response of XPS spectrometer over the whole energy scale [5]. Au, Ag and Cu foils were ion-etched for three minutes prior to the analysis. The energy beam was 6 keV. The $Au4f_{7/2}$, $Cu2p_{3/2}$, $Ag3d_{5/2}$ and Cu LVV spectral lines were used to perform the calibration. The accuracy attained was ± 0.05 eV.

Charging, whenever observed, was corrected by referring all photoelectron signals to that of the aliphatic carbon from residual oil to 285 eV.

### 4.2.3.1 X-ray excited Auger electron spectroscopy

Al Kα source allows the measure of the SKLL line that is found at ca. 2115 eV using the bremsstrahlung. To ensure an appropriate alignment at higher binding energies near SKLL peak, the position of the $AuM_4N_7N_7$ Auger peak at 2101.2 eV was also checked [6, 7] In this work it was found at 2101.1 eV.

### 4.2.4 SIGMA 2

The SIGMA 2 instrument is installed in the Laboratory for Surface Science and Technology at the ETH [Eidgenössische Technische Hochschule - Politecnico Federale Svizzero] in Zürich. In this case too, the analysis chamber is of mu-metal (an alloy with high magnetic permeability made of 80% Ni, 14.48% Fe, 5%Mo, 0.5% Si and 0.02% Cu) and the ultra-high vacuum ($5*10^{-8}$ Pa) is achieved by means of the turbo-molecular pump and the titanium sublimation pump that are mounted on it. Samples are loaded on a sample carrier arm of the fast entry air lock and the high-vacuum is achieved in about 15 minutes thanks to a turbo-molecular pump and a rotary pump that are mounted on a different line from the one which is operating on the analysis chamber. A twin source with aluminium and magnesium anodes is fitted. The in focus positioning of the sample surface is achieved by means of a microscope. The analyser worked in fixed analyser transmission mode being the pass energy equal to 20 eV and to 50 eV for collecting the high-resolution spectra and the survey spectra respectively. In this case also the instrument operated in the large area mode (LAXPS); the applied potentials to the lens were: lens 1 = 5.194 V; lens 2 = 2.092 V; lens 3= 2.798 V.

An ion source, EX05, with its digital power supply allows the argon ion etching of the metal samples for the calibration and the collection of composition in-depth profile.


*Figure 4.5:* SIGMA 2 Thermo Fisher Scientific Inc. at LSST ETH Zurich.

*Table 4.7:* Angles of the main components of the SIGMA 2. Symbols are those of figure 4.3.

| | |
|---|---|
| *Emission Angle ($\Theta_e$)* | 0° |
| *Incident Angle ($\Psi_i$)* | 50° |
| *Source-to-Analyzer Angle ($\Theta_s$)* | 50° |
| *Specimen Azimuthal Angle ($\Phi_s$)* | 180° |
| *Sputter Source Incident Angle ($\Psi_{ig}$)* | 45° |
| *Sputter Source Polar Angle ($\Theta_{ig}$)* | 45° |
| *Sputter Source Azimuthal Angle ($\Phi_{ig}$)* | 100° |

Also in this case the calibration of the spectrometer was performed according to ISO 15472 and the $AuM_4N_7N_7$ Auger peak at 2101.3 eV was collected.

*Table 4.8:* Acquired regions and relative energy ranges used for the experiments. Step sizes and times per step are listed too.

| Name | Energy Range (eV) | Step size (eV) | Time per step (ms) |
|---|---|---|---|
| Survey (Al) | 0-1400 | 1 | 50 |
| Valence Band | -5 - 40 | 0.1 | 50 |
| S2p | 150-175 | 0.05 | 50 |
| SKLL | -500-630 | 0.1 | 50 |
| S2s | 221-244 | 0.05 | 50 |
| SLMM | 1200-1280 | 0.1 | 50 |
| S2p – S2s | 160-250 | 0.1 | 50 |
| C1s | 275-300 | 0.1 | 50 |
| O1s | 520-545 | 0.05 | 50 |
| Cations | | | |
| Cu2p | 925-970 | 0.1 | 100 |
| Cu3p | 65-85 | 0.1 | 100 |
| Fe2p | 694-750 | 0.05 | 50 |
| FeLMM | 760-820 | 0.1 | 50 |
| K 2p | 285-317 | 0.05 | 50 |
| KLMM | 1190-1300 | 0.1 | 50 |

When charging was observed it was corrected by referring all photoelectron signals to that of the aliphatic carbon from residual oil to 285 eV.

### 4.2.5 Data processing and quantitative analysis

The high-resolution spectra were processed with CASA XPS software (v. 2.3.15 Casa Software Ltd., Wilmslow, Cheshire, UK). An iterated Shirley-Sherwood background subtraction was applied prior to curve fitting with a product of Gaussian-Lorentzian curves. The Gaussian-Lorentzian ratio for each peak was determined from measurements on reference compounds. To calculate the atomic percentage of the elements, the first principle method was applied. The final formula is:

$$A\ atomic\ \% = \frac{I_A/S_A}{\sum_i I_i/S_i} * 100 \quad (1)$$

where A is the element or the chemical species, $I_i$ is the experimental intensity (counts/s∗eV) of the chosen XPS peak generated from species $i$, $S_i$ is the sensitivity factor for that particular XPS peak generated from the species $i$:

$$S_i = \sigma_i \cdot L_i(\gamma) \cdot Q_i(KE) \cdot \Lambda_i$$

- $\sigma_i$ is the photoemission cross-section, available on the tables of the Scofield's work [8].
- $L_i(\gamma) = 1 + \frac{1}{2}\beta_i\left(\frac{3}{2}sen^2\gamma - 1\right)$ is the asymmetry function, because for the ESCALAB 200 the value of γ is 49.1° $L_i(\gamma) = 1 + \frac{1}{2}\beta_i(-0.143)$. $\beta_i$, asymmetry parameter, can be found in the tables of Reilman's work [9];
- $Q_i(KE) = \frac{1}{\sqrt{KE}}$ is the analyzer transmission function for the ESCALAB 200;
- $\Lambda_i = \lambda cos\theta$ is the attenuation length. θ, angle formed by the normal at the surface of the sample and the axis of the lenses which collect emitted photoelectrons, for the ESCALAB 200 is 0° if the sample is rotated of 15° compared to ground (data collection at 0°) and therefore $\Lambda_i = \lambda$. $\lambda = \frac{A}{KE^2} + B\sqrt{KE}$ is the inelastic mean free path IMFP. The most widely used predictive formulas are the Seah and Dench [10], the TPP-2M [11] and the G-1 [12]. In this work has been used Seah and Dench formula.

  Signal intensity correction for taking into account the electron attenuation due to the contamination layer was applied using the algorithm proposed by Smith [13].

Signal intensity correction for taking into account the electron attenuation due to the contamination layer was applied using the algorithm proposed by Smith [13].

The effect of hydrocarbon overlayer is the preferential attenuation of the signal by those elements with higher binding energy (lower kinetic energy) peaks resulting in a wrong evaluation of the quantitative composition of the sample surface. The presence of the hydrocarbon overlayer results in an apparent carbon concentration that depends on the layer thickness. Overlayer thickness can be evaluated my means of equation 2:

$$d = -\lambda_{C1s,C}\cos\theta \ln\left(1 - \frac{x}{100}\right) \quad (2)$$

where x is the carbon atomic percentage (determined assuming that sample composition is homogeneous) by means of equation 1, θ is the photoelectron emission

angle relative to the surface normal and $\lambda_{C1s,C}$ is the effective electron attenuation length for C1s photoelectrons in the hydrocarbon overlayer that can be estimated by equation 3:

$$\lambda_{contam}=0.016E^{0.7608} \quad (3)$$

as suggested by Smith as the best fit for inelastic mean free path in organic contamination.

The knowledge of contamination layer thickness allows the correction of the preferential attenuation of signals by elements with higher binding energies by means of equation

$$At_i\%_{corr} = At_i\%_{meas} \exp\left(\frac{d}{\lambda_i \cos\theta}\right) \quad (4)$$

where $At_i$%meas is the atom percentage of the element i determined applying equation (1) to all elements constituting the sample surface without taking into account the carbon, d is the hydrocarbon contamination thickness determined by equation (2), and $\lambda$i is the effective electron attenuation length for photoelectrons from the element i and line of interest in the hydrocarbon overlayer determined by using eq. 3.

In table 4.9, 4.10 and 4.11 the parameters used for calculating the sensitivity factors, using the three different spectrometers are shown.

*Table 4.9:* Parameters for the calculation of the sensitivity factors when using the Theta Probe at Università di Cagliari.

| Element | Ref. BE | $\sigma_\iota$ | $L_\iota(\gamma)$ | $Q_\iota$ (KE) | $\lambda_\iota \cos\theta$ | $s_\iota$ |
|---|---|---|---|---|---|---|
| As 3d $_{doublet}$ | 43.5 | 1.821 | 1.146 | 3.420 | 2.195 | 26.030 |
| C 1s | 285 | 1.000 | 1.278 | 3.444 | 2.003 | 14.652 |
| Cu $2p_{3/2}$ | 932.9 | 16.37 | 1.196 | 3.508 | 2.261 | 155.275 |
| Fe $2p_{3/2}$ | 707.6 | 10.82 | 1.202 | 3.488 | 1.613 | 121.547 |
| K 2p $_{doublet}$ | 292.8 | 3.97 | 1.171 | 3.446 | 1.996 | 53.135 |
| O 1s | 530.6 | 2.93 | 1.278 | 3.470 | 1.787 | 38.578 |
| S 2p $_{doublet}$ | 162.7 | 1.677 | 1.156 | 3.432 | 2.102 | 23.237 |

*Table 4.10:* Parameters for the calculation of the sensitivity factors when using the ESCALAB MKII at Università di Cagliari.

| Element | Ref. BE | $\sigma_t$ | $L_t(\gamma)$ | $Q_t$ (KE) | $\lambda_t \cos\theta$ | $s_t$ |
|---|---|---|---|---|---|---|
| As 3d $_{doublet}$ | 44.4 | 1.821 | 0.925 | 0.026 | 3.646 | 0.162 |
| C 1s | 285 | 1.000 | 0.857 | 0.029 | 3.329 | 0.082 |
| Cu $2p_{3/2}$ | 932.4 | 16.73 | 0.899 | 0.043 | 2.262 | 1.445 |
| Fe $2p_{3/2}$ | 707.8 | 10.82 | 0.896 | 0.036 | 2.680 | 0.931 |
| K2p $_{doublet}$ | 292.7 | 3.97 | 0.912 | 0.029 | 3.318 | 0.348 |
| Li 1s | 54.9 | 0.0568 | 0.857 | 0.026 | 3.633 | 0.005 |
| Na1s | 1071.3 | 8.52 | 0.857 | 0.049 | 1.960 | 0.702 |
| O 1s | 531.5 | 2.93 | 0.857 | 0.032 | 2.968 | 0.241 |
| S 2p $_{doublet}$ | 161.5 | 1.677 | 0.920 | 0.028 | 3.495 | 0.148 |
| Pb 4f $_{doublet}$ | 137.7 | 22.74 | 0.927 | 0.027 | 3.526 | 2.024 |

*Table 4.11:* Parameters for the calculation of the sensitivity factors when using the SIGMA 2 at Zürich.

| Element | BE (eV) | $\sigma_t$ | $L_t(\gamma)$ | $Q_t$ (KE) | $\lambda_t \cos\theta$ (nm) | $s_t$ |
|---|---|---|---|---|---|---|
| C 1s | 285 | 1.000 | 0.881 | 4.688 | 3.328 | 13.746 |
| Cu $2p_{3/2}$ | 932.5 | 16.73 | 0.916 | 4.947 | 2.262 | 171.480 |
| Fe $2p_{3/2}$ | 709.2 | 10.82 | 0.914 | 4.833 | 2.678 | 127.958 |
| K 2p $_{doublet}$ | 292.9 | 3.97 | 0.923 | 4.690 | 3.317 | 56.998 |
| O 1s | 530.5 | 2.93 | 0.881 | 4.764 | 2.969 | 36.511 |
| S 2p $_{doublet}$ | 169.0 | 1.677 | 0.933 | 4.658 | 3.485 | 25.410 |

In the case of a resolved doublet, i.e. Cu2p and Fe2p, the sensitivity factors were calculated considering the Cu2p3/2 and the Fe2p3/2 peaks, whereas for a not resolved doublet, i.e. As3d, K2p, S2p and Pb4f the whole area under the photoelectron signal was taken. In this last case, $\sigma_i$ is equal to the sum of the $\sigma$'s of two components of the doublet.

## References


[1] Atzei D., Elsener B., Fantauzzi M., Rossi A., *Analisi XPS di superfici di minerali: un nuovo sistema chiuso per il trasferimento del campione in ultra alto vuoto.* XVIII Congresso Nazionale di Chimica analitica – Parma 19-23/09/04

[2] Surface Science Spectra in Instructions for Contributors – American Vacuum Society

[3] ISO 15472 Surface Chemical Analysis – X-ray Photoelectron Spectrometers – Calibration of Energy Scales, (2001)

[4] Buckley A.N., Woods R., Wouterlood H.J., *Aust. J. Chem* 1988; 41: 1003-11

[5] Seah M.P., Briggs D. in *Pratical Surface Analysis* 1990; 2nd ed., Vol.1: J. Wiley & Sons, Chichester, eds. by D. Briggs and M.P. Seah

[6] Fantauzzi M., Atzei D., DaPelo S., Elsener B., Frau F., Lattanzi P.F., and Rossi A., *Surface Science Spectra* 2002; vol.9; 266

[7] Wagner C.D., Taylor J.A., *J. Electron Spectrosc. Relat. Phenom.* 1980; 20: 83-93

[8] Scofield J.H., *J. Electron Spectrosc. Relat. Phenom*. 1976; 8: 129-137

[9] Reilman R.F., Msezane A., Manson S.T., *J. Electron Spectrosc. Relat. Phenom*.; 8, 1976: 389-384

[10] Seah M.P.and Dench W.A., *Surf. Interf. Anal.*; 1979; 1: 2-11

[11] Tanuma S., Powell C.J., Penn D.R., *Surf. Interf. Anal.* 1993; 21: 165

[12] Gries W.H., *Surf. Interf. Anal*. 1979; 24 :, 38-50

[13] Smith G.C, *J. Electron Spectrosc. Relat. Phenom.* 2005; 148: 21-28

# Chapter 5

# Results and Discussion

*In this chapter the X-ray photoelectron spectroscopy (XPS) and X-ray excited Auger electron spectroscopy (XAES) analyses on alkaline and transition metal sulphide and sulphates, polysulphides and sulphide minerals are presented. In particular the spectra of the S2p and S KLL lines of the sulphides and sulphates were used for getting the peak fitting parameters and apply them to the model systems obtained by mixing sulphur with sodium tetrasulphide. Minerals were analysed freshly cleaved, ground and after air exposure. The chemical state of sulphur in sulphates, sulphides (alkali- and transition metal compounds, minerals) and polysulphide is discussed. For the first time the X-ray excited Auger SKLL lines were fitted with parameters based on standards. In this way, which can be considered as an extension of previous work, a separation of the different components and a more precise determination of their kinetic energy were achieved. The Auger parameter and the chemical state plot were obtained by combining the S2p photoelectron lines and the SKLL Auger lines. On this basis a clear distinction of the chemical state of sulphur in sulphates, in alkali sulphides and in transition metal sulphides was possible. The chemical state of sulphur in the bulk of minerals such as enargite or pyrite was determined. The chemical state of sulphur that formed on the surface of compounds after exposure to air or after grinding was found to vary according the coordinating metal and its concentration.*

## 5.1 Reference compounds

Reference compounds used for this work were group IA sulphates ($Li_2SO_4*H_2O$, $Na_2SO_4$, $K_2SO_4$, $Rb_2SO_4$ and $Cs_2SO_4$), elemental sulphur ($S_8$), various sulphides ($Li_2S$, $Na_2S$, $Na_2S_4$, $K_2S_n$, $Cu_2S$, CuS and FeS) and model systems prepared by mixing $Na_2S_4$ and $S_8$. The spectra of these compounds were recorded in order to obtain curve-fitting parameters, necessary for modelling the XPS and XAES spectra of mineral samples. The samples were prepared in a glove box, they were mounted as pellets on bi-adhesive tape and they were inserted into the spectrometer analysis chamber by means of a bell device [1]. For each sample survey spectra and high-resolution spectra were acquired.

### 5.1.1 Group IA sulphates

In this section the survey spectra, the high resolution photoelectron and X-ray induced Auger electron spectra of sulphur, as well as the photoelectron lines of the cations for the following sulphates: $Li_2SO_4*H_2O$, $Na_2SO_4$, $K_2SO_4$, $Rb_2SO_4$ and $Cs_2SO_4$ are presented. In a recently published paper on the alkali metals sulphates (group IA) the photoelectron lines were only shown [2].

The survey spectra acquired with Al Kα source (Figure 5.1) confirm the absence of elements different from those expected. In the case of $Na_2SO_4$ also the Mg Kα source had to be used in order to avoid the problem of signal overlapping of the O1s with the NaKLL signals. This approach allows the achievement of more accurate quantitative results. Figure 5.2 shows the high-resolution spectra of photoelectron S2p peaks and Auger SKLL signals for the group IA of sulphates.

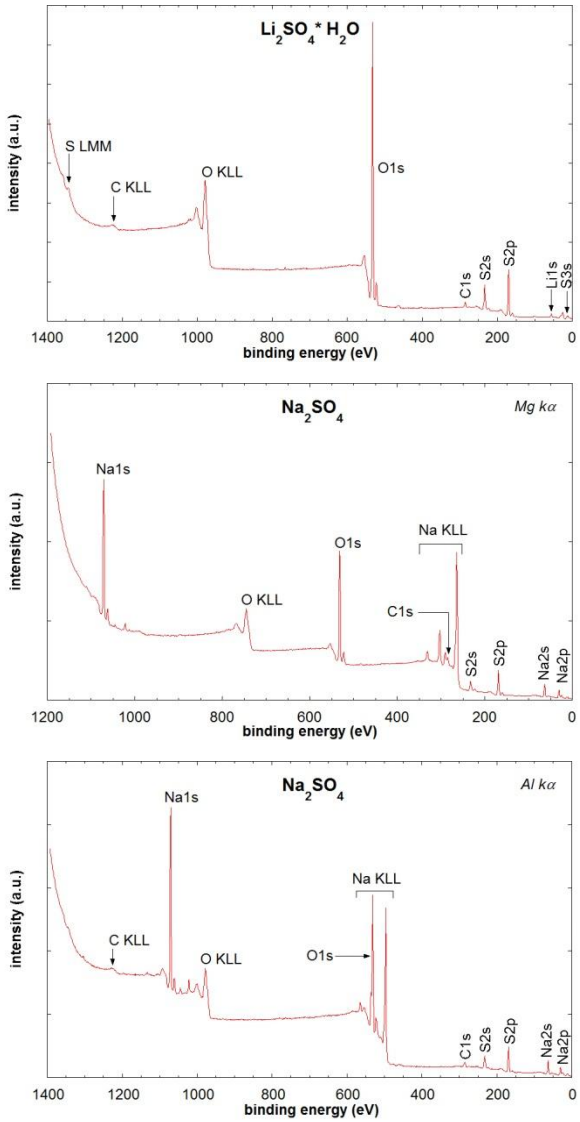
Li2SO4 * H2O
intensity (a.u.)
S LMM
C KLL
O KLL
O1s
C1s
S2s
S2p
Li1s
S3s
1400
1200
1000
800
600
400
200
0
binding energy (eV)
Na2SO4
Mg kα
Na1s
O1s
Na KLL
O KLL
C1s
S2s
S2p
Na2s
Na2p
1200
1000
800
600
400
200
0
binding energy (eV)
Na2SO4
Al kα
Na1s
Na KLL
C KLL
O KLL
O1s
C1s
S2s
S2p
Na2s
Na2p
1400
1200
1000
800
600
400
200
0
binding energy (eV)

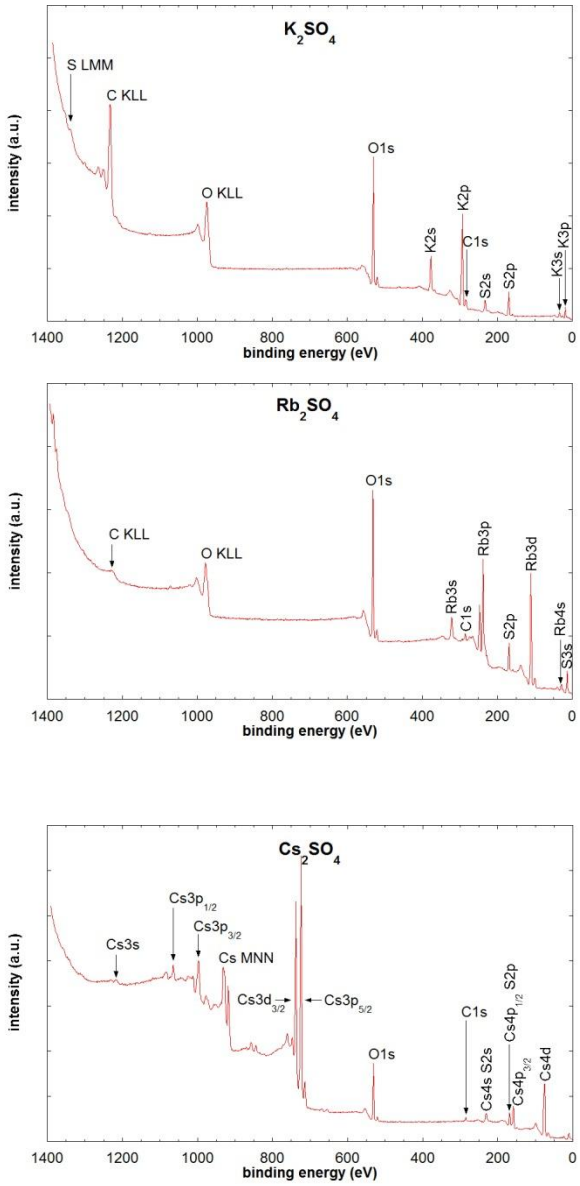


*Figure 5.1:* survey spectra of group IA sulphates.

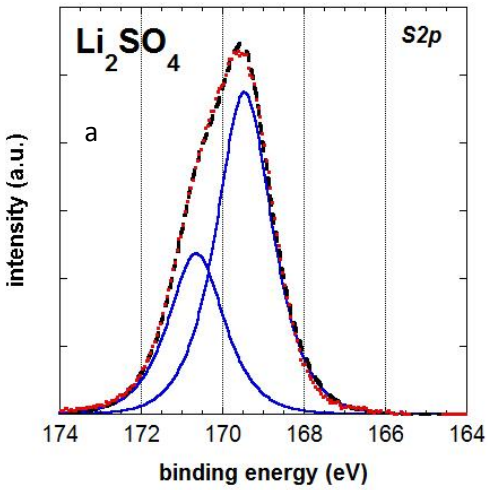
Li2SO4
S2p
a
intensity (a.u.)
174
172
170
168
166
164
binding energy (eV)

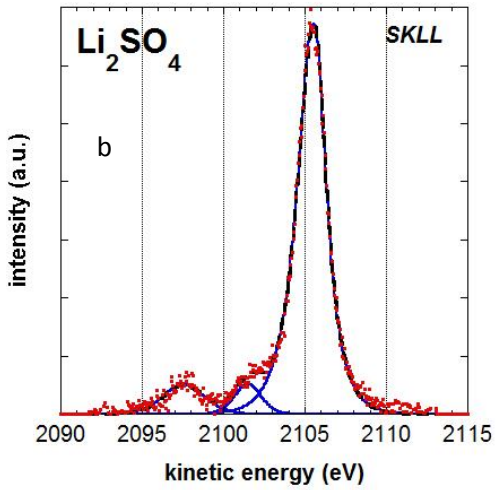
Li2SO4
SKLL
b
intensity (a.u.)
2090
2095
2100
2105
2110
2115
kinetic energy (eV)

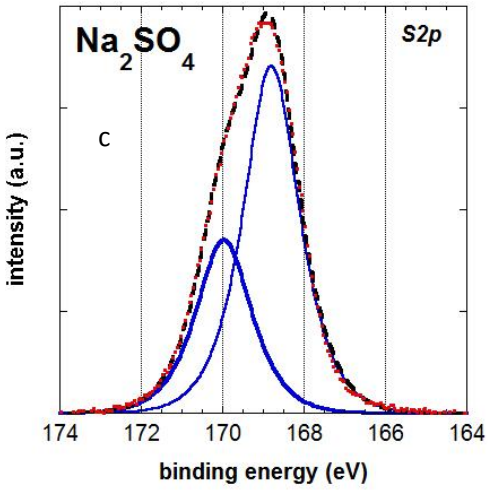
Na2SO4
S2p
c
intensity (a.u.)
174
172
170
168
166
164
binding energy (eV)

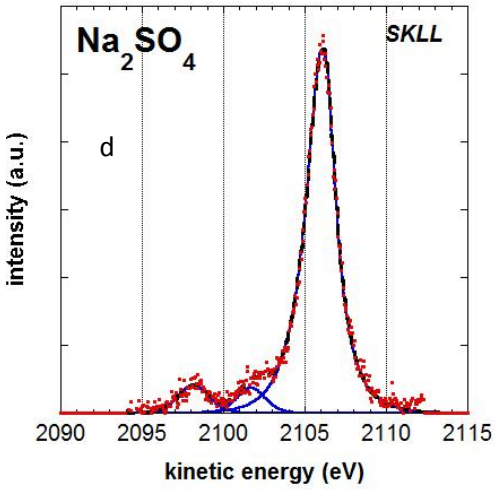
Na2SO4
SKLL
d
intensity (a.u.)
2090
2095
2100
2105
2110
2115
kinetic energy (eV)

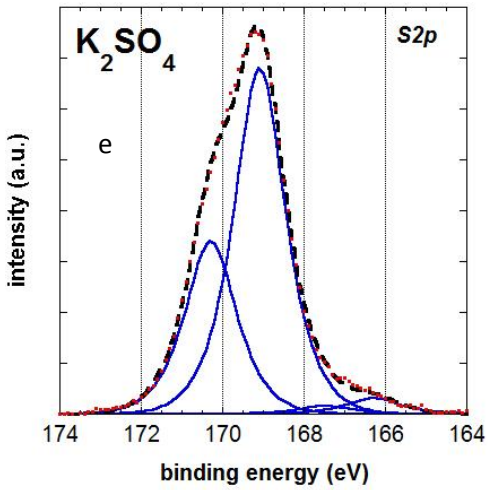
K2SO4
S2p
e
intensity (a.u.)
174
172
170
168
166
164
binding energy (eV)

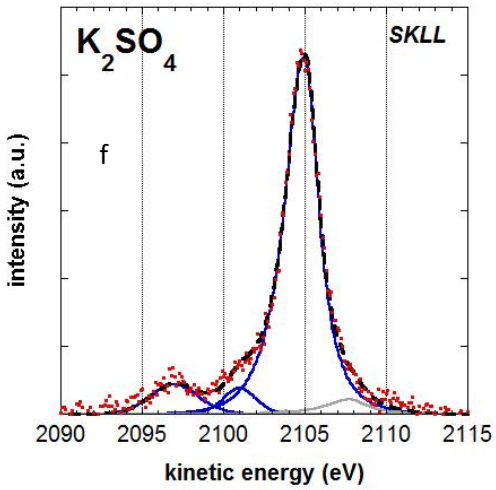
K2SO4
SKLL
f
intensity (a.u.)
2090
2095
2100
2105
2110
2115
kinetic energy (eV)

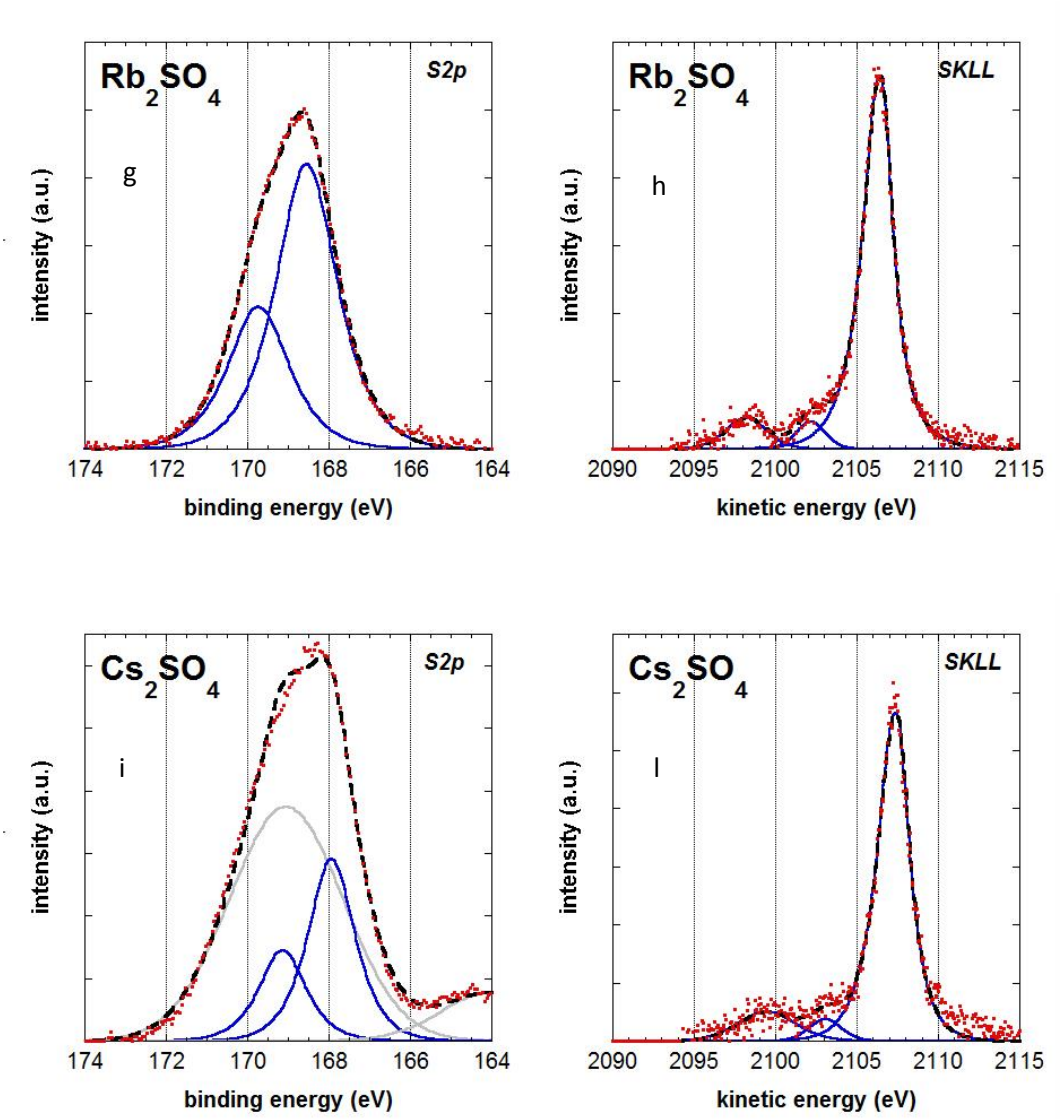


*Figure 5.2:* High-resolution photoelectron and X-ray induced Auger electron spectra

As figure 5.2 shows, all the S2p signals consist of a doublet, owing to the spin-orbit coupling. The most intense component corresponds to the quantic number of total angular momentum j=3/2, while the least intense component corresponds to j=1/2. The area of the least intense peak was always constrained to be 1/2 of the most intense one, in agreement with the theoretical value. The binding energy difference between the two components was found being 1.18 eV in agreement with [3]. The binding

energy values of the S2p signal (see table 5.1) are also in agreement with literature [2,4].

Table 5.1 lists the curve-fitting parameters obtained for the photoelectron signals $S2p_{3/2}$ of the group IA sulphates, after satellite removal and Shirley-Sherwood background subtraction. Binding energy of the signal, full-width-at-half-maximum (FWHM) height and Gaussian/Lorentzian (GL) ratio obtained using Casa XPS software are reported.

*Table 5.1:* Position (eV), FWHM (eV) and line shape of photoelectron signals of group IA sulphates. Standard deviation of three independent measurements is given.

| **Sulphates** | **$S2p_{3/2}$ Binding Energy (eV)** | **FWHM (eV)** | **Line Shape** |
|---|---|---|---|
| $Li_2SO_4*H_2O$ | 169.6±0.1 | 1.6 | GL(75) |
| $Na_2SO_4$ | 168.8±0.1 | 1.6 | GL(75) |
| $K_2SO_4$ | 169.0±0.1 | 1.5 | GL(75) |
| $Rb_2SO_4$ | 168.4±0.2 | 1.8 | GL(75) |
| $Cs_2SO_4$ | 167.8±0.1 | 1.4 | GL(75) |

The X-ray induced Auger Signal S KLL (see figure 5.2) consists of three components. The most intense, $^1D$, is due to the $KL_{2,3}L_{2,3}$ transition that corresponds to $2s^22p^4$ final configuration. The second signal at lower kinetic energies, $^1S$, is due to the other possible transition, $KL_1L_1$, that corresponds instead to $2s^02p^6$ final configuration. The different intensity of these two components reflects the different probability of each transition (see § 3.3.2). There is also a third component between $^1D$ and $^1S$ lines,

probably an excitation line due to a satellite. This component is present in all SKLL sulphate spectra.

XAES spectra of the SKLL line were fitted using a linear background subtraction. Table 5.2 lists curve-fitting parameters for each components of the SKLL signals i.e. KE position, FWHM GL ratio.

*Table 5.2:* Kinetic energy (eV), FWHM (eV) and line shape of X-ray induced Auger signals of group IA sulphates. Standard deviation is calculated over three independent measurements.

| Compounds | S $KL_{2,3}L_{2,3}$ ($^1D$) | | | satellite | | | S $KL_1L_1$ ($^1S$) | | |
|---|---|---|---|---|---|---|---|---|---|
| | **KE (eV)** | **FWHM (eV)** | **Line Shape** | **KE (eV)** | **FWHM (eV)** | **Line Shape** | **KE. (eV)** | **FWHM (eV)** | **Line Shape** |
| $Li_2SO_4*H_2O$ | 2105.1±0.1 | 1.7 | GL(90) T(1.8) | 2101.3±0.2 | 1.9±0.1 | GL(30) | 2097.5±0.1 | 2.9 | GL(30) |
| $Na_2SO_4$ | 2106.2±0.1 | 1.8±0.1 | GL(95) T(1.8) | 2101.8±0.2 | 2.0±0.1 | GL(30) | 2098.1±0.1 | 3.2±0.2 | GL(30) |
| $K_2SO_4$ | 2105.1±0.1 | 2.0±0.1 | GL(95) T(1.8) | 2101.0±0.1 | 1.9±0.1 | GL(30) | 2097.0±0.1 | 3.6±0.5 | GL(30) |
| $Rb_2SO_4$ | 2106.8±0.3 | 1.9 | GL(95) T(1.8) | 2102.6 | 3.0±0.1 | GL(30) | 2098.5 | 3.0±0.1 | GL(30) |
| $Cs_2SO_4$ | 2107.5±0.2 | 1.9 | GL(95) T(1.8) | 2103.3±0.2 | 2.3 | GL(30) | 2099.4±0.1 | 4.0±0.2 | GL(30) |

The high-resolution spectra of the different cations (Li1s, Na1s, K2p, Rb3d and Cs3d) as well as the O1s region of the group IA sulphates are shown in figure 5.3. Li1s and Na1s spectra were fitted with a singlet, reflecting (as for the S2p spectra), the presence of only one chemical state of the cation. The binding energies of Li1s and Na1s respectively 56.0±0.1 eV and 1071.5±0.1 eV (table 5.3) are in good agreement with the literature [5, 4, 6]. The spectrum of K2p (figure 5.3e) is a doublet with a binding energy difference of 2.8 eV [3]; the peak at 292.9±0.1 eV, can be assigned to a sulphate [7].

Rb3d and Cs3d spectra were fitted with a doublet, the area of the less intense peak was always assumed to be 2/3 of the most intense one, as predicted by the ratio of their respective degeneracies (2j+1). Separation between $Rb3d_{5/2}$ - $Rb3d_{3/2}$ and $Cs3d_{5/2}$ - $Cs3d_{3/2}$ signals were found to be respectively 1.49 eV and 13.94 eV in agreement with [3]. The binding energy values of $Rb3d_{5/2}$ and $Cs3d_{5/2}$ are found to be 109.8±0.2 eV and 723.9±0.2 eV respectively, in good agreement with [2, 8].

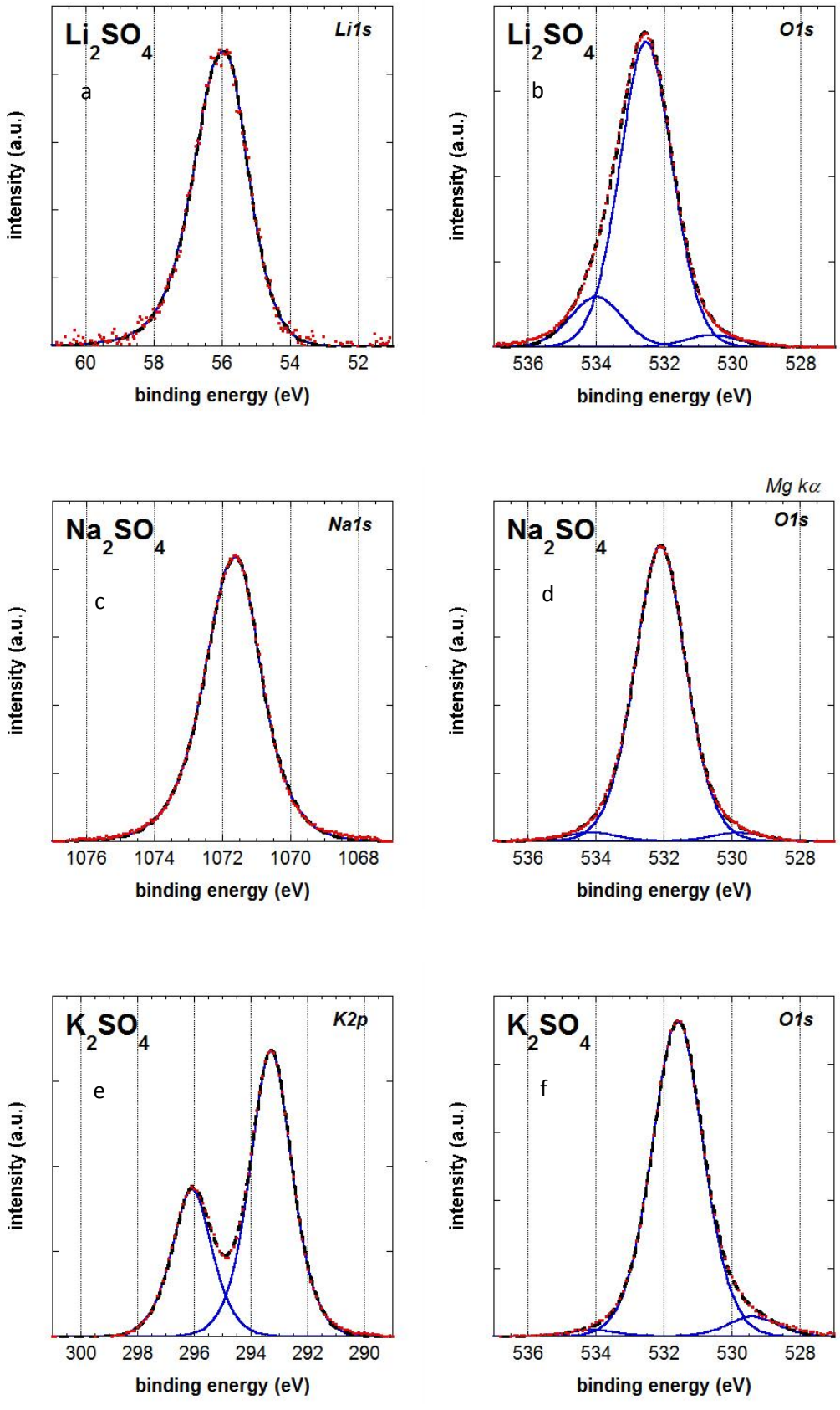
Li2SO4
Li1s
a
intensity (a.u.)
60
58
56
54
52
binding energy (eV)
Li2SO4
O1s
b
intensity (a.u.)
536
534
532
530
528
binding energy (eV)
Na2SO4
Na1s
c
intensity (a.u.)
1076
1074
1072
1070
1068
binding energy (eV)
Mg kα
Na2SO4
O1s
d
intensity (a.u.)
536
534
532
530
528
binding energy (eV)
K2SO4
K2p
e
intensity (a.u.)
300
298
296
294
292
290
binding energy (eV)
K2SO4
O1s
f
intensity (a.u.)
536
534
532
530
528
binding energy (eV)

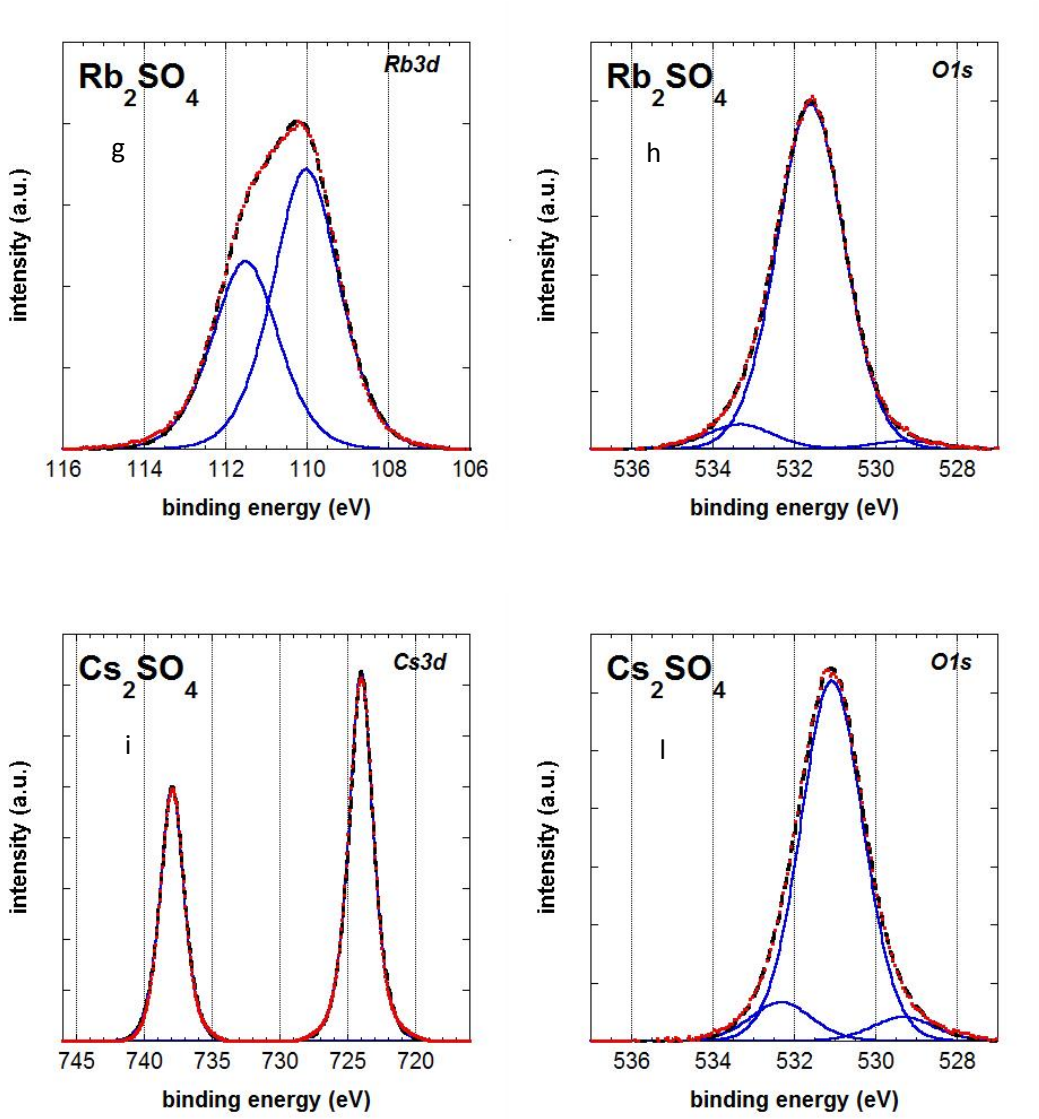


*Figure 5.3:* High-resolution photoelectron spectra of the cations Li1s, Na1s, K2p, Rb3d, Cs3d and O1s regions of group IA sulphates.

*Table 5.3*: Binding energy (eV), FWHM (eV) and line shape of photoelectron signals of group IA sulphates cations. Standard deviation is calculated on three independent measurements.

| **Compounds** | **BE (eV) cation** | **FWHM (eV)** | **Line Shape** |
|---|---|---|---|
| $Li_2SO_4*H_2O$ | Li1s = 56.0±0.1 | 1.7±0.1 | GL(55)T(2) |
| $Na_2SO_4$ | Na1s = 1071.6±0.1 | 1.7 | GL(76)T(2.4) |
| $K_2SO_4$ | $K2p_{3/2}$ = 293.3±0.1 | 1.7 | GL(60) |
| $Rb_2SO_4$ | $Rb3d_{5/2}$ = 109.8±0.2 | 1.9 | GL(50) |
| $Cs_2SO_4$ | $Cs3d_{5/2}$ = 723.9±0.2 | 2.0 | GL(75) |

*Table 5.4:* Binding energy (eV), FWHM (eV) and line shape of the O1s photoelectron signal of group IA sulphates. Standard deviation is calculated on three independent measurements.

| **Compounds** | **O1s BE (eV)** | **FWHM (eV)*** | **Line Shape** |
|---|---|---|---|
| $Li_2SO_4*H_2O$ | 532.6±0.1 | 1.8 | GL(45) |
| $Na_2SO_4$ | 532.0±0.1 | 1.8 | GL(45) [a] |
| $K_2SO_4$ | 531.6 | 1.8 | GL(45) |
| $Rb_2SO_4$ | 531.4±0.2 | 1.8 | GL(45) |
| $Cs_2SO_4$ | 531.0±0.1 | 1.8 | GL(45) |

[a]This spectrum has been acquired with Mg kα

* FWHM was constrained to 1.8 eV

The O1s spectrum (figure 5.3 right column) consists of three components in all cases: the most intense one corresponds to oxygen in sulphate, the less intense corresponds to oxygen in hydroxide and the third one corresponds to oxygen of hydration water. In the O1s of $Li_2SO_4*H_2O$, that exhibits hydroxide and water components more intense

than other sulphates, the ratio between the oxygen assigned to water and the total oxygen in the molecule is 0.20, in good agreement with the ratio equal to 0.20±0.03, found experimentally. The binding energy for O1s hydroxide $Li_2SO_4*H_2O$ agrees with literature [9].

### 5.1.2 Chemical state of sulphates

In sulphates ($SO_4^{2-}$ ions), sulphur is coordinated to four oxygen atoms: the charge balance is established with cations. In this work alkali sulphates were studied. The S2p binding energy of sulphur in sulphates decreases from Li to Cs (table 5.1), in agreement also with literature data. A similar trend (figure 5.4) can be found for the binding energy of the O1s signal, also here in good agreement with literature [2].

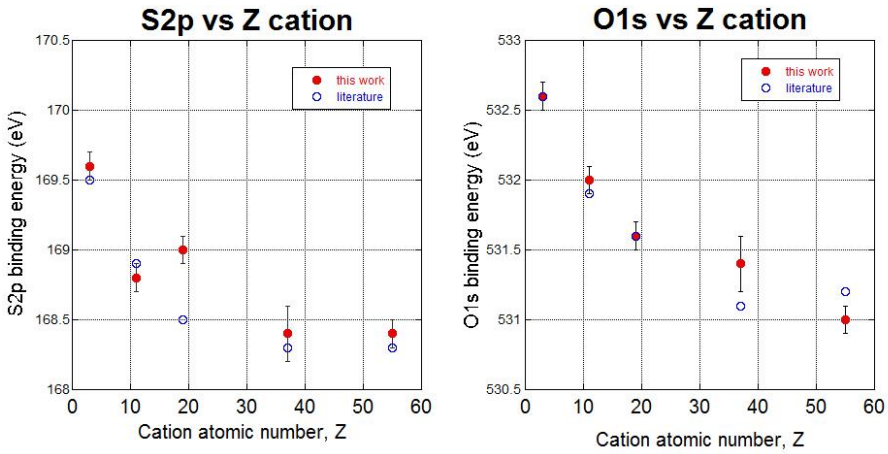


*Figure 5.4:* Trends of S2p and O1s binding energy values versus the atomic number in sulphate samples.

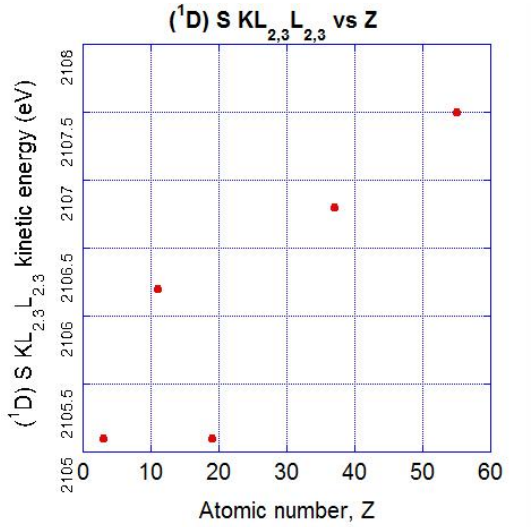


*Figure 5.5:* S KLL kinetic energy value of group I sulphates vs the atomic number of the cation (see table 5.2).

In a first step, the modified Auger parameter ($\alpha'$) can be determined by combining the information from S2p binding energy and SKLL kinetic energy (table 5.2). Wagner originally defined the Auger parameter as the difference between the kinetic energy of the most intense Auger line and the most intense photoelectron line, making reference to the Fermi level rather than the vacuum level. The definition of the Auger parameter $\alpha'$ most frequently used is

$$\alpha' = \alpha + h\nu = E_k \text{ (Auger)} + E_b \text{ (photoelectron)} \qquad (6.1)$$

The modified parameter $\alpha'$ defined this way is then independent of $h\nu$ and always positive and it is simply the sum of the kinetic energy of the Auger signal and the binding energy of the photoelectron signal. A further advantage is that this sum will be the same independent of sample charging. The Auger parameter for the different alkali sulphates is reported in table 5.5.

*Table 5.5:* S2p and S 2s binding energy values (eV), SKLL kinetic energy (eV) and Auger parameter (eV) of sulphates.

| **Compound** | **S2p BE (± 0.1 eV)** | **SKLL KE (± 0.1 eV)** | **α' (eV)** | **S 2s BE (± 0.1 eV)** |
|---|---|---|---|---|
| $Li_2SO_4$ | 169.6 | 2105.1 | 2274.7 | 233.7±0.1 |
| $Na_2SO_4$ | 168.8 | 2106.2 | 2275.0 | 233.1±0.1 |
| $K_2SO_4$ | 169.0 | 2105.1 | 2274.1 | 233.0±0.1 |
| $Rb_2SO_4$ | 168.4 | 2106.8 | 2275.2 | $Rb3p_{3/2}$ overlaps |
| $Cs_2SO_4$ | 167.8 | 2107.5 | 2275.3 | 232.7±0.1 |

It can be observed that the calculated Auger parameter α' is fairly constant, indicating that the chemical environment of sulphur in the sulphates does not change. A two-dimensional representation, the so called Wagner plot or chemical state plot, can be obtained (Figure 5.6) by combining binding energy and kinetic energy of the respective S2p and SKLL lines,.

The Auger parameter α' previously calculated is represented in the Wagner chemical state plot by a diagonal line with the slope -1 (note that the binding energy axis is plotted reversed). In particular, the diagonal line which is most close to the points of the sulphate compounds has the Auger parameter α' = 2277 ± 0.2 eV.

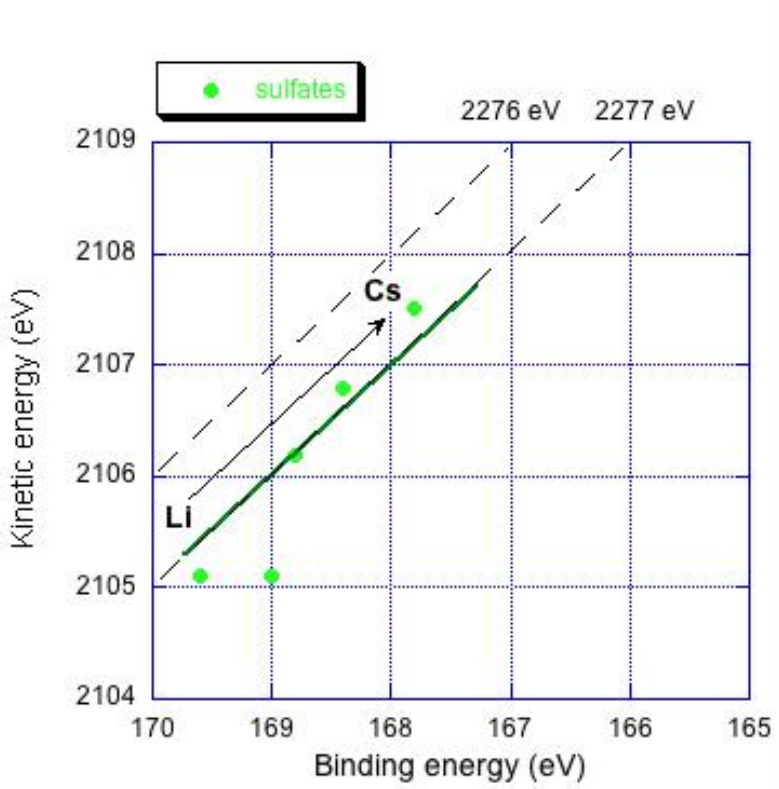


*Figure 5.6:* Wagner chemical state plot of sulphur in alkali sulphates (Li, Na, K, Rb, Cs)

Additional information can be obtained from the S2s signals (table 5.5): the binding energy of the S2s signals also decreases from Li to Cs sulphates similarly to the S2p binding energy. The chemical shifts observed in sulphates (difference between the binding / kinetic energy of Li and Cs for different signals) increase from S2s, O1s, S2p to SKLL (1, 1.6, 1.8 and 2.4 eV respectively). The largest difference was found for the SKLL signals, confirming that the use of these lines is a very powerful tool for the identification of the chemical states of the elements. As the corresponding SLMM signals showed a poor signal-to-noise ratio, no reliable data were obtained. An

exception is the $K_2SO_4$, recorded with the SIGMA 2 equipped with Alpha 100 analyser: the kinetic energy of the SLMM signal was found equal to 149.9 ± 0.1 eV.

### 5.1.3 Elemental sulphur ($S_8$)

All modifications of crystalline sulphur contain a cyclic molecule consisting of 6 to 20 sulphur atoms; the most common is the molecule with 8 atoms that exists in 3 allotropic main forms: $S_\alpha$, $S_\beta$ and $S_\gamma$ [10]. Figure 5.7 shows the survey spectrum and the high-resolution S2p and SKLL signals recorded on elemental sulphur.

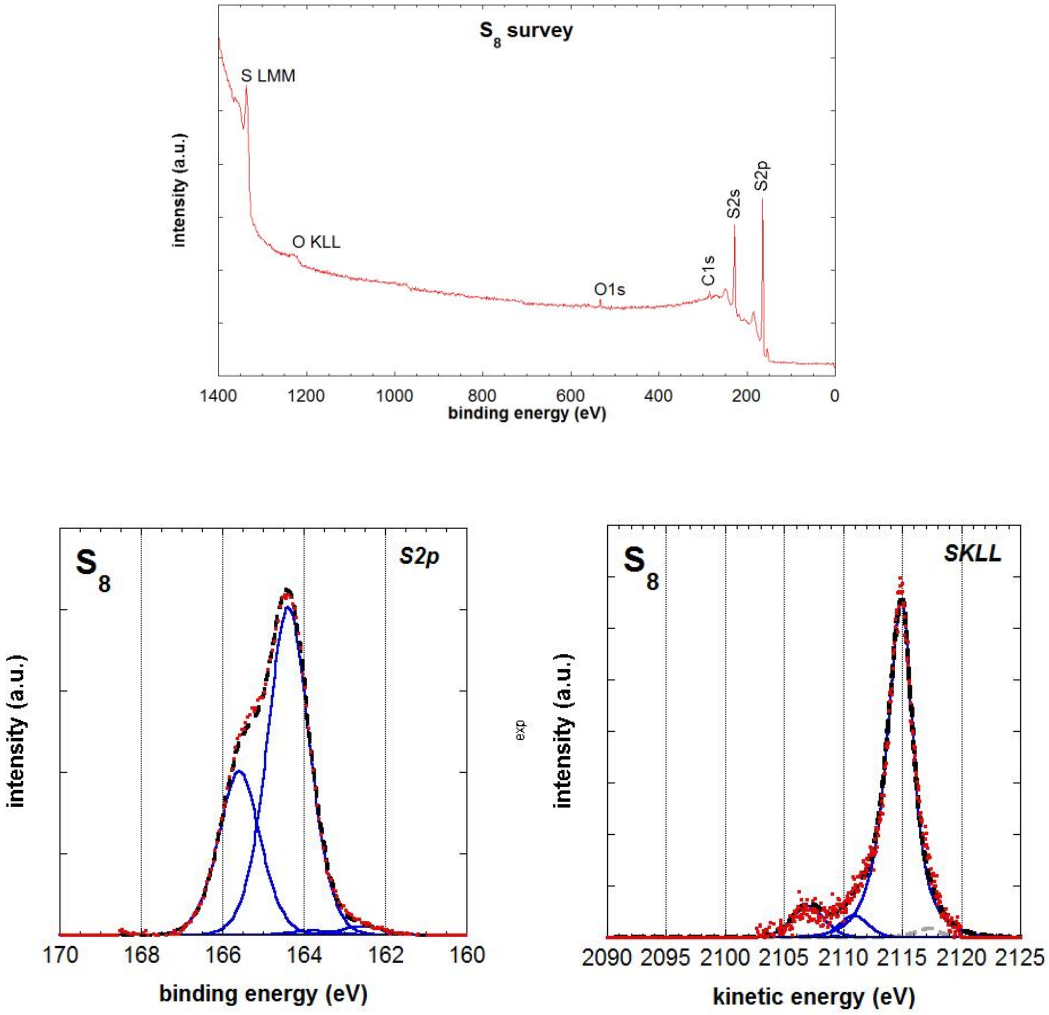


*Figure 5.7:* survey and high-resolution spectra of S2p and SKLL of elemental sulphur.

Also in this case, the S2p signal consists of a single doublet. The curve-fitting parameters for the S2p spectra are listed in table 5.6; the binding energy of the $S2p_{3/2}$ signal at 164.3±0.1 eV is in good agreement with previous investigations [11].

*Table 5.6:* Binding energy (eV), FWHM (eV) and line shape of photoelectron signals of elemental sulphur. Standard deviation is calculated on three independent measurements.

| **$S2p_{3/2}$ BE (eV)** | **FWHM (eV)** | **Line Shape** |
|---|---|---|
| 164.3±0.1 | 1.3±0.1 | GL(45) |

*Table 5.7:* Kinetic energy (eV), FWHM (eV) and line shape of X-ray induced Auger signals of elemental sulphur. Standard deviation is calculated on three independent measurements.

| **S $KL_{2,3}L_{2,3}$ ($^1D$)** | | | **satellite** | | | **S $KL_1L_1$ ($^1S$)** | | |
|---|---|---|---|---|---|---|---|---|
| **KE (eV)** | **FWHM (eV)** | **Line Shape** | **KE (eV)** | **FWHM (eV)** | **Line Shape** | **KE (eV)** | **FWHM (eV)** | **Line Shape** |
| 2112.8±0.3 | 2.1 | GL(90) T(1.8) | 2108.7±0.2 | 2.7±0.1 | GL(30) | 2104.8±0.2 | 3.8 | GL(30) |

### 5.1.4 Sulphides and polysulphides of group I elements

A series of sulphides of group I elements ($Li_2S$, $Na_2S$, $Na_2S_4$ and $K_2S_n$) were analysed. As in the case of sulphates (par. 5.1.1), XPS survey and S2p and SKLL high-resolutions spectra were measured together with the spectra of the cations and oxygen O1s. The spectra presented in this section were recorded after 5 minutes grinding of the samples. The effect of grinding time on $Na_2S$ and $Na_2S_4$ samples is presented in detail in paragraph 5.1.8.

The survey spectra (Figure 5.8) acquired with Al Kα source indicate the presence of a small C1s signal that demonstrates the quality of the sample preparation, whereas the O1s is quite intense despite the fact that these sulphides were sent enclosed in a sealed bottle. They were apparently oxidized owing to a contact with air prior to their shipment. The S2p and SKLL high-resolutions spectra of sulphides and poly-sulphides of group I elements are given in Figure 5.9.

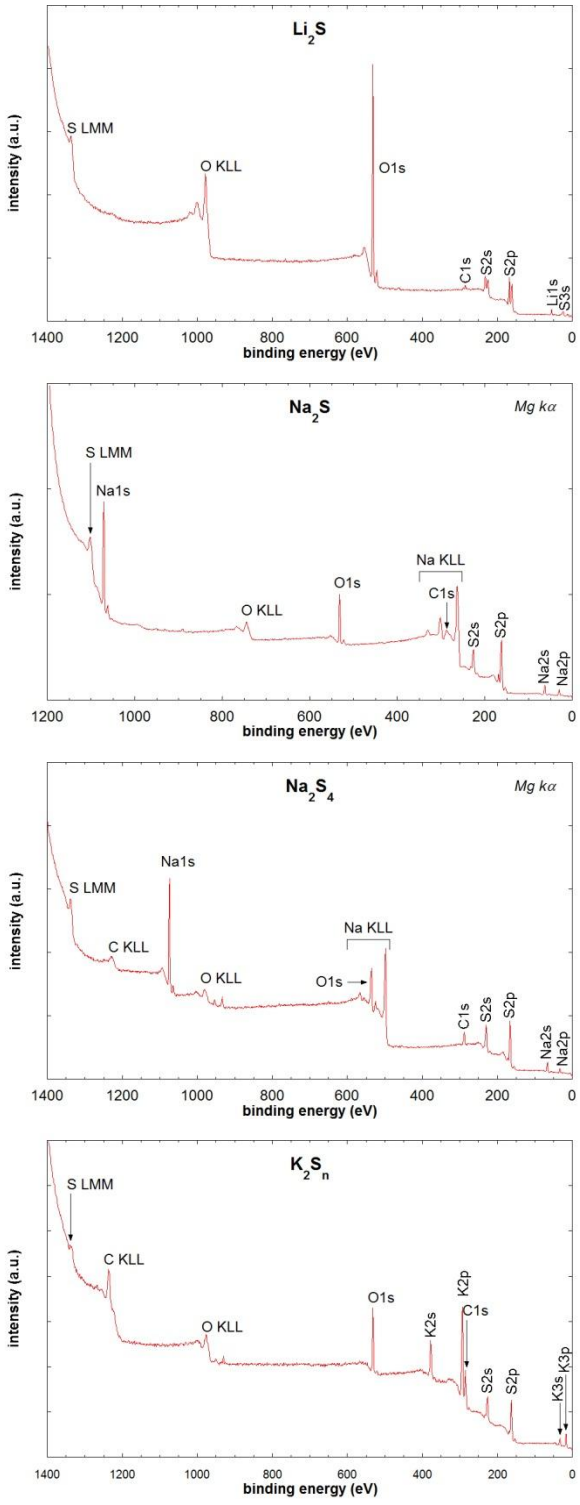


*Figure 5.8:* Survey spectra of the group I sulphides and poly-sulphides measured on powdered samples

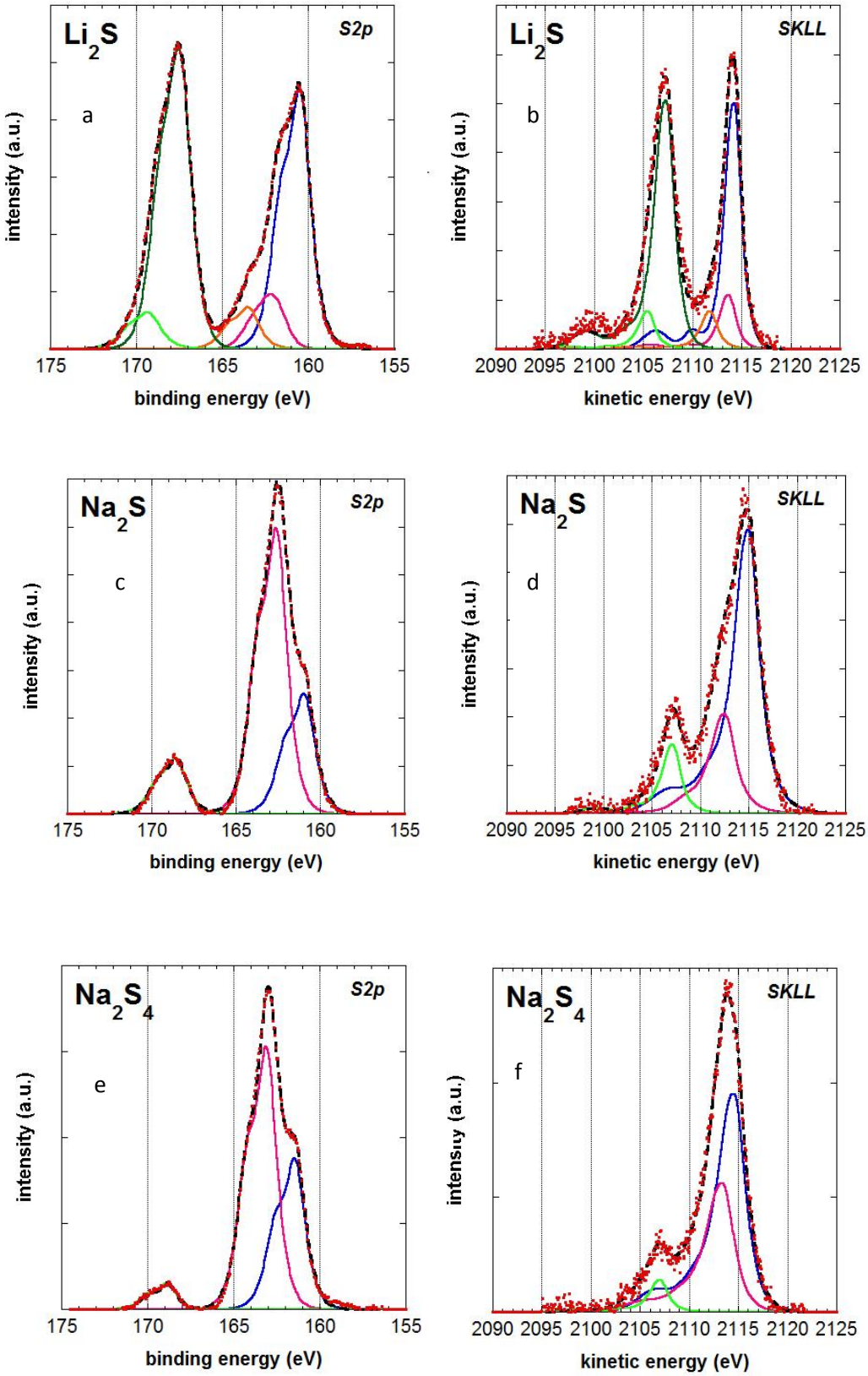
Li2S
S2p
a
intensity (a.u.)
175 170 165 160 155
binding energy (eV)
Li2S
SKLL
b
intensity (a.u.)
2090 2095 2100 2105 2110 2115 2120 2125
kinetic energy (eV)
Na2S
S2p
c
intensity (a.u.)
175 170 165 160 155
binding energy (eV)
Na2S
SKLL
d
intensity (a.u.)
2090 2095 2100 2105 2110 2115 2120 2125
kinetic energy (eV)
Na2S4
S2p
e
intensity (a.u.)
175 170 165 160 155
binding energy (eV)
Na2S4
SKLL
f
intensity (a.u.)
2090 2095 2100 2105 2110 2115 2120 2125
kinetic energy (eV)

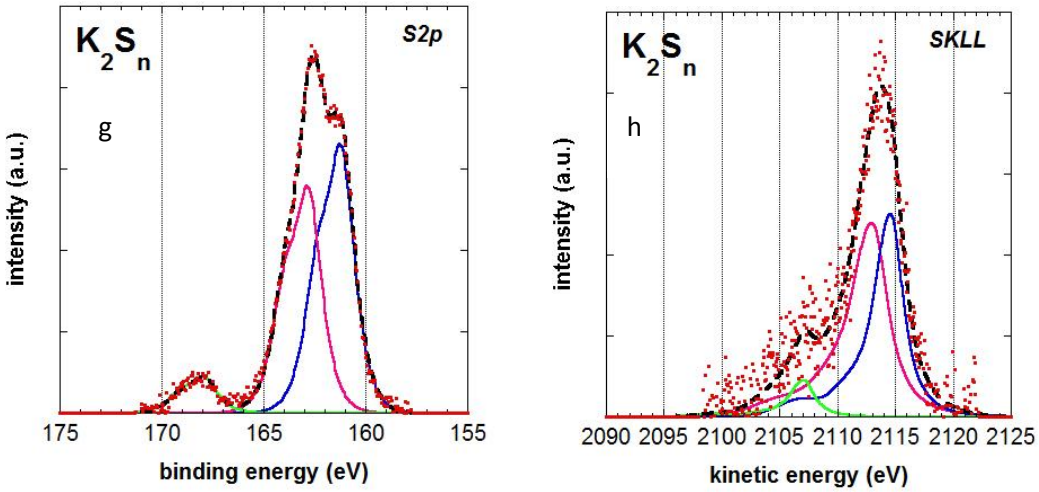


*Figure 5.9:* High-resolution spectra of the group I sulphides and poly-sulphides measured on powdered samples

As can be seen from figure 5.9, the S2p spectra of sulphides and poly-sulphides show several components that were fitted using the parameters listed in table 5.8 and described in the experimental section (paragraph 4.2.5). At high binding energies (at ca. 168.4 eV) a component that can be assigned to sulphates (this chapter, paragraph 5.1.1) is always detected. Its intensity is particularly pronounced in the case of $Li_2S*H_2O$. The signal attributed to sulphide shows always a shoulder, resulting in the presence of two components (each consisting of a S2p doublet). Curve fitting reveals one component at lower binding energy, ca. 160.5 eV, and one at higher binding energy, ca. 163.4 eV. The resulting binding energies and the curve fitting parameters are given in table 5.8.

*Table 5.8*: Binding energy and Kinetic energy (eV), FWHM (eV) and line shape of the components in the SKLL signals of Li, Na, K sulphides and polysulphide. Standard deviation is calculated on three independent measurements.

| | | **S2p peak fitting parameters** | | | **SKLL peak fitting parameters** | | |
|---|---|---|---|---|---|---|---|
| **Compound** | **Component** | **Bindig Energy (eV) $S2p_{3/2}$** | **FWHM (eV)** | **Line Shape** | **Kinetic Energy (eV) $(^1D)SKL_{2,3}L_{2,3}$** | **FWHM (eV)** | **Line Shape** |
| $Li_2S$ | (I) | 160.5±0.1 | 1.4 | GL(75) | 2114.4±0.3 | 1.7 | GL(80)T(2) |
| | (II) | 162.1±0.1 | 1.4 | GL(75) | 2113.7±0.1 | 1.7 | GL(80)T(2) |
| | (III) | 163.4±0.1 | 1.4 | GL(75) | 2111.8±0.2 | 1.7 | GL(80)T(2) |
| | (IV) | 167.4±0.2 | 1.4 | GL(75) | 2107.3±0.2 | 1.9 | GL(80)T(2) |
| | (V) | 169.3±0.2 | 1.4 | GL(75) | 2105.5±0.2 | 1.9 | GL(80)T(2) |
| $Na_2S$ | (I) | 160.8 ± 0.1 | 1.5 | GL(75) | 2115.0±0.1 | 2.6 | GL(80)T(1.5) |
| | (II) | 162.5 ±0.1 | 1.5 | GL(75) | 2112.4±0.1 | 2.6 | GL(80)T(1.5) |
| | (III) | 168.4 ±0.1 | 1.5 | GL(75) | 2107.2±0.1 | 2.6 | GL(95)T(1.8) |
| $Na_2S_4$ | (I) | 161.5±0.1 | 1.5 | GL(75) | 2114.8 | 2.7 | GL(80)T(1.5) |
| | (II) | 163.1±0.2 | 1.5 | GL(75) | 2113.4 | 2.7 | GL(80)T(1.5) |
| | (III) | 168.6±0.2 | 1.5 | GL(75) | 2107.0 | 1.9 | GL(95)T(1.8) |
| $K_2S_n$ | (I) | 161.7±0.1 | 1.5 | GL(75) | 2114.2±0.2 | 3.0 | GL(80)T(1.5) |
| | (II) | 163.3±0.2 | 1.5 | GL(75) | 2112.6±0.1 | 2.9 | GL(80)T(1.5) |
| | (III) | 168.4±0.1 | 1.5 | GL(75) | 2106.2±0.1 | 2.0 | GL(95)T(1.8) |

In the following, the individual compounds are described in more detail. Lithium sulphide showed five S2p doublets between 160.5 eV and 169.3 eV (Fig. 5.9a). The former is ascribed to sulphide $S^{2-}$ species and the latter to $SO_4^{2-}$. The intermediate components might be assigned to polysulphide species with different chain-length (162.1 eV and 163.4 eV) and to sulphite $SO_3^{2-}$ (167.4 eV). This last assignment is in agreement with published data on $Na_2SO_3$ [12]. Also the SKLL spectrum was fitted with five components (Fig. 5.9b), each of them constituted by three peaks (SKLL $^1$D, SKLL $^1$S and SKLL SAT). The area ratio between SKLL $^1$D components was kept constant and equal to the ratio calculated from photoelectron signals. Li1s peak shows two components. The less intense at ca. 56 eV can be assigned to lithium bound to S-O groups while the most intense at about 54.4 eV could be assigned to Li-sulphide/polysulphide. (Figure 5.10a)

Commercial sodium sulphide $Na_2S$ showed three S2p doublets (Fig. 5.9c). Sulphide is found at 160.8 eV, and sulphate at 168.4 eV. The intermediate peak (B.E. 162.5 eV) is ascribed to polysulphide sulphur. S2p peak of sulphide is in good agreement with [13]. They reported the S2p signal at 159.4 eV but they used the C1s at 283.7 eV as internal reference for charge correction: adding 1.3 eV to 159.4 eV the value of 160.7 eV is found in excellent agreement with this work. SKLL was fitted with three components.

Also sodium tetrasulphide, $Na_2S_4$, showed three components in the S2p spectrum (Fig. 5.9e): the one at lower binding energy is found at 161.5 eV. The polysulphide component is found at 163.1 eV and the sulphate one at 168.6 eV. It is interesting to notice that the first peak exhibits a higher binding energy than that measured on the sulphide of $Na_2S$ (160.8 eV). This component could be due to a polysulphide with a

shorter chain length compared to the polysulphides that origin the peak at 163.1 eV. Sodium Na1s was found at 1071 eV in both $Na_2S$ and $Na_2S_4$ (Figure 5.10c and e).

$K_2S_n$ is a commercial polysulphide. The chain-length of the polysulphide is not provided by the supplier. The sulphur S2p peak shows three components (Fig. 5.9g), at 161.7 eV, 163.3 eV and 168.4 eV respectively. ($^1$D) $SKL_{2,3}L_{2,3}$ lines are found at 2112.6 eV, 2114.2 eV and 2106.2 eV (Fig. 5.9h). $K2p_{3/2}$ is found at ca. 298.7 eV (Figure 5.7g).

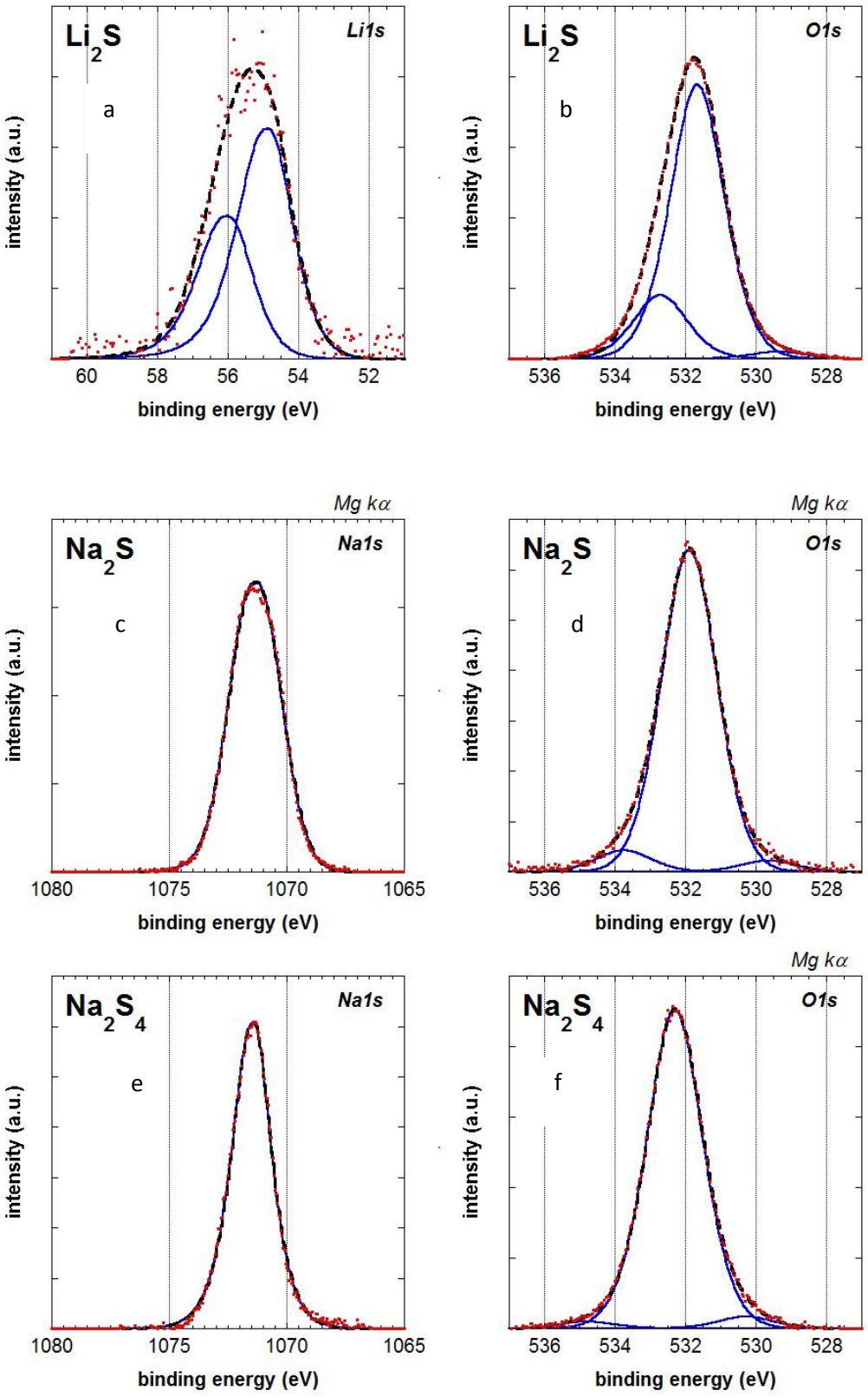
Li2S
Li1s
a
intensity (a.u.)
60
58
56
54
52
binding energy (eV)
Li2S
O1s
b
intensity (a.u.)
536
534
532
530
528
binding energy (eV)
Mg kα
Na2S
Na1s
c
intensity (a.u.)
1080
1075
1070
1065
binding energy (eV)
Mg kα
Na2S
O1s
d
intensity (a.u.)
536
534
532
530
528
binding energy (eV)
Na2S4
Na1s
e
intensity (a.u.)
1080
1075
1070
1065
binding energy (eV)
Mg kα
Na2S4
O1s
f
intensity (a.u.)
536
534
532
530
528
binding energy (eV)

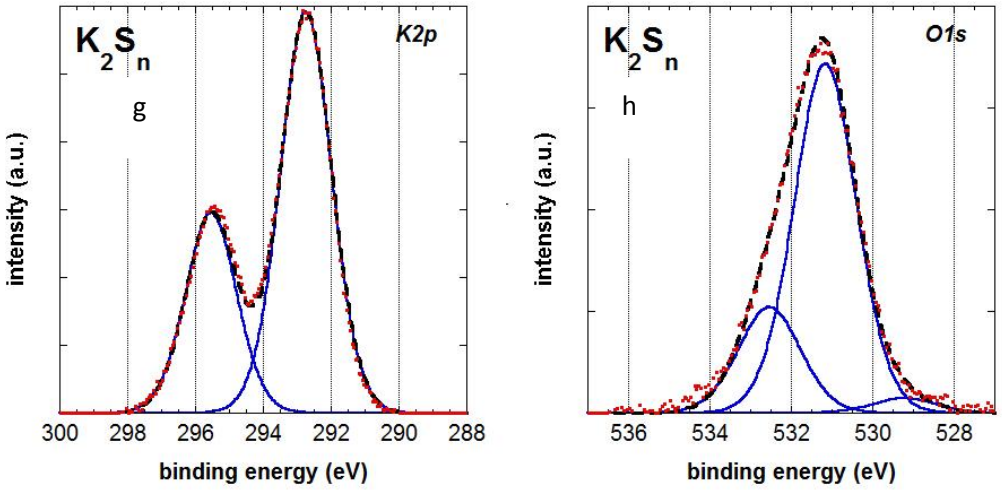


*Figure 5.10:* High-resolution spectra of the cations (Li, Na, K) and O1s line of group I sulphides and poly-sulphides measured on powdered samples

### 5.1.5 Chemical state of sulphides

Sulphide $S^{2-}$ is the formal most negative charge on sulphur atom. Sulphides have got the lowest binding energies that are ranging between 161 eV and 163 eV: they thus clearly differ from sulphates (binding energy ca. 168.5 eV – 170 eV). The alkali sulphides studied in this work (figure 5.9, table 5.8) fall in the "upper right" region of the chemical state plot. The Auger parameter is calculated and it is found being 2275.6 ± 0.2 eV. A second smaller peak, identified in the S2p (binding energy ca. 163 eV) and in the SKLL spectra (kinetic energy 2113 eV), is found in the chemical state plot on the same diagonal line as the sulphide, with Auger parameter $\alpha' = 2275.6 \pm 0.2$ eV.

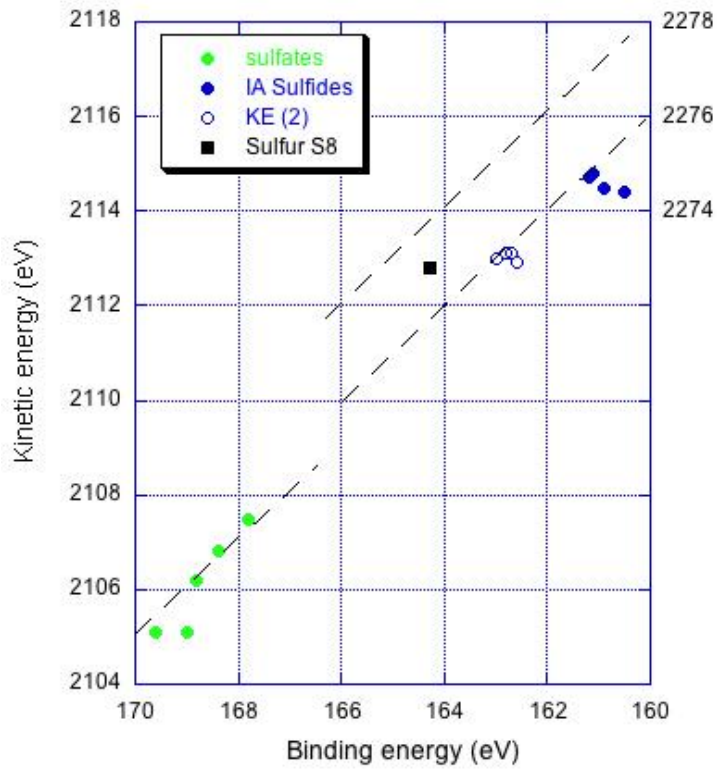


*Figure 5.11*: Chemical state plot of alkali sulphides, sulphates and elemental sulphur.

### 5.1.6 Copper and iron sulphides

Copper and iron sulphides were also investigated in this work in the frame of the surface characterization of natural sulphide minerals such as enargite ($Cu_3AsS_4$), pyrite and arsenopyrite. As for all the other compounds studied, XPS survey and S2p and SKLL high-resolutions spectra were recorded together with the spectra of the cations and the oxygen O1s. The spectra showed in this section were taken on powdered samples after five minutes of grinding in agate mortar.

The survey spectra (Figure 5.12) acquired with the Al Kα source confirm the absence of contaminants: in these cases both C1s and O1s signals are much less intense than the main photoelectronic signals of the cations. The S2p and S KLL high-resolutions spectra of transition metal sulphides are shown in Figure 5.13.

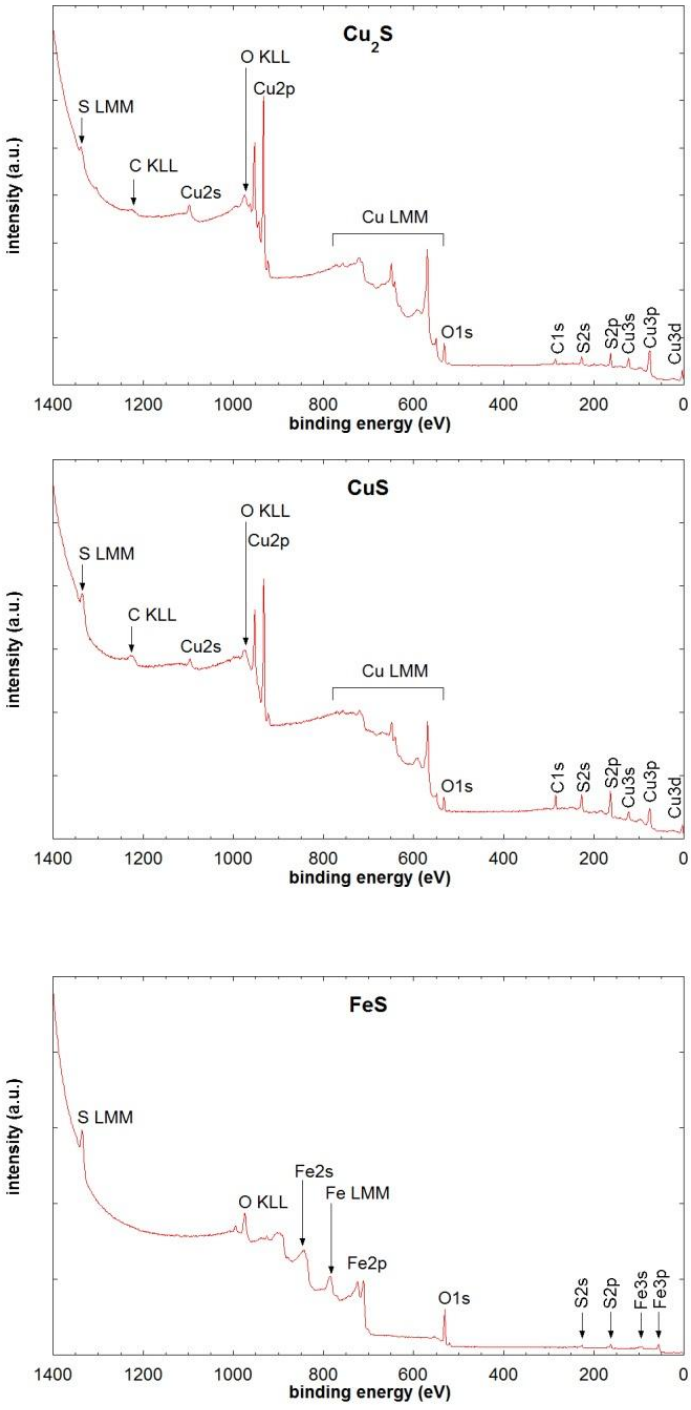


*Figure 5.12:* survey spectra of transition metal sulphides studied in this work.

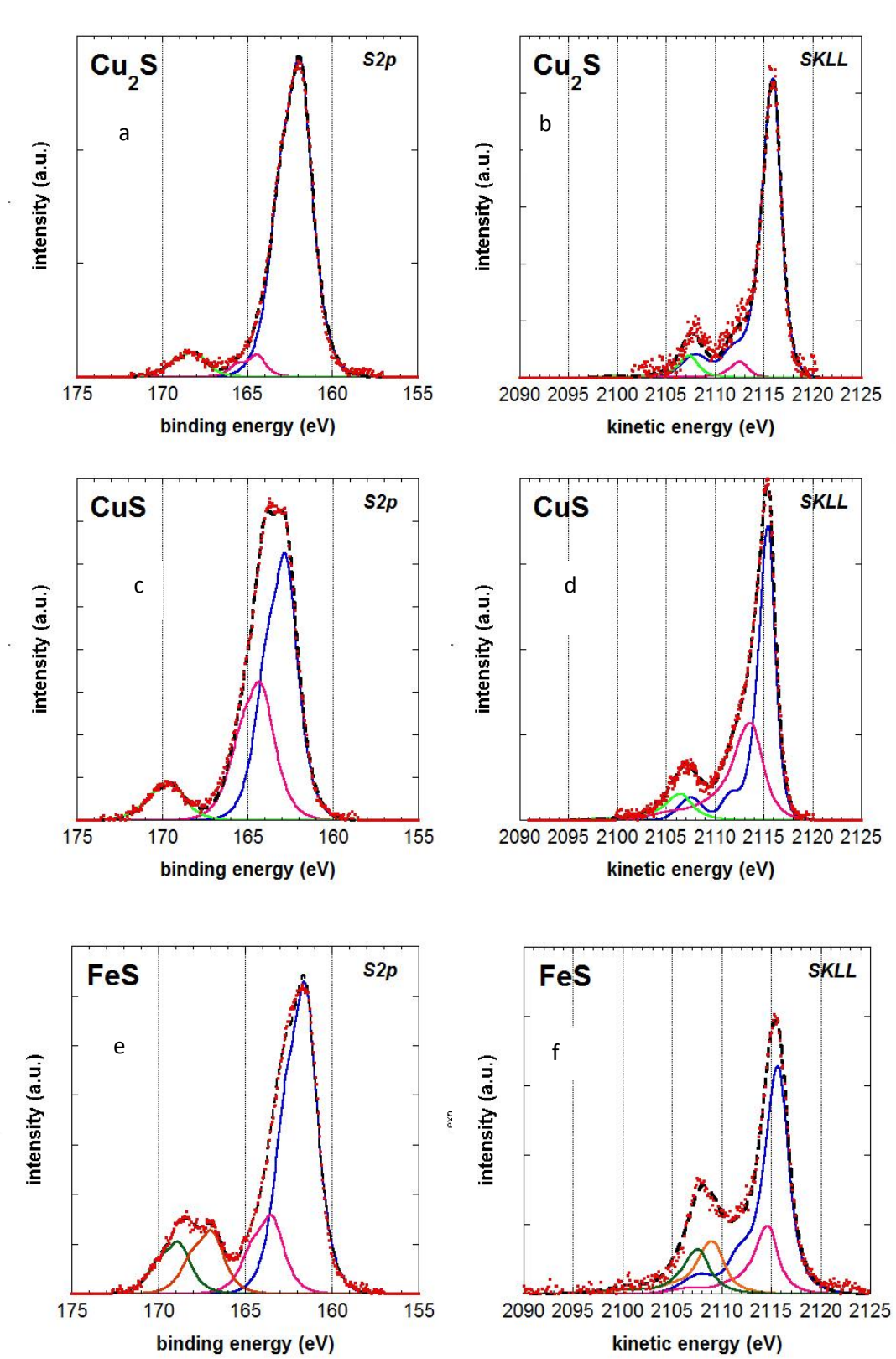


*Figure 5.13:* High-resolution photoelectron and X-ray induced Auger spectra for sulphur of $Cu_2S$ (a and b), CuS (c and d) and FeS (e and f).

*$Cu_2S$*

$Cu_2S$ (Fig. 5.13a) showed an intense peak at 161.9 eV that is close to the value reported for Cu (I) sulphide [14] and two additional small components at 164.4 eV and at 168.1 eV respectively. The component at 164.4 eV may be ascribed to elemental sulphur as it is substantiated by the kinetic energy of the corresponding SKLL line (2112.7 eV) (Fig 5.13b). The peak at higher binding energy is due to small amounts of sulphate on the sample surface. Cu2p (Fig. 5.14a; table 5.9) shows an intense peak at 932.2 eV which is in very good agreement with results reported by [14]. A small component at 934.5 eV is also detectable: it can be assigned to copper (II) sulphate as confirmed by the satellite structure at higher binding energy (941. 6 eV and 943.7 eV).

*CuS*

The S2p of CuS shows three peaks (Fig 5.13c). The signal at 162.7 eV and the one at 164.2 eV are due to two different kinds of sulphur atoms in CuS. In effect it is known [15] that in covellite (CuS) exists both $S^{2-}$ and $S_2^{2-}$ ions. In agreement with literature the area ratio of these two components is 2:1 [15]. The peak at 169.4 is ascribed to sulphate and it is closed to value reported by [14]. SKLL shows three components as well; the first one (KE= 2115.5 eV) could be assigned to $S^{2-}$, the component at 2113. 7 eV at $S_2^{2-}$ and the third one at sulphur in $SO_4^{2-}$ ions. Copper Cu2p3/2 (fig. 5.14c) was found at 932.6 in agreement with [14].

The iron sulphide sample (FeS) showed four different oxidation states in the S2p spectrum (Fig 5.13e) and four different components were used also for curve fitting the SKLL spectrum (Fig 5.13f). The most intense peak at 161.5 eV could be ascribed to disulphide and the one at 163.4 to polysulphide according to [16]. Peaks at higher binding energy values are due to S-O species at the sample surface, probably Fe (II) - sulphate and Fe (III) – sulphate. [17]. The presence of Fe (III) – sulphate is also confirmed by the component at 713 eV (Fig. 5.14e and tab. 5.10) in the Fe2p3/2 signal [17]. The surface of FeS was very oxidized and together with Fe (III) sulphate component, $Fe_2O_3$ at 710.5 eV [18] and Fe (III) – sulfide at 708.6 eV [19] were detected. No signals from Fe (II) compounds are present.

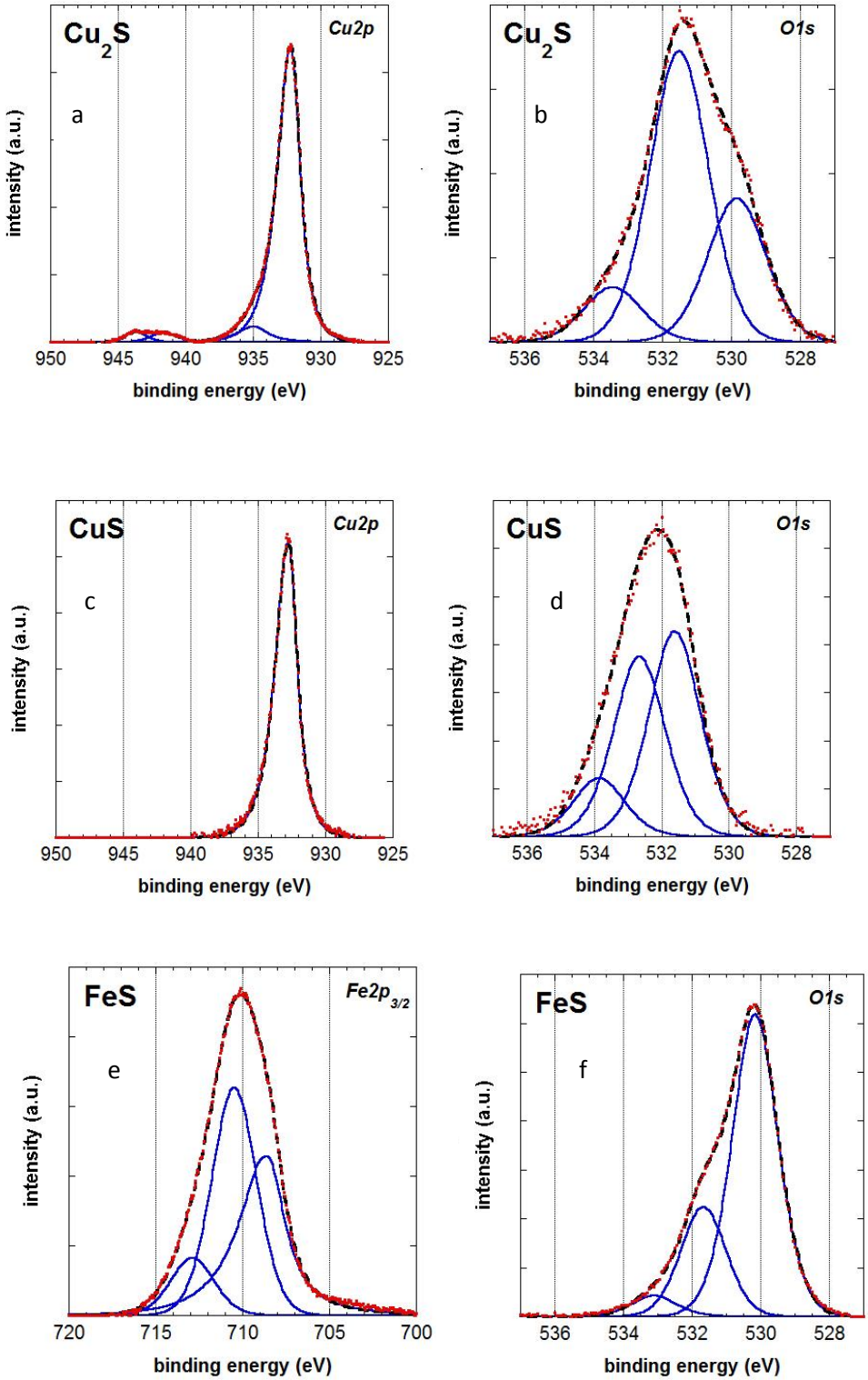


*Figure 5.14:* high-resolution photoelectron spectra of copper $Cu2p_{3/2}$ and iron $Fe2p_{3/2}$ and O1s regions of $Cu_2S$ (a and b), CuS (c and d) and FeS (e and f).

*Table 5.9:* Binding energy (eV), FWHM (eV) and line shape of the components in the S2p signals of transition metal sulphides. Standard deviation on three independent measurements is listed.

| | | **S2p peak fitting parameters** | | | **SKLL peak fitting parameters** | | |
|---|---|---|---|---|---|---|---|
| **Compound** | **Component** | **Bindig Energy (eV) $S2p_{3/2}$** | **FWHM** | **Line Shape** | **Kinetic Energy (eV) ($^1$D)SK$L_{2,3}L_{2,3}$** | **FWHM** | **Line Shape** |
| $Cu_2S$ | (I) | 161.9±0.1 | 1.7 | GL(75) | 2116.0±0.2 | 1.9 | GL(95)T(1.8) |
| | (II) | 164.4±0.2 | 1.7 | GL(75) | 2112.7±0.2 | 1.9 | GL(95)T(1.8) |
| | (II) | 168.1±0.1 | 1.7 | GL(75) | 2107.5±0.2 | 1.9 | GL(95)T(1.8) |
| CuS | (I) | 162.7±0.1 | 1.7 | GL(75) | 2115.5±0.1 | 1.7 | GL(80)T(1.8) |
| | (II) | 164.2±0.2 | 1.7 | GL(75) | 2113.7±0.1 | 1.7 | GL(80)T(1.8) |
| | (II) | 169.4±0.1 | 1.7 | GL(75) | 2106.6±0.2 | 1.7 | GL(80)T(1.8) |
| FeS* | (I) | 161.5±0.1 | 1.7 | GL(75) | 2115.8±0.2 | 2.3 | GL(90)T(1.5) |
| | (II) | 163.4±0.2 | 1.7 | GL(75) | 2114.7±0.1 | 2.3 | GL(90)T(1.5) |
| | (III) | 166.9±0.1 | 1.7 | GL(75) | 2109.1±0.2 | 2.3 | GL(90)T(1.5) |
| | (IV) | 168.9±0.1 | 1.7 | GL(75) | 2107.7±0.1 | 1.7 | GL(90)T(1.5) |

*Table 5.10:* Copper and iron sulphides peak fitting parameters

| **Compounds** | **Line** | **BE Position (eV) cation** | **FWHM** | **Line Shape** |
|---|---|---|---|---|
| $Cu_2S$ | Cu2p (I) | 932.2 ±0.1 | 1.6 | GL(90)T(1.5) |
| | Cu2p (II) | 934.8 ±0.1 | 2.0 | GL(90)T(1.5) |
| CuS | Cu2p (I) | 932.6±0.2 | 1.7 | GL(90)T(1.5) |
| FeS | Fe2p (I) | 708.6±0.1 | 1.7 | GL(75) |
| | Fe2p (II) | 710.5±0.1 | 1.7 | GL(75) |
| | Fe2p (III) | 713±0.1 | 1.7 | GL(75) |

### 5.1.7 The chemical state plot of metal sulphides

Sulphur of transition metals (FeS, CuS, $Cu_2S$) in the freshly-cleaved state show S2p binding energies at ca. 162 eV. The S2p and SKLL spectra (figure 5.13) exhibit (to a varying extent) two peaks in addition to the signal from sulphates. In the chemical state plot (figure 5.15) the transition metal sulphides appear as a distinct group with the most positive kinetic energies and an Auger parameter of 2278 ± 0.2 eV. The position of the second, weak peak at a binding energy of ca. 164 eV in the chemical state plot (open circles) decreases from FeS to $Cu_2S$. Thus, the chemical state of the sulphur compound on the surface of the cleaved samples is strongly influenced by the type of cation. It is interesting to notice that the position of the small peak of $Cu_2S$ falls on the line where elemental sulphur and the weak peak of the alkali sulphides are located (Auger parameter 2277 eV).

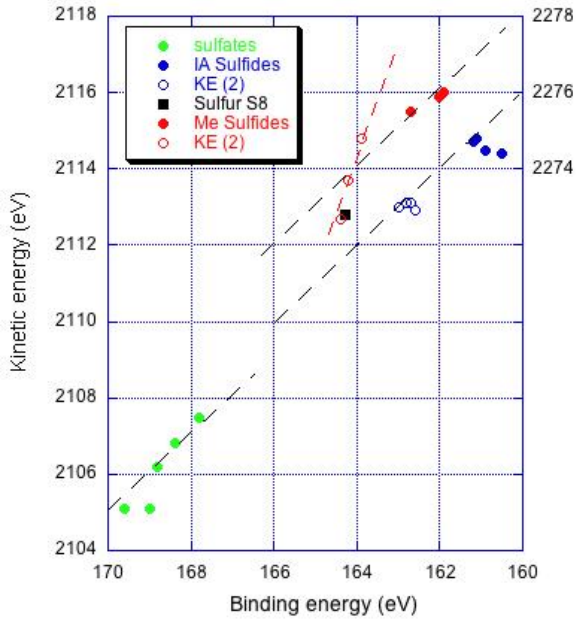


*Figure 5.15:* Chemical state plot of transition metal sulphides (the other compounds are shown for comparison)

## 5.1.8 Effect of grinding time of polysulphides

*a) Sodium tetrasulphide ($Na_2S_4$)*

Sodium tetrasulphide is tetragonal, crystallized in space group I42d and the crystal structure is built up of unbranched $S_4^{2-}$ ions surrounded by $Na^+$ ions [20]. The sodium-sulphur system was studied in the past and the existence and stability of $Na_2S_n$ with n=1, 2, 3, 4 and 5 was proven. Sodium hexasulphide does not exist [21]. Sodium tetrasulphide can be used as mercury capturing agent in a novel mercury control technology for solid waste incineration [22]. This sample appears as a yellow/brown powder and was analyzed "as received" and after different grinding times (5 and 20 minutes). The high-resolution spectra after different grinding times are shown in figure 5.16.

Figures 5.16 (a), (c) and (e) show the high-resolution spectra of the S2p region. In all the spectra three components can be distinguished. The first component is found at 160.3 eV in the as received sample and can be ascribed to sulphide [11]. This component exhibits a shift at higher binding energy values with grinding time. After 20 minutes grinding it is found at 161.3 eV. The second component is found at 162.0 eV in the as received sample and its binding energy increases upon grinding time; after 20 minutes it is found at 163.0 eV. This component is assigned to polysulphide. The component at higher B.E. values (168.4 eV) is assigned to the sulphate. The intensity of the sulphate component decreases from 14% in the as received sample to 4% after 20 minutes grinding. The area ratio between sulphide and polysulphide components increases from 0.17 in the as received sample to 0.63 after 20 minutes grinding. The binding energies of the S2p signals, the kinetic energies of the SKLL signals and all curve-fitting parameters are summarized in table 5.11.

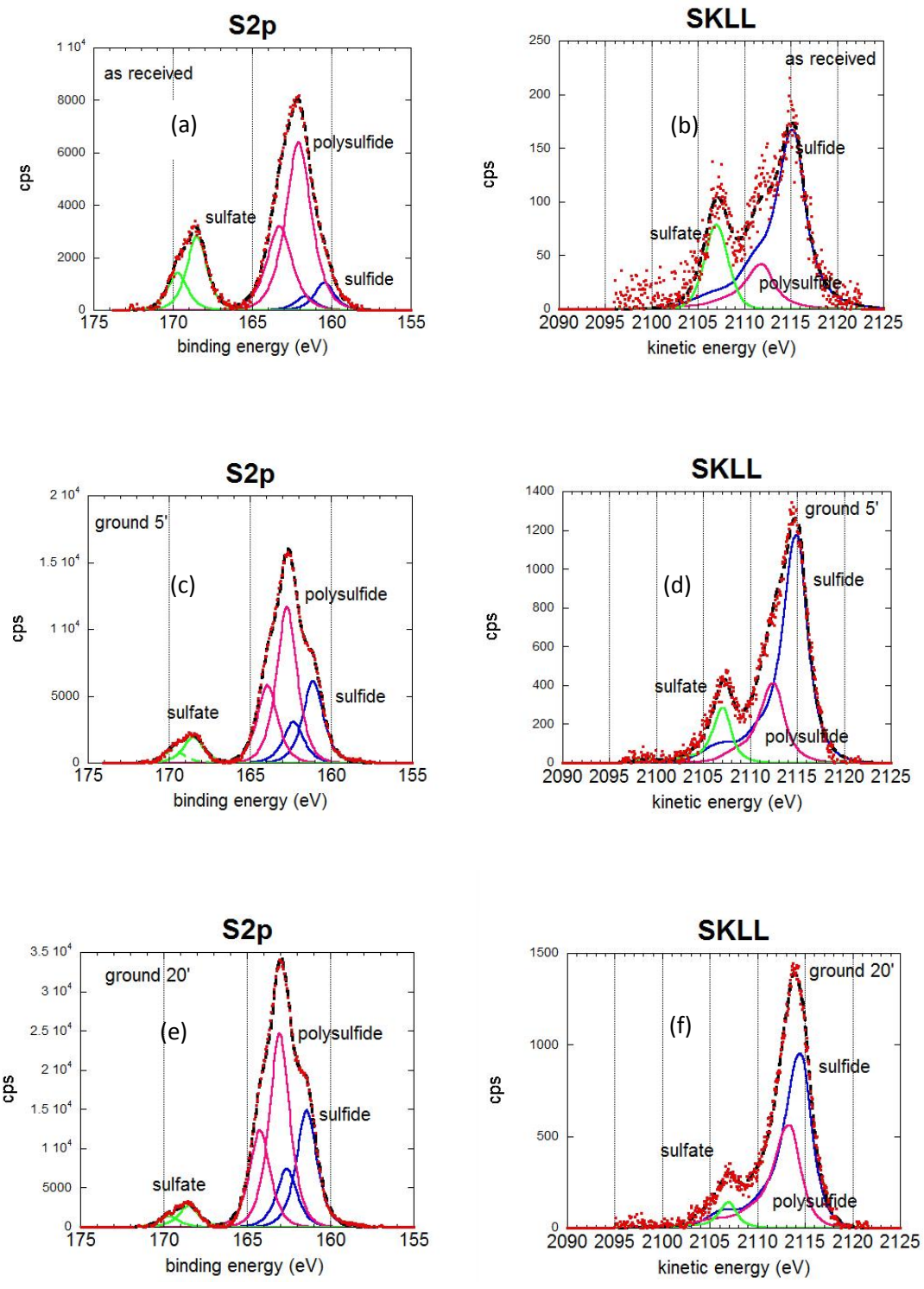


*Figure 5.16:* S2p and SKLL high-resolution spectra of sodium tetrasulphide analysed as received and after different grinding times: as received (a and b); 5 minutes (c and d); 20 minutes (e and f). ESCALAB MK II - Source: Al Kα (15mV * 20mA)

*Table 5.11:* S2p binding energies, SKLL kinetic energies and fitting parameters of the different components in sodium tetrasulphide after different times of grinding

| **Sample** | **Signal** | **BE (eV)** | **KE (eV)** | **FWHM** | **Line Shape** | **$A_{signal}/A_{main\ peak}$** | **$KE_{polysulphide}$-$KE_{line}$** |
|---|---|---|---|---|---|---|---|
| As received | $S2p_{sulphide}$ | 160.3 | - | 1.5 | GL(75) | 0.13 | - |
| | $S2p_{polysulphide}$ | 162.0 | - | 1.5 | GL(75) | 1 | - |
| | $S2p_{sulphate}$ | 168.4 | - | 1.5 | GL(75) | 0.36 | - |
| | $SKLL_{sulphide}$ | - | 2115.3 | 3.0 | GL(80)T(1.5) | - | 3.4 |
| | $SKLL_{polysulphide}$ | - | 2111.9 | 3.0 | GL(80)T(1.5) | - | 0 |
| | $SKLL_{sulphate}$ | - | 2107.2 | 2.1 | GL(95)T(1.8) | - | 8.1 |
| Ground 5’ | $S2p_{sulphide}$ | 160.8 | - | 1.5 | GL(75) | 0.50 | - |
| | $S2p_{polysulphide}$ | 162.5 | - | 1.5 | GL(75) | 1 | - |
| | $S2p_{sulphate}$ | 168.4 | - | 1.5 | GL(75) | 0.17 | - |
| | $SKLL_{sulphide}$ | - | 2115.1 | 2.5 | GL(80)T(1.5) | - | 1.5 |
| | $SKLL_{polysulphide}$ | - | 2113.6 | 2.5 | GL(80)T(1.5) | - | 0 |
| | $SKLL_{sulphate}$ | - | 2107.4 | 1.9 | GL(95)T(1.8) | - | 7.7 |
| Ground 20’ | $S2p_{sulphide}$ | 161.3 | - | 1.4 | GL(75) | 0.60 | - |
| | $S2p_{polysulphide}$ | 163.0 | - | 1.4 | GL(75) | 1 | - |
| | $S2p_{sulphate}$ | 168.4 | - | 1.4 | GL(75) | 0.11 | - |
| | $SKLL_{sulphide}$ | - | 2114.8 | 2.9 | GL(80)T(1.5) | - | 1.4 |
| | $SKLL_{polysulphide}$ | - | 2113.4 | 2.9 | GL(80)T(1.5) | - | 0 |
| | $SKLL_{sulphate}$ | - | 2107.0 | 1.8 | GL(95)T(1.8) | - | 7.8 |

Figure 5.16 (b), (d) and (f) shows the high-resolution spectra of the x-ray induced SKLL region. The kinetic energy of sulphide component decreases from 2115.3 eV in the as received sample to 2115.1 eV to 2114.8 eV in the sample ground for 20’ (Table 5.11) . In contrast the kinetic energy of the polysulphide component first increases

from 2111.9 eV in the as received sample to 2113.4 eV after 20 minutes grinding. The difference between the two components decreases from 3.4 eV to 1.4 eV after 20 minutes grinding.

*b) Sodium disulphide ($Na_2S$)*

$Na_2S$ is characterized by the antifluorite structure, which means that the $Na^+$ centers occupy sites of the fluoride in the $CaF_2$ lattice, and the larger $S^{2-}$ occupy the sites for $Ca^{2+}$. This sample appears as white irregular and small pieces that was analysed as received and after different grinding times (5 minutes and 20 minutes). During the analysis the colour of the sample became purple.

Figures 5.17 (a), (c) and (e) show the high-resolution spectra of the S2p region. In all the spectra three components can be observed. The first component is found at 161.1 eV in the as received sample and at 160.8 in the sample ground for 20 minutes; it can be ascribed to sulphide [11]. The second component is found at 163.1 eV in the as received sample and at 162.5 eV in the sample ground for 20 minutes. This component is assigned to polysulphide and the one at 168.4 eV to sulphate. The kinetic energies of the first component (sulphides) in the SKLL spectra (Fig. 5.17 (b), (c) and (d)) increases from 2112.8 eV to 2115.0 eV with increasing grinding time. The second component, assigned to polysulphides increases as well from 2109.9 eV to 2112.6 eV. All the curve-fitting parameters are summarized in table 5.12.

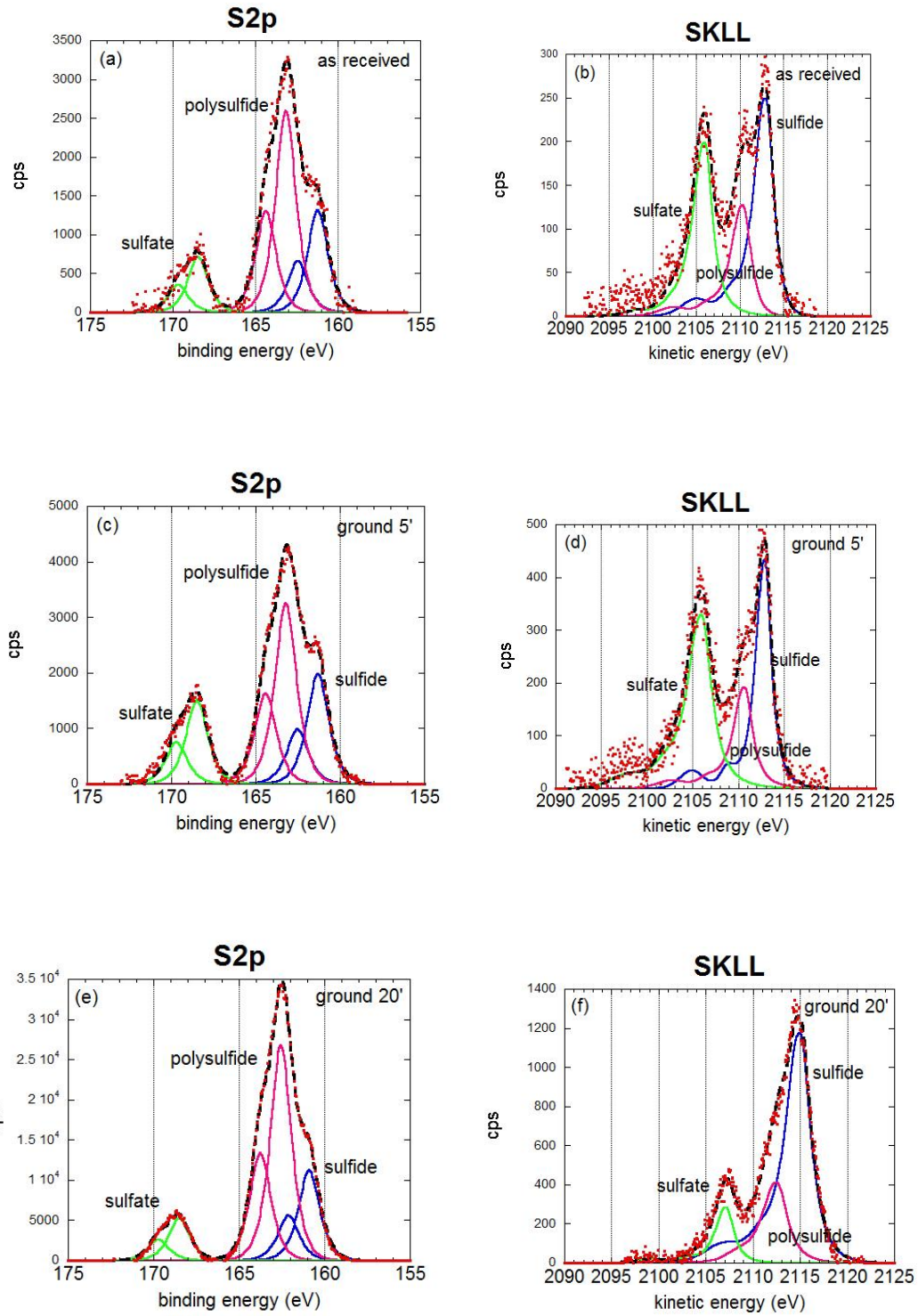


*Figure 5.17:* high-resolution spectra of S2p and SKLL regions of sodium sulphide analysed as received and after different grinding time: as received (a and b); 5 minutes

grinding (c and d); 20 minutes grinding (e and f). ESCALAB MK II - Source: Al Kα (15mV * 20mA)

*Table 5.12:* S2p Binding energy, SKLL kinetic energy and curve fitting parameters of the different components in sodium disulphide. Kinetic energies of the main peak $^1$D SKLL are only listed

| **Sample** | **Signal** | **BE (eV)** | **KE (eV)** | **FWHM** | **Line Shape** | **$A_{signal}$/ $A_{polysulphide}$** | **$KE_{polysulphide}$- $KE_{line}$** |
|---|---|---|---|---|---|---|---|
| As received | $S2p_{sulphide}$ | 161.1 | - | 1.4 | GL(75) | 0.51 | - |
| | $S2p_{polysulphide}$ | 163.1 | - | 1.4 | GL(75) | 1 | - |
| | $S2p_{sulphate}$ | 168.4 | - | 1.4 | GL(75) | 0.28 | - |
| | $SKLL_{sulphide}$ | - | 2112.8 | 3.0 | GL(95) T(1.8) | 0.5 | 2.9 |
| | $SKLL_{polysulphide}$ | - | 2109.9 | 3.0 | GL(95) T(1.8) | 1 | 0 |
| | $SKLL_{sulphate}$ | - | 2105.7 | 2.0 | GL(95) T(1.8) | 0.88 | 7.1 |
| Ground 5’ | $S2p_{sulphide}$ | 161.2 | - | 1.5 | GL(75) | 0.61 | - |
| | $S2p_{polysulphide}$ | 163.1 | - | 1.5 | GL(75) | 1 | - |
| | $S2p_{sulphate}$ | 168.4 | - | 1.5 | GL(75) | 0.46 | - |
| | $SKLL_{sulphide}$ | - | 2113.0 | 2.3 | GL(95) T(1.8) | 0.55 | 2.5 |
| | $SKLL_{polysulphide}$ | - | 2110.5 | 2.3 | GL(95) T(1.8) | 1 | 0 |
| | $SKLL_{sulphate}$ | - | 2105.8 | 2.3 | GL(95) T(1.8) | 1.15 | 7.2 |
| Ground 20’ | $S2p_{sulphide}$ | 160.8 | - | 1.4 | GL(75) | 0.42 | - |
| | $S2p_{polysulphide}$ | 162.5 | - | 1.4 | GL(75) | 1 | - |
| | $S2p_{sulphate}$ | 168.4 | - | 1.4 | GL(75) | 0.20 | - |
| | $SKLL_{sulphide}$ | - | 2115.0 | 2.6 | GL(95) T(1.8) | - | 2.4 |
| | $SKLL_{polysulphide}$ | - | 2112.6 | 2.6 | GL(95) T(1.8) | - | 0 |
| | $SKLL_{sulphate}$ | - | 2107.2 | 2.6 | GL(95) T(1.8) | - | 7.6 |

*Grinding effect on $Na_2S_4$*

With increasing time of grinding the percentages of Na and S at the surface of $Na_2S_4$ are changing in parallel to the decreasing oxygen (sulphate) content. The sample that underwent the longest grinding time exhibits a composition close to the stoichiometric one (Fig. 5.18).

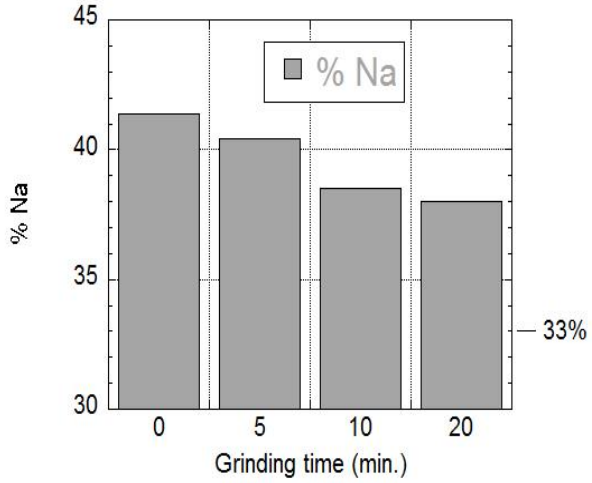


*Figure 5.18 :* $Na_2S_4$ surface composition versus grinding time.

With increasing grinding time not only the surface composition reaches the stoichiometric one but the binding energies of sulphides and polysulphides S2p line of $Na_2S_4$ increase and the kinetic energies of the SKLL lines decrease. No conclusion may be drawn from this information alone. Combining the binding energy of S2p photoelectron signals with the kinetic energy of SKLL lines the two-dimensional chemical state plot is obtained (figure 5.19). From this plot different information can be drawn. First, it is possible to clearly distinguish between the region of existence of

sulphides (red and blue full dots), sulphates (green dots) and polysulphides (open dots).

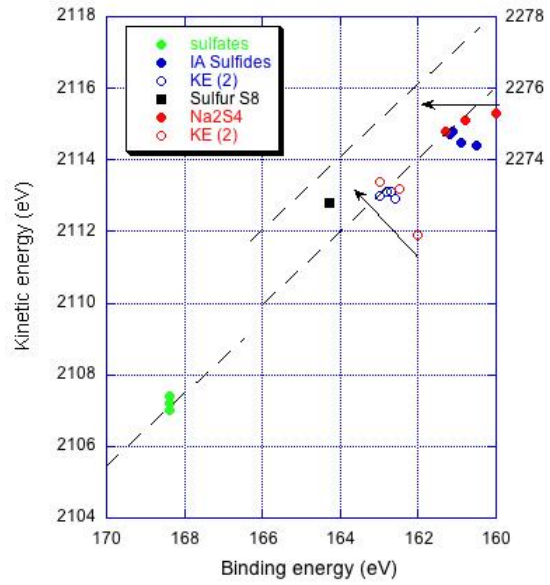


*Figure 5.19:* Chemical state plot of $Na_2S_4$ samples after different grinding times.

Second the Auger parameter is found to be between 2275.6 eV and 2276.1 eV for the sulphides, between 2273.9 eV and 2276.4 eV for the polysulphides, and it is 2275.6 eV for the sulphates.

It might be concluded that prolonged grinding seems to promote the sulphur polymerization that might end with the formation of elemental sulphur. This finding suggests that the chemical state plot allows to following the changes in the surface chemistry of sulphide-bearing materials subjected to different processes.

## 5.2 Model systems: mixtures of sodium tetrasulphide and elemental sulphur

In order to test to what extent the contribution of sulphide and of polysulphide in the S2p and SKLL signals could be separated, two model systems made mixing sodium tetrasulphide and elemental sulphur, $Na_2S_4$ - $S_8$ were prepared by separately grinding each compound in an agate mortar for 5 minutes and then mixing them together and grinding for five further minutes. The two mixtures were made up with two different ratios of the components: 42% $Na_2S_4$ - 58% $S_8$ and 16% $Na_2S_4$ - 84% $S_8$. Figure 5.20 shows the survey spectra of the two mixtures, acquired with Al Kα source. The survey spectra confirm the absence of elements different from those expected.

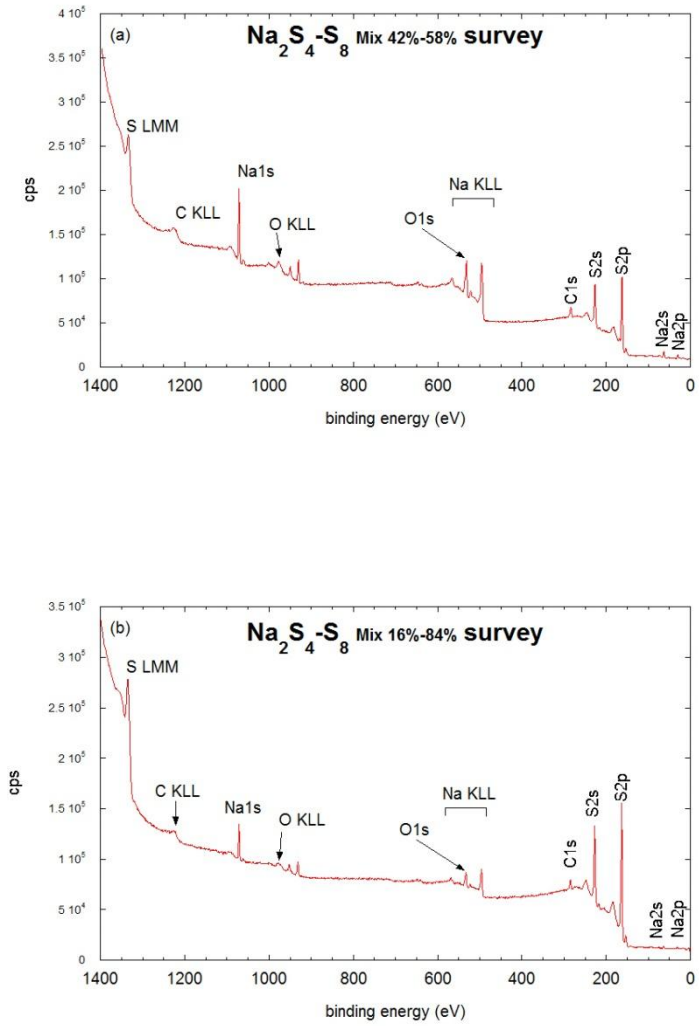


*Figure 5.20:* survey spectra of sodium tetrasulphide-elemental sulphur mixtures: (a) 42% $Na_2S_4$ - 58% $S_8$ and (b) 16% $Na_2S_4$ - 84% $S_8$

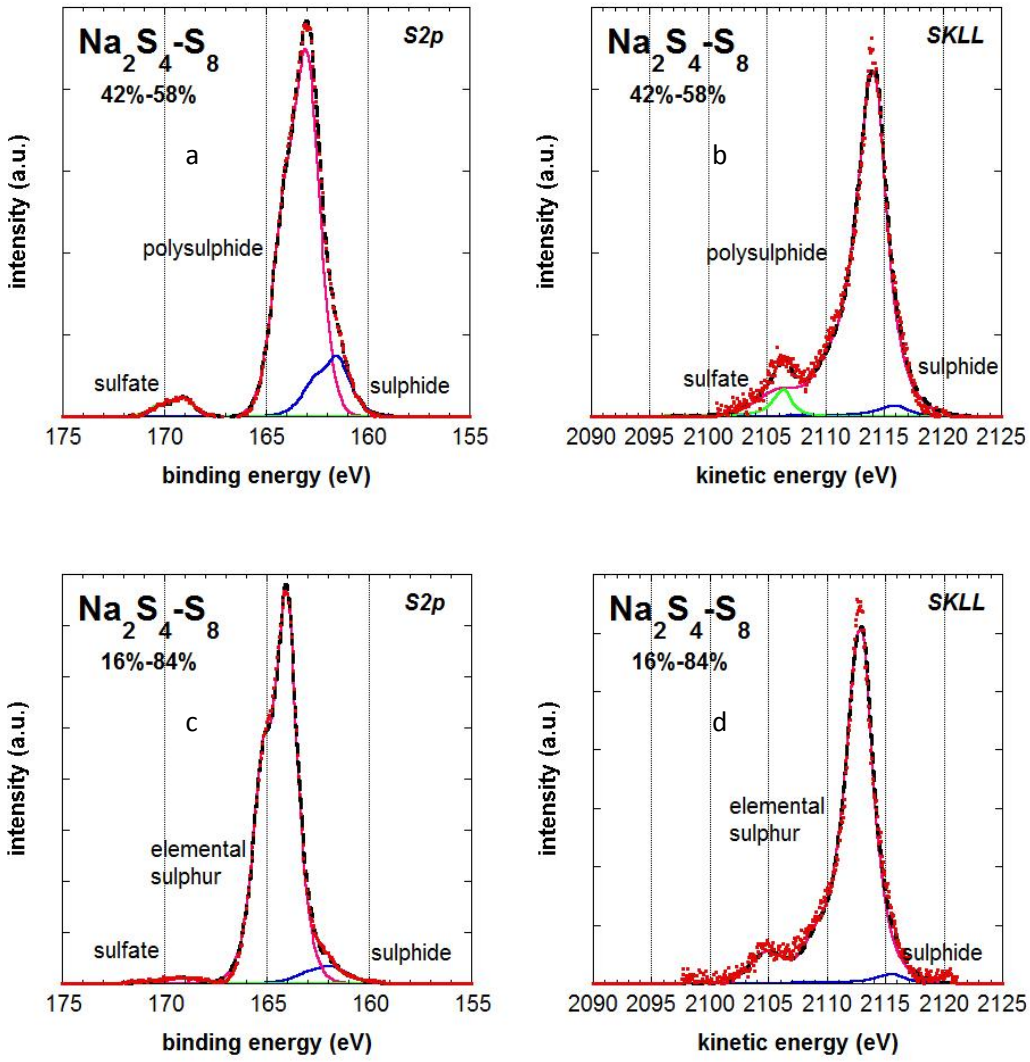


*Figure 5.21:* High-resolution spectra of S2p and SKLL regions of sodium tetrasulphide-elemental sulphur mixtures: 42% $Na_2S_4$ - 58% $S_8$ (a) and (b); 16% $Na_2S_4$ - 84% $S_8$ (c) and (d). Source: Al Kα.

Figure 5.21a shows the high-resolution spectrum of the S2p signal of 42% $Na_2S_4$ - 58% $S_8$ mixture, acquired with the Al Kα source. This signal presents three doublets. The component which is found at the lowest binding energy value, 161.5 eV, can be assigned to the sulphide (figure 5.21, table 5.13), the second one at 163.0 eV can be assigned to the polysulphide and the third one, at 169.1 eV, can be assigned to

sulphates. Figure 5.21c shows the high-resolution spectrum of S2p signal of 16% $Na_2S_4$ - 84% $S_8$ mixtures, acquired with Al Kα source. This signal too presents three components, but the contribution of the minor constituent of the mixture, sodium tetrasulphide, is very low. The assignment of the components is the same as above: at the lowest binding energy, 161.8 eV, sulphide component is found, whereas the second component at 164.0 eV can be assigned to elemental sulphur and the third one 169.1 eV to sulphate. The curve fitting components for S2p signals of the mixtures are reported in table 5.13.

*Table 5.13*: S2p Binding energies, SKLL kinetic energies and fitting parameters of the components in sodium tetrasulphide - elemental sulphur mixtures.

| **$Na_2S_4$-$S_8$ mix** | **Signal** | **BE (eV)** | **KE (eV)** | **FWHM** | **Line Shape** |
|---|---|---|---|---|---|
| 42%-58% | $S2p_{sulphide}$ | 161.5 | - | 1.4 | GL(75) |
| | $S2p_{polysulphide}$ | 163.0 | - | 1.4 | GL(75) |
| | $S2p_{sulphate}$ | 169.1 | - | 1.2 | GL(75) |
| | $SKLL_{sulphide}$ | - | 2116.4 | 2.1 | GL(95)T(1.8) |
| | $SKLL_{polysulphide}$ | - | 2114.2 | 2.1 | GL(95)T(1.8) |
| | $SKLL_{sulphate}$ | - | 2106.5 | 2.1 | GL(35) |
| 16%-84% | $S2p_{sulphide}$ | 161.8 | - | 1.4 | GL(75) |
| | $S2p_{el.sulphur}$ | 164.0 | - | 1.3 | GL(75) |
| | $S2p_{sulphate}$ | 169.1 | - | 1.5 | GL(75) |
| | SKLL(1D) | - | 2115.7 | 3.1 | GL(90)T(3.5) |
| | SKLL(sat) | - | 2112.9 | 3.1 | GL(75) |

Figure 5.21b shows SKLL Auger spectrum of 42% $Na_2S_4$ - 58% $S_8$ mixture acquired with Al Kα source. Also in this spectrum three components can be revealed as in the

S2p photoelectron signal. Sulphide component has the higher values, 2116.4 eV in KE, at 2114.2 eV there is a polysulphide component and at 2106.5 eV the sulphate component is found. Only two peaks at 2115.7 eV and 2112.9 eV are detected for sulphide and elemental sulphur in 16% $Na_2S_4$ - 84% $S_8$ mixture.

In the chemical state plot of the $Na_2S_4$ - $S_8$ mixtures (figure 5.22) the points for the two mixtures can be found on the same diagonal line as elemental sulfur, the points for the sulfides show a slightly higher Auger parameter α'. Thus, even if the binding energy and the kinetic energy of the sulphur contribution in the mixture do not match those of elemental sulfur, the chemical state remains that of elemental sulphur.

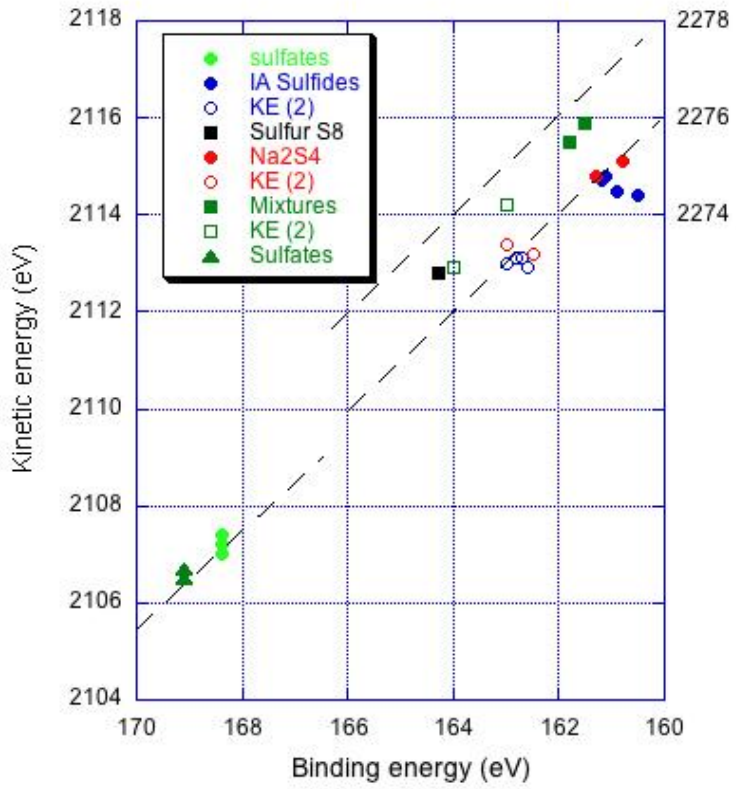


*Figure 5.22:* Chemical state plot of the $Na_2S_4$ - $S_8$ mixtures. Sulfides and elemental sulphur are given for comparison.

In 42% $Na_2S_4$ - 58% $S_8$ both the binding energies and kinetic energies values are different from those observed for elemental sulphur (§ 5.1.2) and for $Na_2S_4$ (§5.1.4). The reason of the observed shifts could be attributed to the reaction that can occur between sulphur and sulphide/polysulphide leading to polymerization and production of polysulphides with different chain lengths.

## 5.3 Minerals

The minerals used are various sulfides such as pyrite ($FeS_2$), enargite ($Cu_3AsS_4$), arsenopyrite (FeAS), chalcopyrite ($CuFeS_2$). S2p photoelectron and SKLL x-ray induced Auger signals were studied, for the first time by means of accurate analysis of SKLL signals, for a more clear assignment of the sulfur component located in the proximity of binding energy of 163.5 eV. All minerals (except pyrite, $FeS_2$) were analyzed immediately after cleavage, after grinding and after one week air exposed. The minerals were fractured and ground inside a glove box, and with the powders thus produced pellets were pressed and mounted on bi-adhesive tape. The transfer to the spectrometer analysis chamber was performed without contact to the atmosphere, using a bell device [1] that could be closed inside the glove box and opened inside the analysis chamber. All spectra acquired were fitted using the parameters obtained on the reference compounds (§ 5.1). For each sample survey spectra and high-resolution spectra of S2p, SKLL and various ions bonded to sulfur were recorded.

### 5.3.1 Pyrite

Pyrite is a most common sulfide mineral Figure 5.23 shows survey spectra of pyrite freshly cleaved and after 10 min grinding in acetone or in air. The spectra show that no contaminants are present. The signal of adventitious carbon, fixed at 285.0 eV, was used to compensate for sample charging. Afterwards curve fitting of XPS/XAES signals and quantitative analysis were performed; the high-resolution spectra of S2p and SKLL are shown in figure 5.24 In table 5.14 binding energy values of

photoelectron S2p and Fe2p signals as well as kinetic energy values for SKLL Auger signals are summarized, together with peak fitting parameters.

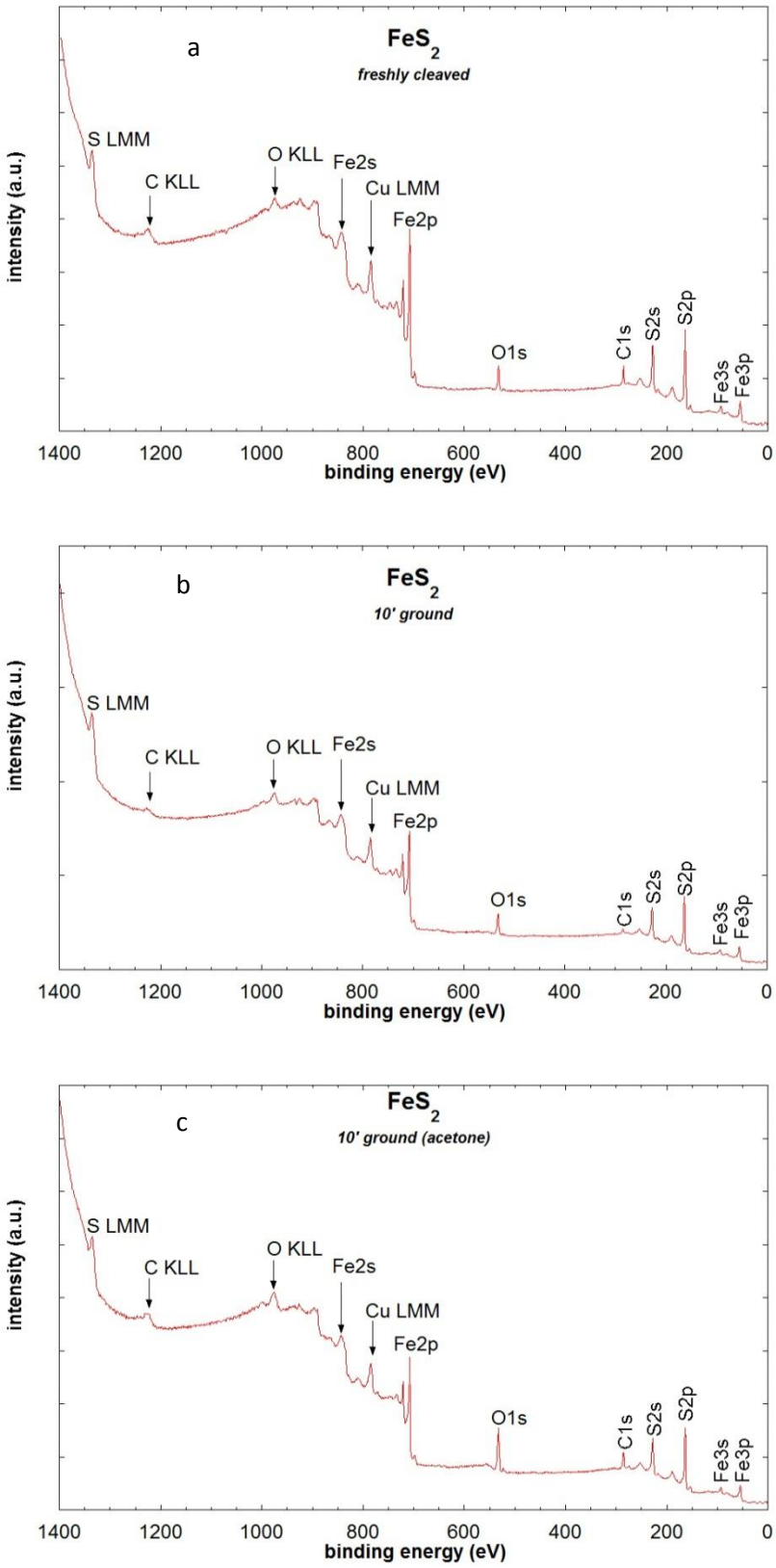


*Figure 5.23:* survey spectra of pyrite (a) freshly cleaved, (b) 10 min grinding, (c) 10 min grinding in acetone

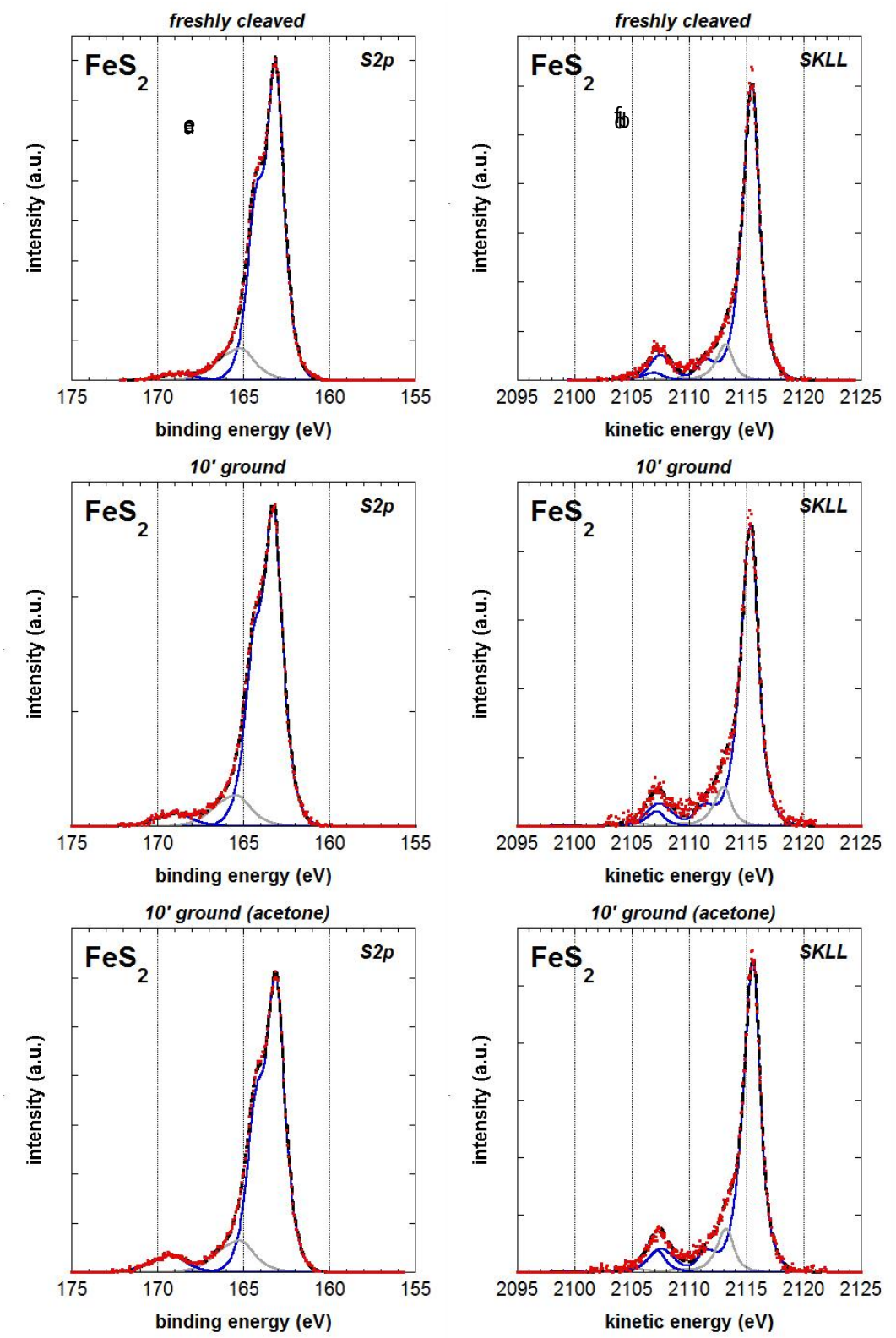


*Figure 5.24:* High-resolution spectra of S2p and SKLL of pyrite freshly cleaved (a, b), after 10 minutes grinding in air (c, d) and after10 minutes grinding in acetone (e, f).

Figure 5.24 (a) shows high resolution spectrum of S2p signal acquired with Al Kα source. Curve fitting parameters are summarized in Table 5.14.

*Table 5.14:* Binding energy, kinetic energy and curve fitting parameters of the different components in the sulfur S2p, Fe2p3/2 and SKLL signals.

| | Line | Bindig/Kinetic Energy (eV ± 0.2) | FWHM (eV) | Line Shape |
|---|---|---|---|---|
| $FeS_2$ Freshly cleaved | S2p 3/2 (a) | 163.0 | 1.2 | GL(75) |
| | S2p 3/2 (b) | 165.1 | 1.9 | GL(75) |
| | S2p 3/2 (c) | 168.9 | 1.9 | GL(75) |
| | SKLL ($^1$D) (a) | 2115.8 | 1.4 | GL(95)T(1.8) |
| | SKLL ($^1$D) (b) | 2113.5 | 1.4 | GL(95)T(1.8) |
| | SKLL ($^1$D) (c) | 2107.2 | 1.7 | GL(95)T(1.8) |
| | Fe2p3/2 | 707.5 | 1.0 | GL(98)T(1.2) |
| | Fe2p3/2 | 710.4 | 3.5 | GL(40) |
| $FeS_2$ 10 min ground air | S2p 3/2 (a) | 163.2 | 1.3 | GL(75) |
| | S2p 3/2 (b) | 165.3 | 1.9 | GL(75) |
| | S2p 3/2 (c) | 168.7 | 1.9 | GL(75) |
| | SKLL ($^1$D) (a) | 2115.4 | 1.5 | GL(95)T(1.8) |
| | SKLL ($^1$D) (b) | 2113.1 | 1.5 | GL(95)T(1.8) |
| | SKLL ($^1$D) (c) | 2107.2 | 1.5 | GL(95)T(1.8) |
| | Fe2p3/2 | 707.8 | 1.0 | GL(98)T(1.1) |
| | Fe2p3/2 | 711.0 | 3.8 | GL(40) |
| $FeS_2$ 10 min ground acetone | S2p 3/2 (a) | 163.1 | 1.2 | GL(75) |
| | S2p 3/2 (b) | 165.1 | 1.9 | GL(75) |
| | S2p 3/2 (c) | 169.0 | 1.8 | GL(75) |
| | SKLL ($^1$D) (a) | 2115.6 | 1.4 | GL(95)T(1.8) |
| | SKLL ($^1$D) (b) | 2113.3 | 1.4 | GL(95)T(1.8) |
| | SKLL ($^1$D) (c) | 2107.4 | 1.6 | GL(95)T(1.8) |
| | Fe2p3/2 | 707.7 | 1.0 | GL(98)T(1.1) |
| | Fe2p3/2 | 711.4 | 3.9 | GL(40) |

The binding energy of the main component is 163.0 (table 5.14) eV for the cleaved pyrite sample and no significant shifts are observed after grinding in air or in acetone.

This component is assigned to pyritic sulfur. A small component 165.1 eV could be due to sulfite, according to [23] and it does not show any shift after grinding The third and less intense component is found at about 169 eV and is ascribed to sulfate.

SKLL spectra show an intense component at 2115.8 eV for the cleaved sample, due to pyritic sulfur. Small shifts are observed for ground samples (2115.4 eV and 2115. 6 in air and acetone respectively). The second component is found at 2113.5 eV for cleaved pyrite and shows a small decrease in its value for acetone ground (2113.3 eV) and for air ground (2113.1 eV). The kinetic energy of the sulfate component is 2107. 2 eV for all samples.

High-resolution $Fe2p_{3/2}$ spectra are shown in Fig. 5.25. For each sample Fe2p3/2 exhibits two components (table 5.14). The most intense one is found at 707.5 eV for freshly cleaved pyrite (Fig. 5.25a) , at 707.8 for pyrite ground in air (Fig. 5.25c) and at 707.7 for pyrite ground in acetone (Fig. 5.25e) . This component can be assigned to pyritic iron. The second component shows a shift from 710.4 eV in freshly cleaved pyrite to 711.4 eV in pyrite ground in acetone. In freshly cleaved pyrite the second component is assigned to Fe (III) oxide, whereas in pyrite ground in acetone it is ascribed to Fe (III) – oxyhydroxide [18].

Figure 5.25(b, d, e) shows high-resolution spectra of O1s signal. There are three components: one at low BE, 530.8 eV, due to hydroxide species, the most intense at 532.2 eV ascribed to sulfate species and the last one at 534.0 eV due to the presence of water.

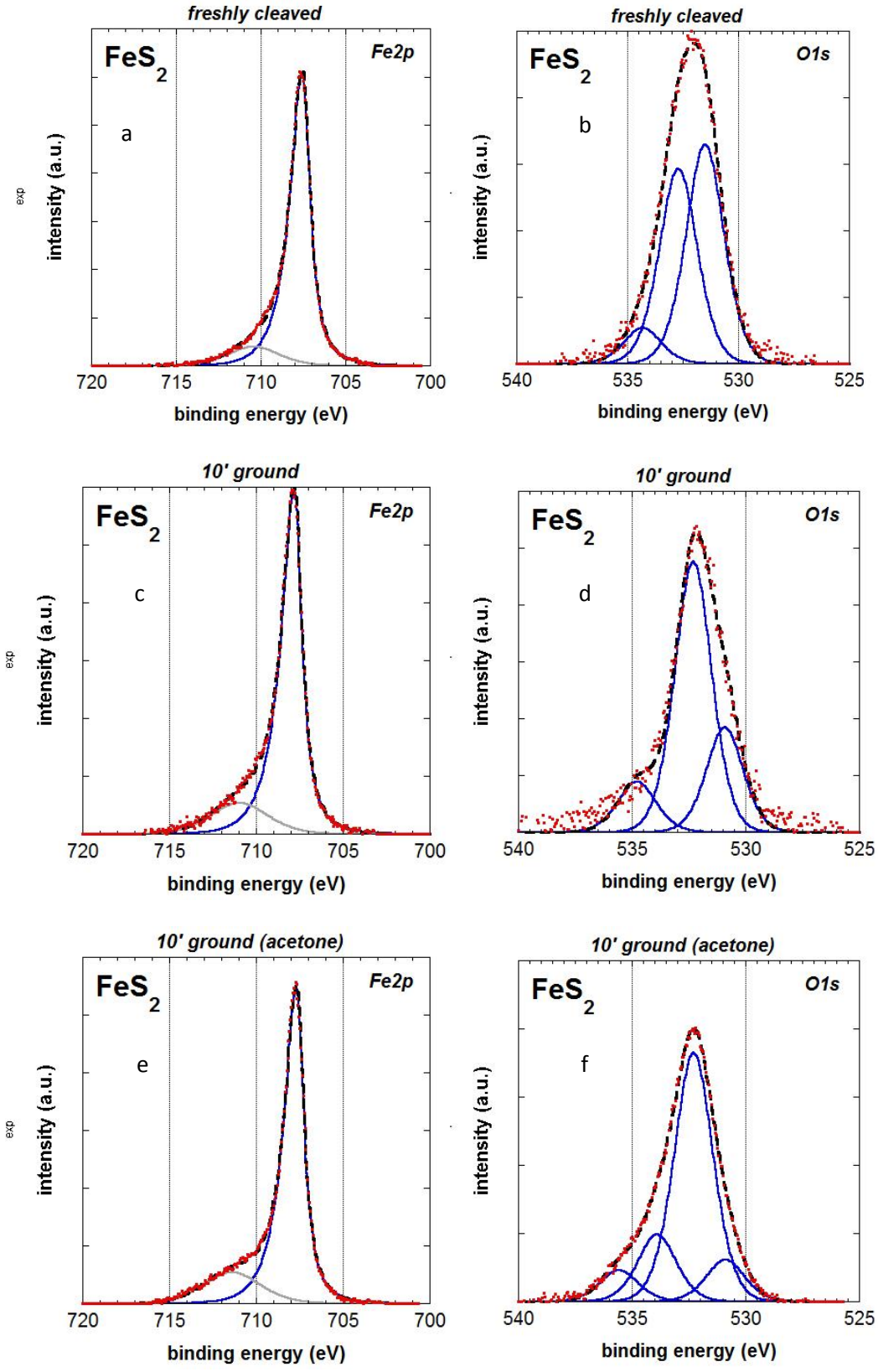


*Figure 5.25:* High-resolution spectra of Fe2p3/2 and O1s of pyrite freshly cleaved (a, b), after 10 minutes grinding in air (c, d) and after 10 minutes grinding in acetone (e, f)

### 5.3.2 Arsenopyrite

Arsenopyrite (FeAsS) crystals from a Chinese mine were analyzed by X-ray photoelectron spectroscopy after cleavage. The same crystal was analyzed after one week exposure to the laboratory atmosphere. XPS experiments on ground samples (10 minutes in glove box under argon atmosphere) were performed. Figure 5.18 shows the survey spectrum of freshly cleaved arsenopyrite. On the surface of freshly cleaved arsenopyrite crystals just elements belonging to FeAsS were detected, together with small amounts of oxygen and carbon. This is in agreement with XRD results that showed the presence of a pure FeAsS phase (§ 4.1.3).

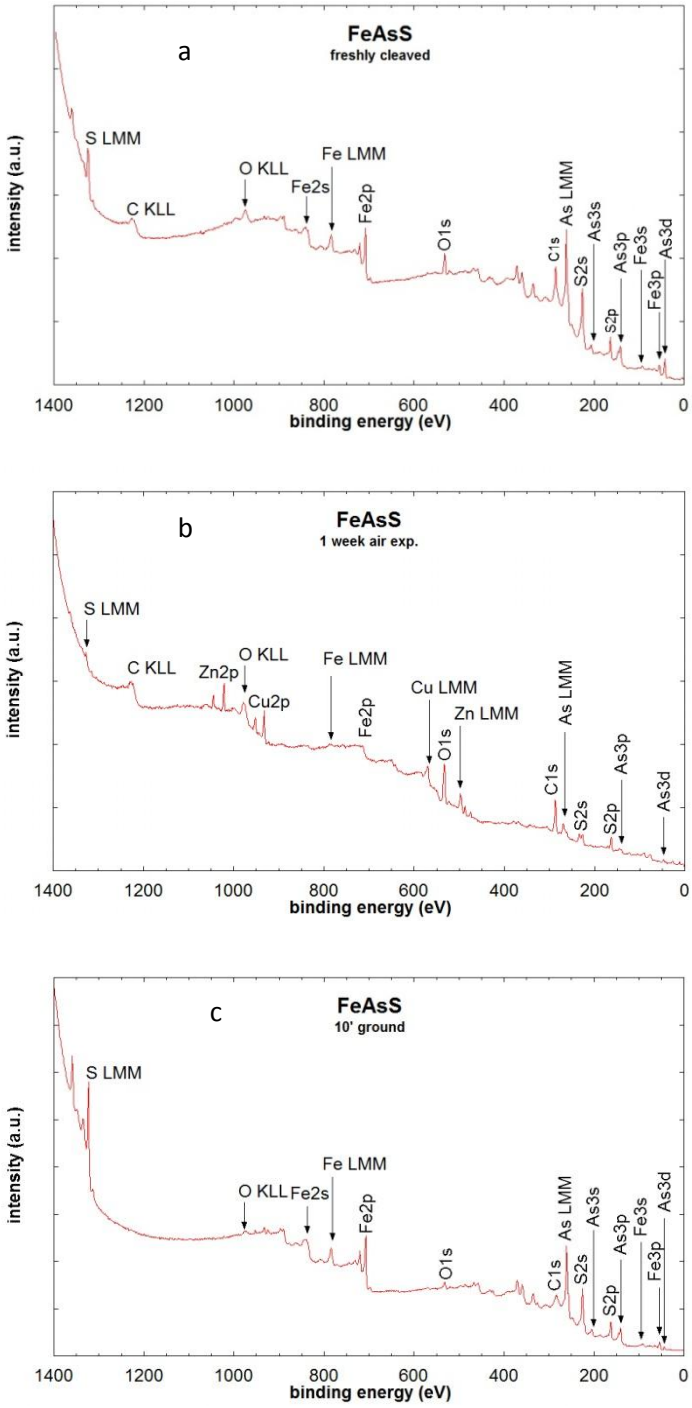


*Figure 5.26:* Survey spectra of arsenopyrite: freshly cleaved (a); exposed to air for one week (b) and ground (c).

S2p and SKLL high-resolution spectra are shown in figure 5.27 and peak fitting parameters are summarized in table 5.15.

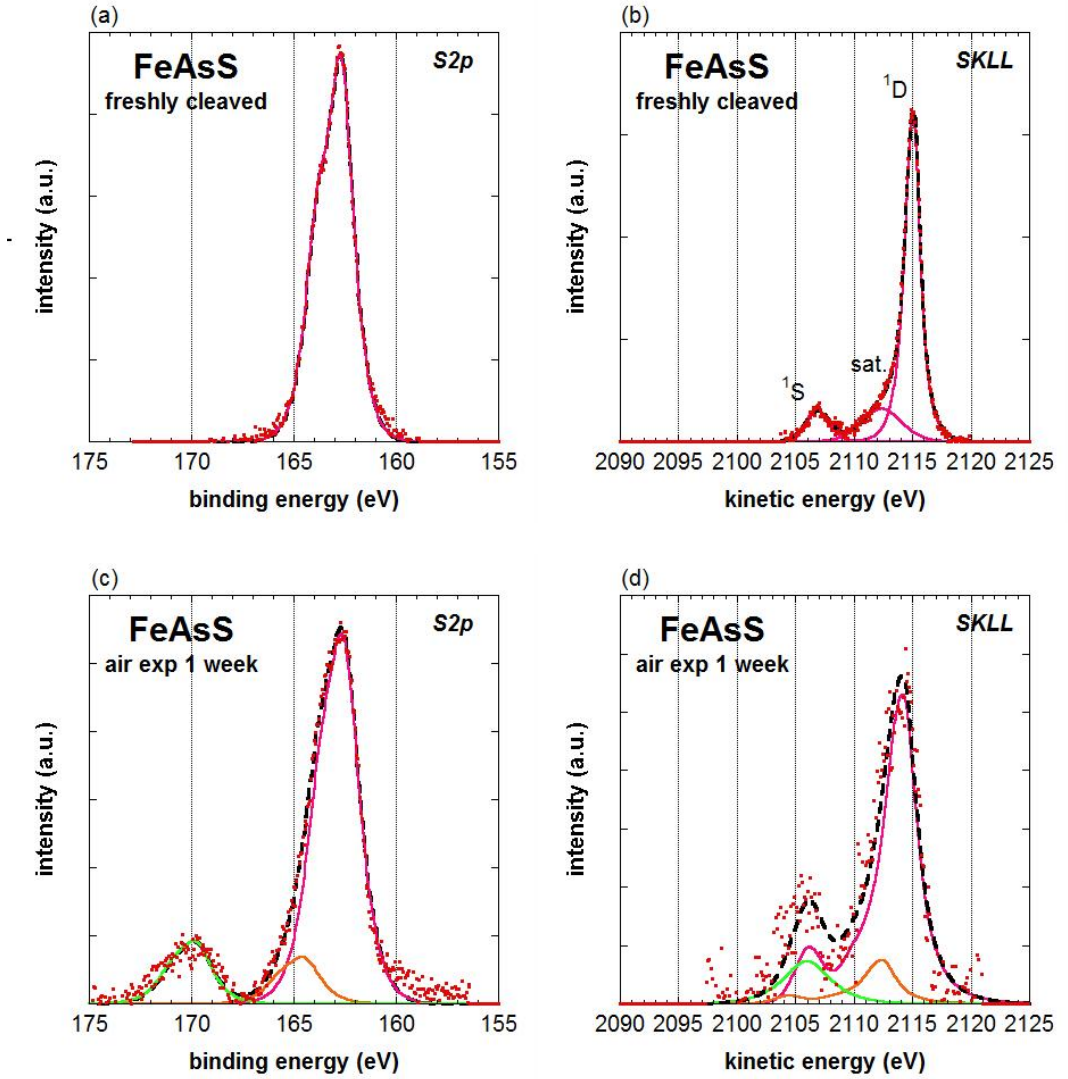

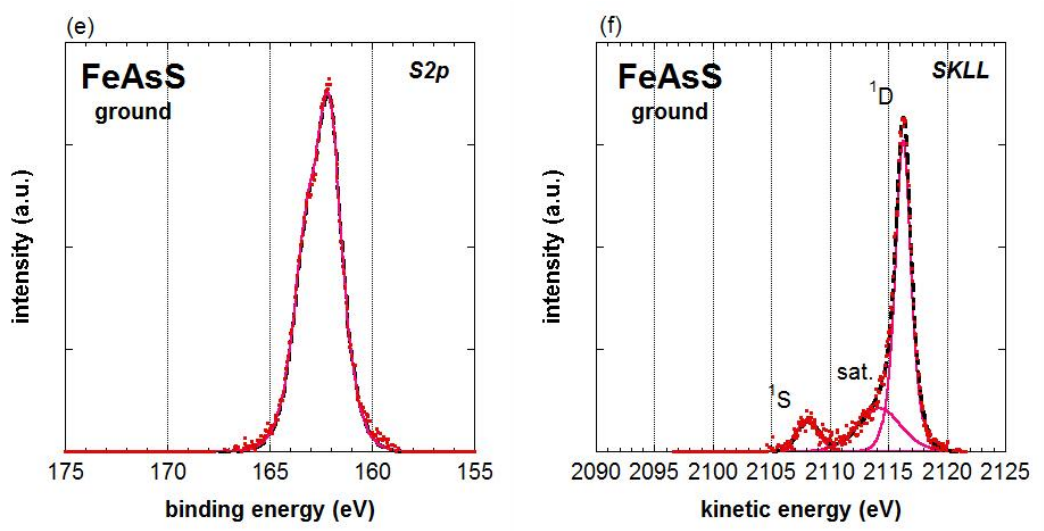


*Figure 5.27:* High-resolution spectra of S2p and SKLL of freshly cleaved arsenopyrite (a, b), after 10 minutes grinding in air (c, d) and 10 minutes grinding in acetone (e, f)

From the comparison of both S2p and SKLL spectra of the three different arsenopyrite samples it is possible to observe that air exposure leads to oxidation of arsenopyrite surface. Freshly cleaved (Fig. 5.27 a and b) and ground samples (Fig. 5.27 e and f) show just one component in the S2p and SKLL spectra (Table 5.15). Air exposure leads to oxidation of the surface and more than one component is present on S2p and SKLL spectra (Fig. 5.27 c and d). The most intense peak of freshly cleaved and air exposed FeAsS crystal can be ascribed to $(Fe\text{-}As)^{2-}$ according to [24]. The peak at 164.1 eV in air exposed arsenopyrite is close to elemental sulfur (see § 5.1.3) and the higher binding energy peak is assigned to sulfate (table 5.15).

*Table 5.15:* S2p and SKLL peak fitting parameters for arsenopyrite (FeAsS).

| | **Line** | **Binding/Kinetic Energy (eV ± 0.2)** | **FWHM (eV)** | **Line Shape** |
|---|---|---|---|---|
| freshly cleaved | S2p 3/2 (a) | 162.6 | 1.5 | GL(75) |
| | SKLL ($^1$D) (a) | 2115.3 | 1.6 | GL(95)T(1.8) |
| 1 week air exposed | S2p 3/2 (a) | 162.5 | 1.6 | GL(75) |
| | S2p 3/2 (b) | 164.1 | 1.9 | GL(75) |
| | S2p 3/2 (c) | 169.8 | 1.9 | GL(75) |
| | SKLL ($^1$D) (a) | 2114.6 | 2.2 | GL(95)T(1.8) |
| | SKLL ($^1$D) (b) | 2112.5 | 2.2 | GL(95)T(1.8) |
| | SKLL ($^1$D) (c) | 2105.7 | 1.8 | GL(95)T(1.8) |
| ground for 10' in glove box | S2p 3/2 (a) | 162.1 | 1.5 | GL(75) |
| | SKLL ($^1$D) (a) | 2116.4 | 1.6 | GL(95)T(1.8) |

### 5.3.3 Chalcopyrite

Chalcopyrite ($CuFeS_2$) samples were analyzed after cleavage inside the glove box. The same crystal was then analysed after one week of exposure to laboratory atmosphere. Chalcopyrite was also analyzed after ten minutes grinding inside the glove box for. Figure 5.28 shows survey spectra of freshly cleaved chalcopyrite.

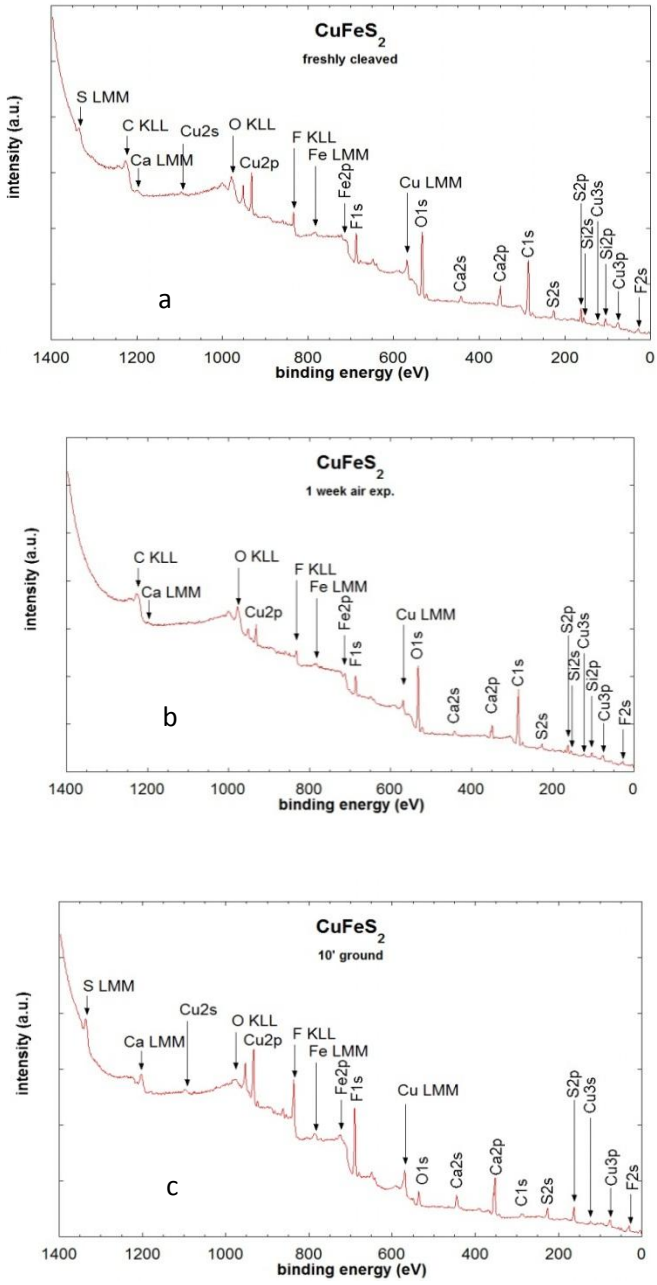


*Figure 5.28*: Survey spectra of freshly cleaved (a), exposed to air for one week (b) and ground (c) chalcopyrite $CuFeS_2$

From survey spectra (Fig. 5.28) it is possible to observe that not only copper, iron and sulfur, but also calcium, fluorine and small amount of silicon are present on the sample surface. These results confirm XRD results on chalcopyrite powder that

showed the presence not only of chalcopyrite phase but also other phases such as silica. S2p and SKLL high-resolution spectra are shown in figure 5.29 and peak fitting parameters are summarized in table 5.16.

*Table 5.16:* S2p and SKLL peak fitting parameter for $CuFeS_2$

| | **Line** | **Bindig/Kinetic Energy (eV ± 0.2)** | **FWHM (eV)** | **Line Shape** |
|---|---|---|---|---|
| freshly cleaved | S2p 3/2 (a) | 161.5 | 1.23 | GL(75) |
| | S2p 3/2 (b) | 163.4 | 1.9 | GL(75) |
| | S2p 3/2 (c) | 170.2 | 1.9 | GL(75) |
| | SKLL ($^1$D) (a) | 2115.3 | 1.6 | GL(95)T(1.5) |
| | SKLL ($^1$D) (b) | 2112.4 | 1.9 | GL(95)T(1.5) |
| | SKLL ($^1$D) (c) | 2106.6 | 1.9 | GL(95)T(1.5) |
| exposed for one week to atmosphere | S2p 3/2 (a) | 162.1 | 1.23 | GL(75) |
| | S2p 3/2 (b) | 164.0 | 1.9 | GL(75) |
| | S2p 3/2 (c) | 169.7 | 1.9 | GL(75) |
| | SKLL ($^1$D) (a) | 2114.7 | 1.5 | GL(95)T(1.5) |
| | SKLL ($^1$D) (b) | 2112.0 | 1.8 | GL(95)T(1.5) |
| | SKLL ($^1$D) (c) | 2106.6 | 2.0 | GL(95)T(1.5) |
| ground in glove box for 10 minutes | S2p 3/2 (a) | 162.2 | 1.23 | GL(75) |
| | S2p 3/2 (b) | 163.5 | 1.9 | GL(75) |
| | S2p 3/2 (c) | 165.1 | 1.9 | GL(75) |
| | SKLL ($^1$D) (a) | 2115.3 | 1.6 | GL(95)T(1.5) |
| | SKLL ($^1$D) (b) | 2112.7 | 1.9 | GL(95)T(1.5) |
| | SKLL ($^1$D) (c) | 2107.3 | 2.0 | GL(95)T(1.5) |

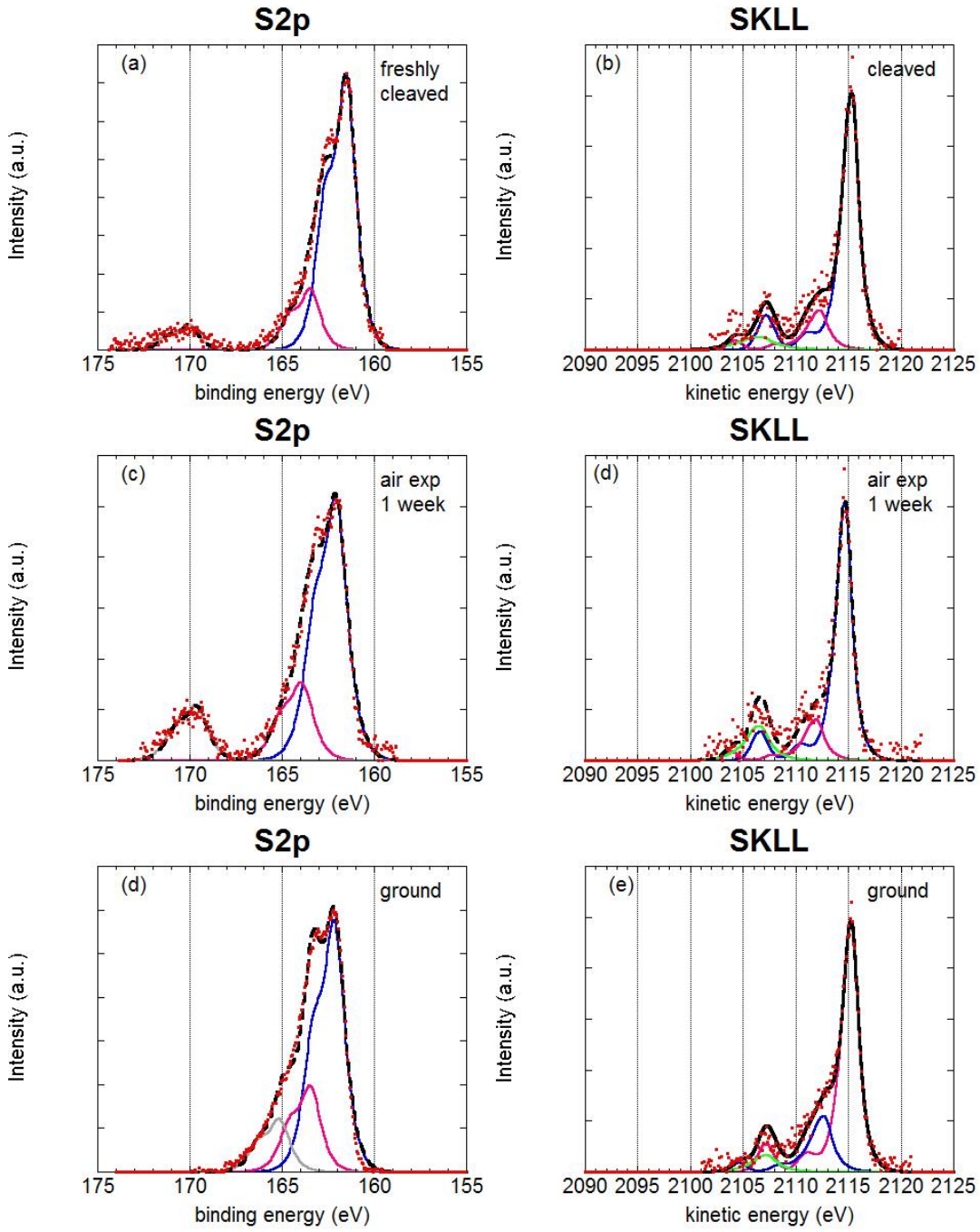


*Figure 5.29:* S2p and SKLL high resolution spectra of: freshly cleaved chalcopyrite crystal (a and b), crystal exposed after one week air exposure (c and d) and ground chalcopyrite (e and f).

The data in table 5.16 show that the most intense S2p peak shifts from 161.5 eV for the cleaved sample to 162.2 eV for the ground sample. The peak at 161.5 eV in the

S2p spectrum of the freshly cleaved sample can be assigned to chalcopyrite sulfide $S^{2-}$, in agreement with [25]. The peaks at higher binding energy values (162.1 eV and 162.2 eV respectively for chalcopyrite exposed to air and ground chalcopyrite) can be assigned to disulfide $S_2^{2-}$, those at 163.6 eV to polysulfide and the peak at 164.0 eV in air exposed chalcopyrite can be due to elemental sulfur or polysulfide. The curve fitting of SKLL and calculation of Auger parameter will permit to identify the chemical state of that sulfur species (see discussion chapter).

### 5.2.3 Enargite

Enargite ($Cu_3AsS_4$) crystals from Leonard Mine, Butte Montana, USA, were analyzed after cleavage inside the glove box. The same crystals were then analyzed after one week of exposure to laboratory atmosphere. Enargite was analyzed also after ten minutes grinding inside the glove box. Figure 5.30 shows survey spectra of freshly cleaved (a), exposed to atmosphere (b) and ground samples (c).

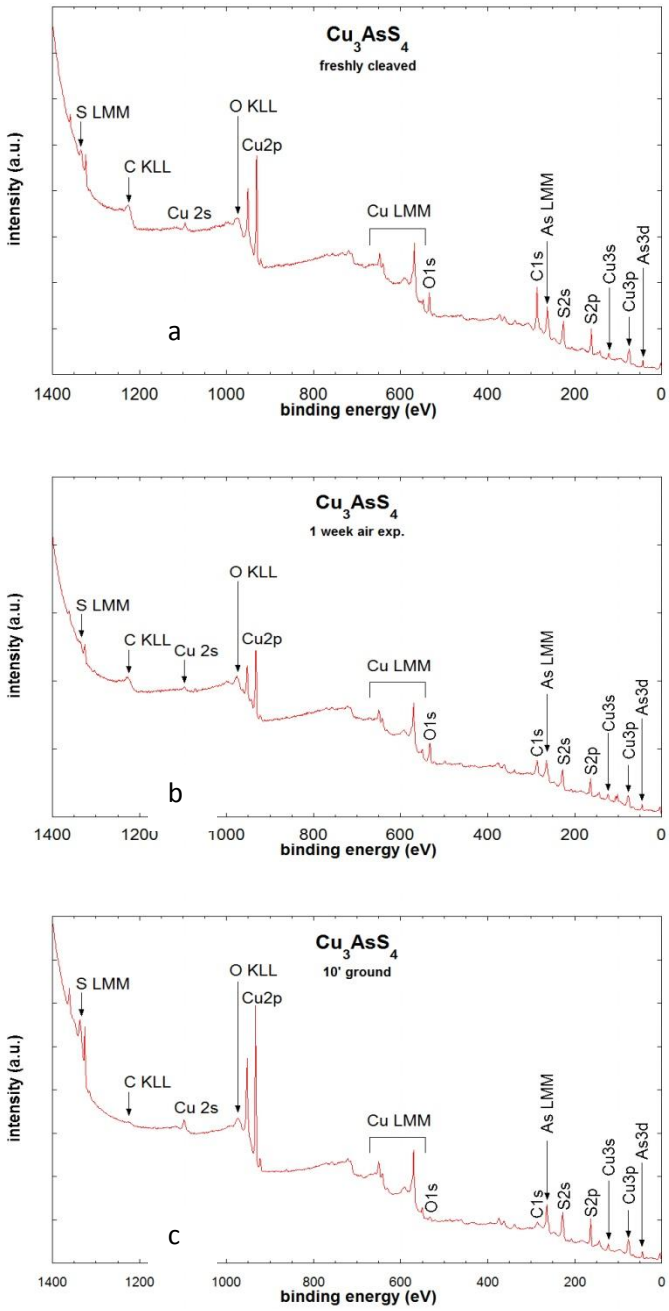


*Figure 5.30:* Survey spectra of freshly cleaved (a), exposed to air for one week (b) and ground (c) enargite $Cu_3AsS_4$

From survey spectra (Fig. 5.30) it is possible to observe that only copper, arsenic and sulfur are present on the sample surface, together with small amounts of carbon and oxygen. These results confirm XRD results on enargite powder that only showed the

presence of the enargite phase. S2p and SKLL high-resolution spectra are shown in figure 5.31 and peak fitting parameters are summarized in table 5.17.

*Table 5.17*: S2p and SKLL peak fitting parameter for $Cu_3AsS_4$.

| **$Cu_3AsS_4$ – freshly cleaved** | | | |
|---|---|---|---|
| Line | Bindig/Kinetic Energy (eV ± 0.2) | FWHM (eV) | Line Shape |
| S2p 3/2 (a) | 161.3 | 1.2 | GL(75) |
| S2p 3/2 (b) | 164.1 | 1.2 | GL(75) |
| SKLL ($^1$D) (a) | 2115.8 | 1.6 | GL(95)T(1.5) |
| SKLL ($^1$D) (b) | 2113.0 | 1.9 | GL(95)T(1.5) |
| | | | |
| **$Cu_3AsS_4$ – one week exposure to atmosphere** | | | |
| Line | Bindig/Kinetic Energy (eV ± 0.2) | FWHM (eV) | Line Shape |
| S2p 3/2 (a) | 162.5 | 1.3 | GL(75) |
| S2p 3/2 (b) | 164.5 | 1.3 | GL(75) |
| S2p 3/2 (c) | 168.9 | 1.3 | GL(75) |
| SKLL ($^1$D) (a) | 2114.5 | 1.9 | GL(95)T(1.5) |
| SKLL ($^1$D) (b) | 2111.8 | 1.8 | GL(95)T(1.5) |
| SKLL ($^1$D) (c) | 2106.7 | 1.9 | GL(95)T(1.5) |
| | | | |
| **$Cu_3AsS_4$ – ground inside the glove box for 10 minutes** | | | |
| Line | Bindig/Kinetic Energy (eV ± 0.2) | FWHM (eV) | Line Shape |
| S2p 3/2 (a) | 161.8 | 1.23 | GL(75) |
| S2p 3/2 (b) | 163.4 | 1.9 | GL(75) |
| SKLL ($^1$D) (a) | 2115.9 | 1.6 | GL(95)T(1.5) |
| SKLL ($^1$D) (b) | 2113.3 | 1.9 | GL(95)T(1.5) |

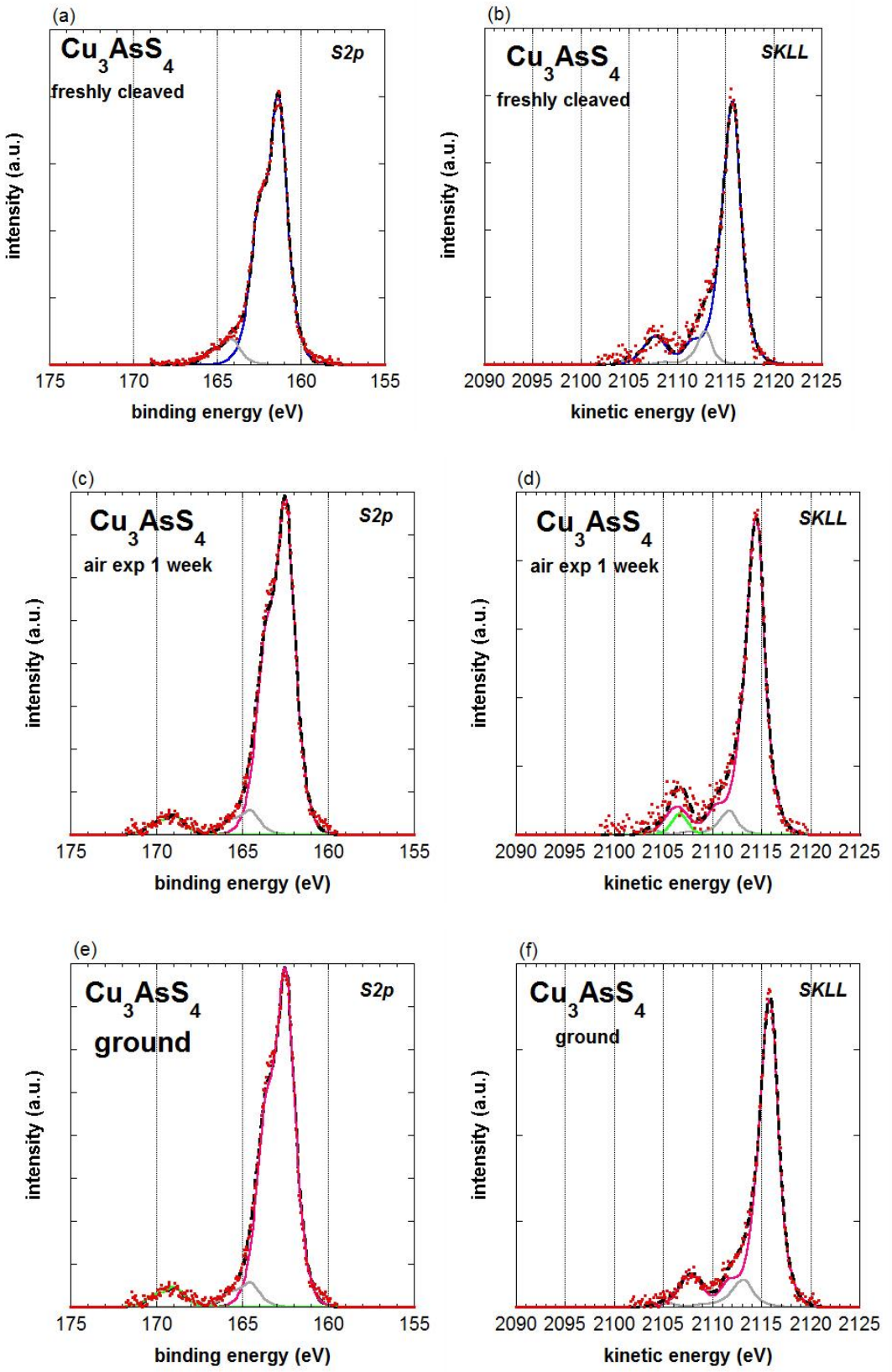


*Figure 5.31:* S2p and SKLL high resolution spectra of: freshly cleaved enargite crystal (a and b), crystal exposed to air for one week (c and d) and ground enargite (e and f).

S2p binding energy value of 161.3 for cleaved enargite sample is in agreement with [14]. The second component at 164.1 will be assigned in the discussion chapter. After air exposure for one week a shift of the most intense peak towards higher binding energy values is observed together with a peak at 168.5 eV ascribed to sulfur in sulfates. After grinding two peaks at 161.8 eV and 163.5 eV are only observed. No sulfate component is present.

### 5.3.5 Chemical state of sulphur in minerals

Various minerals (pyrite $FeS_2$, enargite $Cu_3AsS_4$, arsenopyrite FeAsS and chalcopyrite $CuFeS_2$) - freshly cleaved, after grinding and after air-exposure -were examined in this work (§ 5.3.1 - § 5.3.4). The chemical state plot of these minerals was drawn (figure 5.32), like it was done for sulphates and sulphides.

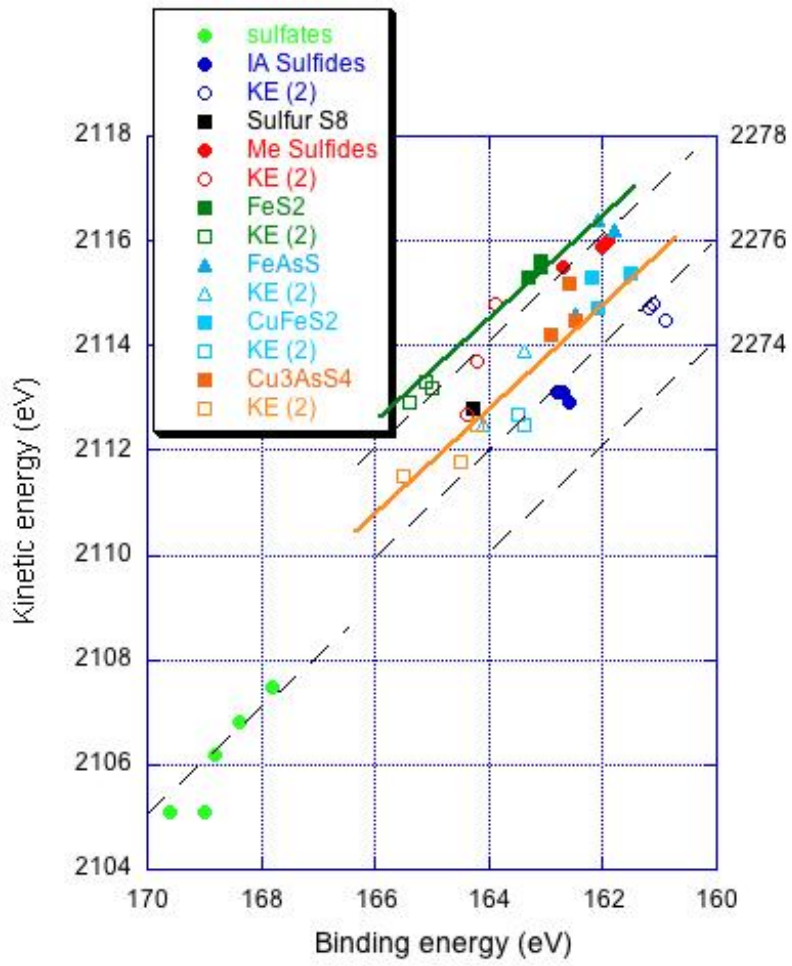


*Figure 5.32:* Chemical state plot of sulphide minerals (other compounds are shown for comparison).

In addition to the already discussed region of sulphates, alkali and transition metal sulphides, essentially two new groups can be distinguished. The first one is pyrite ($FeS_2$). The main S2p peak in the high-resolution photoelectron spectrum is found at

ca. 163 eV, the SKLL peak at ca. 2115 eV (§ 5.3.1). The Auger parameter is calculated being equal to 2278.6 ± 0.2 eV, thus clearly more positive compared to transition metal sulphides. The minor peak associated to sulphur on the surface of pyrite is found at higher binding energies but lower kinetic energies with the same Auger parameter (points are located on the same diagonal line): this suggests the presence of chain-lengths longer than $S_2^{2-}$.

Enargite, $Cu_3AsS_4$, shows a S2p binding energy value for the main peak assigned to sulphur in the bulk of the mineral similar to that of pyrite, the kinetic energy of the SKLL signal being clearly lower (ca. 2114 eV). The Auger parameter results to be: $\alpha'$ = 2276.8 ± 0.2 eV. The points of the sulphur component at the surface of enargite fall on the same diagonal line. On the basis of these results one may confirm that the sulphur at lower binding energy (sulphur in the bulk) is a sulphide – type compound. The component at higher binding energy with the same Auger parameter is supporting the formation of polysulphides on the surface after grinding. The just cleaved and air exposed enargite surface exhibit a component close to the elemental sulphur in the chemical state plot.

References

[1] Atzei D., Elsener B., Fantauzzi M., Rossi A., Analisi XPS di superfici di minerali: un nuovo sistema chiuso per il trasferimento del campione in ultra alto vuoto. XVIII Congresso Nazionale di Chimica analitica – Parma 19-23/09/04

[2] Wahlqvist M., Shchukarev A., J. Electron Spectrosc. Relat. Phenom. 1985; 156-158: 310-314

[3] Moulder H., Stickle W.F., Sobol P.E., Bomden K.D., Handbook of X-ray Photoelectron Spectroscopy 1992; ed. By J. Chastain

[4] Siriwardene R.V., Cook M.J., J. Colloid Interface Sci. 1985; 104: 250

[5] Contarni S., Rabalais J.W., J. Electron Spectrosc. Relat. Phenom. 1985; 35: 191

[6] C.D.Wagner, Discuss. Faraday Soc. 60, 291 (1975)

[7] Turner N.H., Murday J.S., Ramaker D.E., Anal. Chem 1980; 52: 84

[8] Wagner C.D., Chapter 7 in Handbook of X-ray and Ultraviolet Photoelectron Spectroscopy 1977; Ed. Briggs, Heyden and Sons, London

[9] Wagner C.D., Zatko D.A., Raymond R.H., Anal. Chem. 1980; 52: 1445

[10] Lee J.D., Chimica Inorganica 2000; cap. 16: 521 V Ed. Piccin

[11] Smart R.St.C., Skinner W.M., Gerson A.R., 28: 101-105

[12] Peisert H., Chassé T., Streubel P., Meisel A., Sgargan R., Journal of Electron Spectroscopy and Related Phenomena 1994; 68: 321-328

[13] Yu X.-R., Liu F., Wang Z.-Y., Chen Y., Journal of Electron Spectroscopy and Related Phenomena 1990; 50: 159-166

[14] Fantauzzi M., Atzei D., Elsener B., Lattanzi P., Rossi A., Surf. Interface Anal. 2006; 38: 922-930

[15] Nakai I., Sugitani Y., Nagashima N., J. Inorg. Nucl. Chem. 1978; 40 : 789 – 791

[16] Herbert R. B. Jr., Benner S. G., Pratt A.R., Blowes D. W., Chem Geology 1998; 144: 87 – 97

[17] Descostes M., Mercier F., Beaucaire C., Zuddas P., Trocelliner P., Nucl. Instr. And Meth. In Phys. Res B 2001; 181: 603 – 609

[18] M. Olla, G. Navarra, B. Elsener, A. Rossi, Surf. Interface Anal 38: 964 – 974 (2006)

[19] A.V. Kuklinskii, Yu. L. Mikhlin, G.L. Pashkov, V.F. Kargin, I.P. Asanov, Russ. J. Electrochem, 37: 1269 – 1276 (2001)

[20] R. Tegman, Acta Cryst., 1973; B29, 1463

[21] D. Oei, Inorg. Chem., 1973; Vol 12, No2, 438

[22] Y. Liu, X. Shaodong, Y. Li, Y. Liu, Environ. Sci. Technol., 2007; 41, 1735.

[23] W.E. Swartz Jr., K.J. Wynne, D.M. Hercules, Anal. Chem., 1971; 43, No13, 1884.

[24] Y.L. Mikhlin, A.R. Romanchenco, I.P. Asanov, Geochim. Cosmochim. Acta 70 (2006) 4874 – 4888

[25] I. Nakai, Y. Sugitani, N. Nagashima. J. Inorg. Nucl. Chem. 40 (1978), 789 – 791

# Chapter 6

# Conclusions

The chemical state of sulphur at the surface of sulphur-bearing materials (compounds or minerals) is a challenging task that is based on the Auger parameter α' and the two dimensional chemical state plot. Owing to the simultaneous presence of sulphides, polysulphides and sulphates, the S2p photoelectron and the SKLL Auger lines are multi-component. Whereas curve fitting for S2p photoelectron lines is a standard procedure, in this work for the first time the curve fitting of SKLL line of a series of sulfides and sulfates compounds has been attempted. This results in a more accurate determination of the SKLL kinetic energy of the different components compared with the conventional way of using only the centroid. By combining the photoelectron S2p and S2s signals and the Auger SKLL and SLMM lines it has been possible to identify the chemical state of sulfur on the surface of different mineral samples.

From this work the following conclusions can be drawn:

1) The chemical state plot of reference compounds allows to distinguish among three different regions, characterized by three different values of the Auger parameter: the sulphates, the alkali sulphides and the transition metals sulphides regions.

2) In the alkali sulphates series (Li to Cs) the binding energy of S2s, S2p and SKLL decreases from lithium to cesium; this decrease is more pronounced for the SKLL line than for S2p and S2s lines. The difference in binding energies of S2p and kinetic energies of SKLL of these compounds reflects differences in initial state effects: local valence charge and Madelung potential. Being the local valence charge the same for each metal ion and for sulphates anions, differences in Madelung potential should cause the distribution along a line characterized by an α' value of $2276.6 \pm 0.2$ eV.

3) Alkali sulphide compounds ($Li_2S$, $Na_2S$, $K_2S$) show two compounds assigned to sulphide and polysulphide with nearly the same Auger parameter as alkali sulphates. This confirms that initial state effects are dominant in determining the shift in S2p binding and SKLL kinetic energy. Mechanical grinding changes the surface composition towards elemental sulphur increasing the grinding time.

4) In the mixtures of $Na_2S_4$ and elemental sulphur $S_8$ the individual compounds could be detected both in the S2p and SKLL lines. The signals of elemental sulphur show the same Auger parameter as the pure $S_8$ standard. Sulphur in $Na_2S_4$, however, exhibits in the mixtures a higher binding and kinetic energy compared with the pure $Na_2S_4$ and the Auger parameter is close to that of elemental sulphur.

5) The chemical state of sulphur in minerals differs according to the metals present. Pyrite ($FeS_2$) and arsenopyrite (FeAsS) show the highest Auger parameter ($\alpha'$ = 2278.2 ± 0.2 eV), the copper- bearing chalcopyrite ($CuFeS_2$) and enargite ($CuAsS_4$) show Auger parameters of 2277.0 ± 0.2 eV for sulphides. The polysulphides that formed on the mineral surface after air exposure or grinding exhibit a chemical state between those of elemental sulphur and of the polysulphides in the alkali sulphide standards.

From this work it can thus be advanced as a hypothesis that the chemical state of sulphur on mineral surfaces, that is often a metal-deficient sulphur surface layer, can be placed in an interval between a polysulfide and elemental sulphur.

APPENDIX – Example of calibrations.

*Table A1*: Calibration of energy scales [1]of the AlKα (1486.6 eV) and MgKα (1253.6 eV) sources (a, c) and associated errors (b, d) of the VG ESCALAB 200. Position of the Au $M_4N_{6,7}N_{6,7}$ lines are indicated too [2, 3].

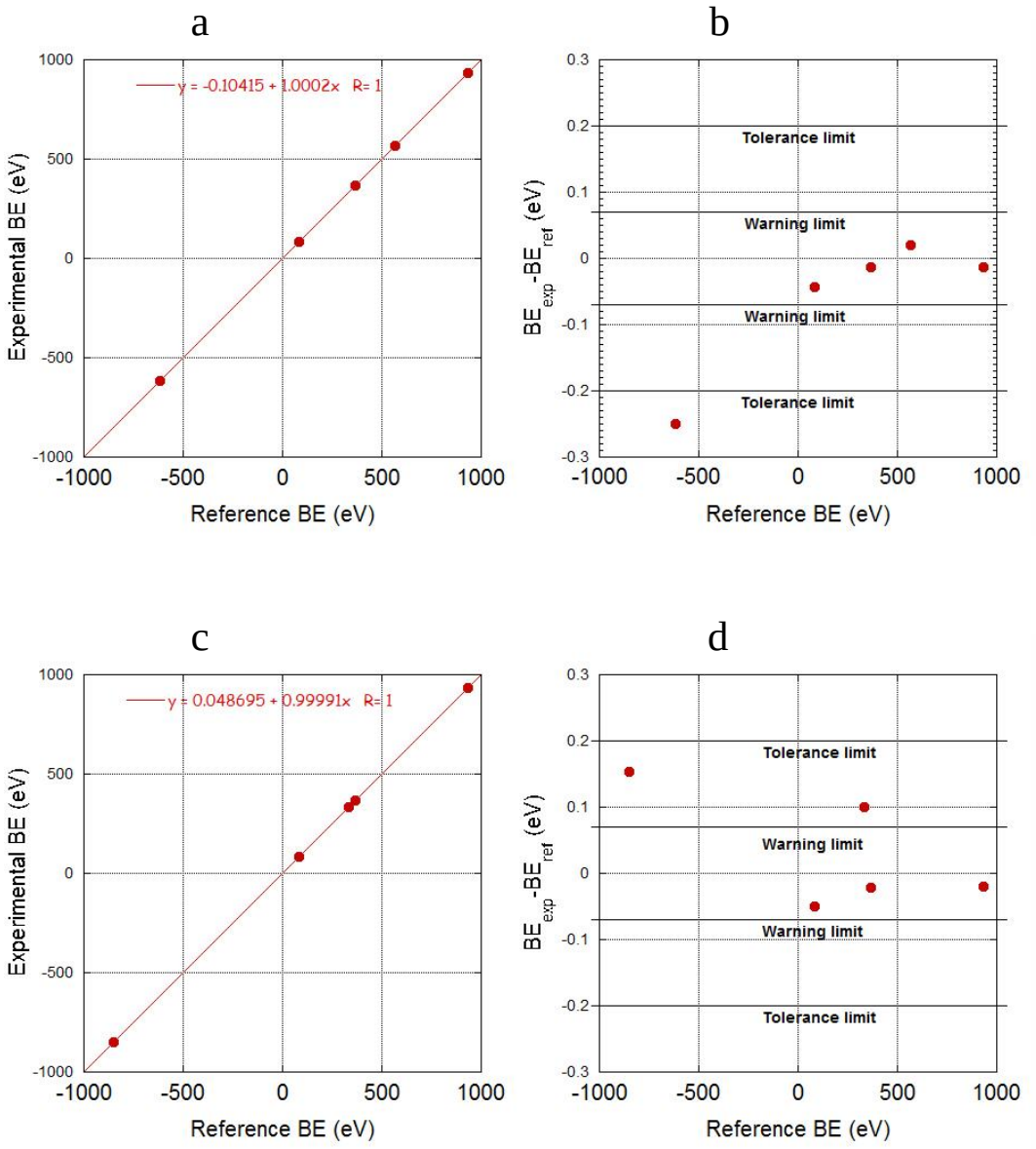

*Table A2*: Calibration of energy scales [1]of the AlKα (1486.6 eV) monochromatic source (a) and associated errors (b) of the Thetaprobe spectrometer.

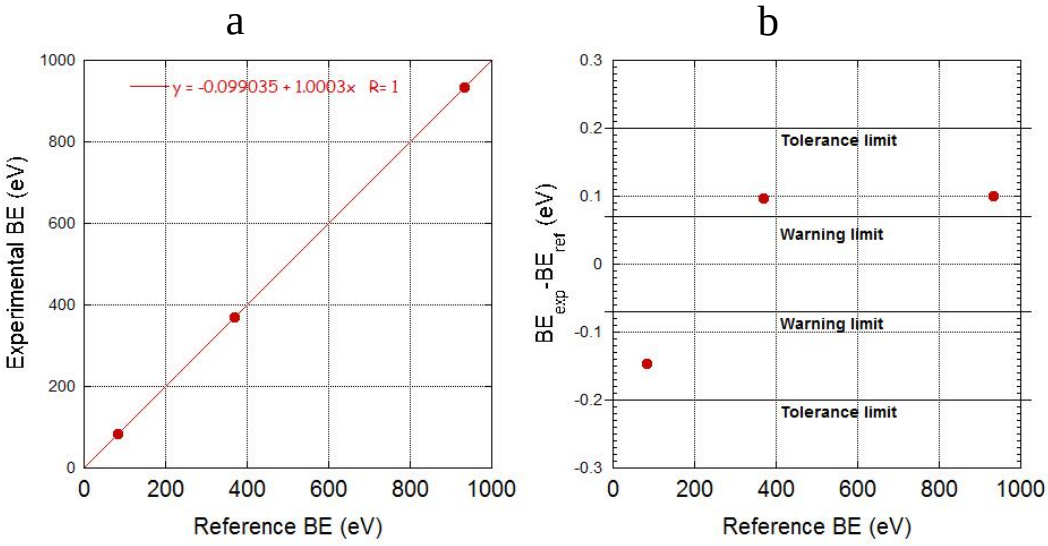


*Table A3:* Experimental binding energies measured during the calibration of spectrometers compared to reference values [4,5,6].

| **Peak** | **Monochromatic Al Kα** | | | | | |
|---|---|---|---|---|---|---|
| | Ref. | Exp. *ESCALAB* | Ref. | Exp. *ESCALAB* | Ref. | Exp. *THETA PROBE* |
| Au $4f_{7/2}$ | 83.95 | 83.907 | 83.95 | 83.900 | 83.96 | 83.713 |
| $Ag3d_{5/2}$ | 368.22 | 567.950 | 368.22 | 335.000 | 368.21 | 368.21 |
| Cu $L_3VV$ | 567.93 | 932.617 | 334.90 | 932.600 | [a] | - |
| Cu $2p_{3/2}$ | 932.63 | 368.207 | 932.62 | 368.199 | 932.62 | 932.68 |
| Au $M_4N_{6,7}N_{6,7}$ | -614.6[b] | -614.850 | -848.6[a] | -847.446 | [c] | - |

[a] not given

[b] according to value of 2101.2 eV in kinetic energy.[2, 3]

[c] not detectable with monochromatic sources

APPENDIX references

[1] ISO 15472:2001 – Surface Chemical Analysis – X-ray Photoelectron Spectrometers – Calibration of Energy Scales and ref. therein.

[2] Peisert H., Chassé T., Streubel P., Meisel A., Szargan R. *Journal of Electron Spectroscopy and Related Phenomena* 1994; 68: 321-328

[3] Wagner C.D., *J. Vac. Sci. Technol.* 1978; 15: 518